CONNECTION OF MODULAR STEEL BEAM PRECAST SLAB UNITS WITH CAST-IN-PLACE CLOSURE POUR SLABS

A Thesis

by

NATALIE CAMILLE BRUSH

Submitted to the Office of Graduate Studies of
Texas A&M University
in partial fulfillment of the requirements for the degree of

MASTER OF SCIENCE

December 2004

Major Subject: Civil Engineering

CONNECTION OF MODULAR STEEL BEAM PRECAST SLAB UNITS WITH CAST-IN-PLACE CLOSURE POUR SLABS

A Thesis

by

NATALIE CAMILLE BRUSH

Submitted to Texas A&M University
in partial fulfillment of the requirements
for the degree of

MASTER OF SCIENCE

Approved as to style and content by:

Ray James (Chair of Committee)	Harry Jones (Member)
Terry Kohutek (Member)	Paul Roschke (Head of Department)

December 2004

Major Subject: Civil Engineering

ABSTRACT

Connection of Modular Steel Beam Precast Slab Units

with Cast-in-Place Closure Pour Slabs. (December 2004)

Natalie Camille Brush, B.S., Texas A&M University

Chair of Advisory Committee: Dr. Ray James

Jointless bridges are advantageous in removing mechanical joints which are a known cause of bridge deterioration. Elimination of joints provides a smoother riding surface and removes the possibility of de-icing salts penetrating the deck and corroding the deck reinforcing and underlying bridge superstructure. Jointless bridges are traditionally constructed by monolithically casting the entire bridge deck on beams after they have been erected. However, this process requires extensive in-field formwork and lengthy traffic closures. The Texas Department of Transportation proposes a new method of constructing jointless bridges using prefabricated girder-and-deck units connected on-site with cast-in-place closure pours. This new system will expedite construction and reduce disturbances to the traveling public.

The objective of this experimental study was to investigate the behavior of the cast-in-place closure pour slab and to determine if it responds to wheel loads in the same way as a traditional monolithic continuous deck. The effects of the cold joints and discontinuous steel details are the focus of the research work.

ACKNOWLEDGEMENTS

I greatly appreciate the financial support from the Texas Department of Transportation which made this study possible. In addition, I wish to thank Project Director, Lloyd Wolf (BRG), Project Coordinator, Ronald E. Koester (WAC), and the Project Monitoring Committee, Dean Van Landuyt (BRG) for their guidance.

Dr. Ray James and Dr. Harry Jones gave their time and energy throughout the project and had a direct impact on the achievements of this thesis. Sincere thanks are extended to them and to Graeme Sharpe for his daily assistance in laboratory testing and preparation. Special appreciation goes to Andrew Fawcett, Jeff Perry, and Matt Potter of the A&M Testing, Machinery, and Repair Facility for all their laboratory help, time, and support. Last but not least, thank you to Jonathan Neubauer, Yateesh Contractor, and Elizabeth Goodwin for assistance in the construction of specimen forms and research work.

TABLE OF CONTENTS

Page

Page

Page

LIST OF FIGURES

Page

Page

Page

Page

Page

LIST OF TABLES

Page

Page

INTRODUCTION

Proposed Design Overview

Jointless bridges are advantageous in removing mechanical joints which are a known cause of bridge deterioration. Elimination of joints provides a smoother riding surface and removes the possibility of de-icing salts penetrating the deck and corroding the deck reinforcing and underlying bridge superstructure. Jointless bridges are traditionally constructed by monolithically casting the entire bridge deck on beams after they have been erected. However, this process requires extensive in-field formwork and lengthy traffic closures. The Texas Department of Transportation proposes a new method of constructing jointless bridges using prefabricated girder-and-deck units connected on-site with cast-in-place closure pours. This new system will expedite construction and reduce disturbances to the traveling public.

Each prefabricated unit consists of a full depth concrete deck attached with shear connectors to a trapezoidal steel girder ("tub-girder") assembly. Fig. 1 shows a transverse cross-section of a module proposed for use on the Interstate 35 expansion near Waco, Texas. The unit is constructed on the ground in a controlled environment instead of over traffic. At the bridge site, the modules are lifted into place and subsequently connected with cast-in-place closure pour slabs both longitudinally and transversely.

This thesis follows the style of *ASCE Journal of Bridge Engineering.*

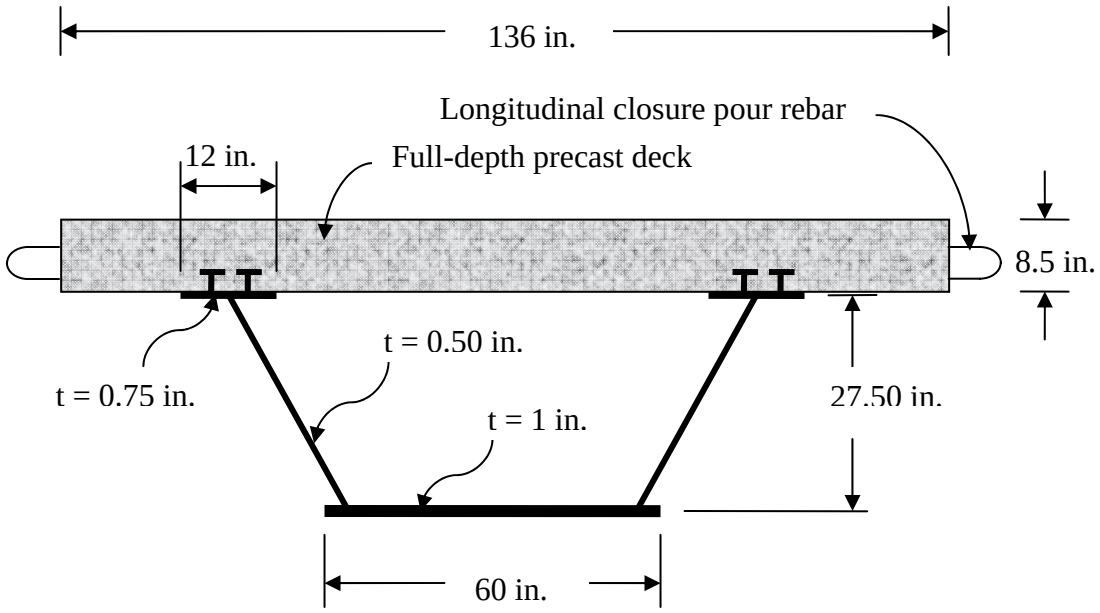

Fig. 1. Transverse cross-section of interior bridge steel tub-girder module

Fig. 2 depicts two interior spans of the newly proposed bridge system after casting both types of closure pours. A plan view of the prefabricated unit is provided in Fig. 3. The steel tub-girder extends beyond the deck slab at each end and rests on elastomeric bearing pads on the pier bent caps as shown in Fig. 4. A 1 in. bituminous pad is provided at the bottom of the transverse closure pour to reduce bearing forces on the transverse closure pour from girder rotations.

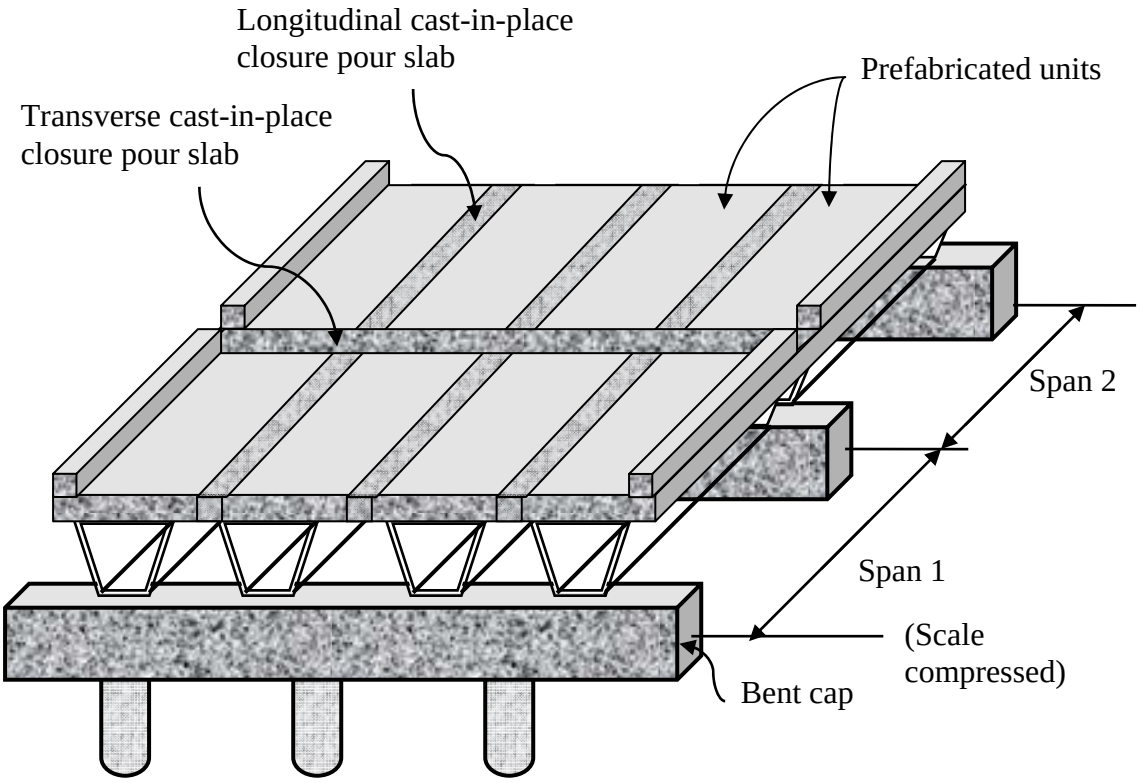

Fig. 2. Two interior bridge spans for the proposed jointless bridge

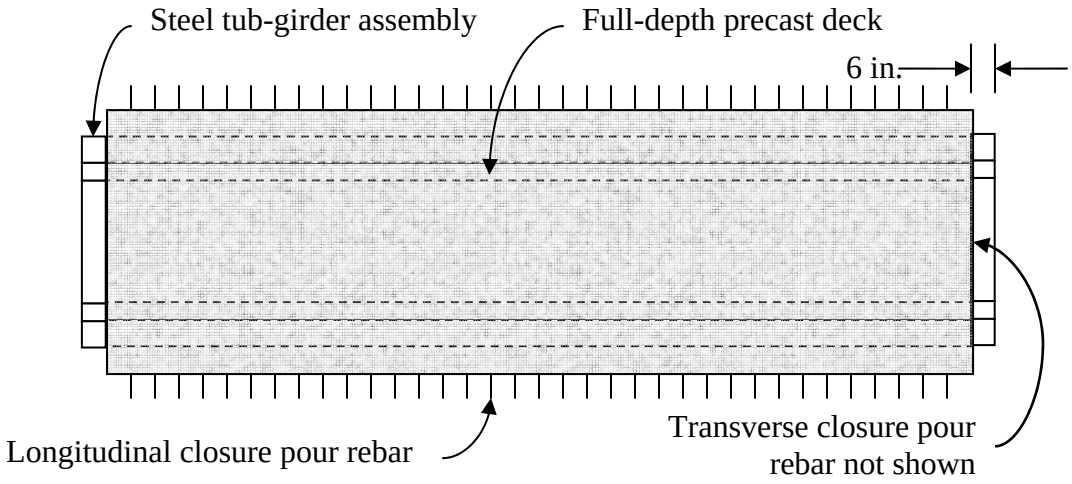

Fig. 3. Plan view of interior bridge steel tub-girder module

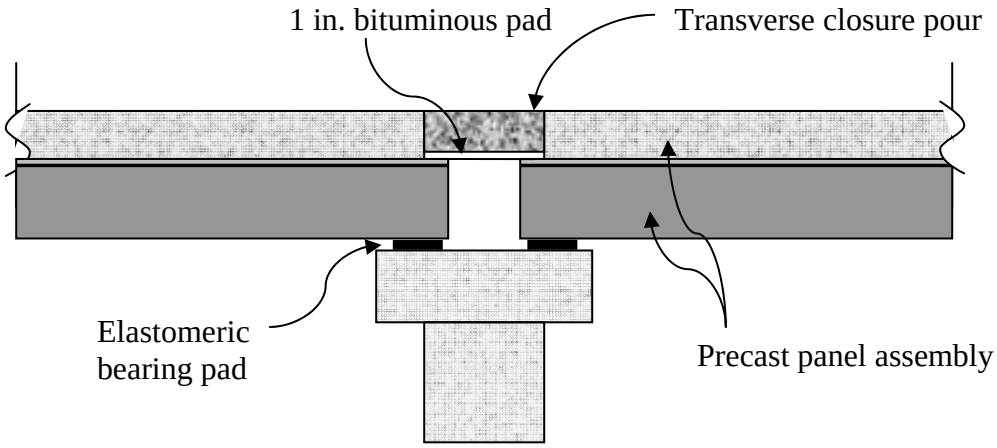

Fig. 4. Section through interior transverse closure pour

The end product of the proposed system is a jointless bridge deck. However, due to the unique construction method, the behavior of the bridge cannot be assumed to be identical to a conventional monolithically cast deck. Although the completed deck looks similar to the typical jointless deck, discontinuous deck reinforcing and presence of closure pour cold joints may result in unusual bridge behavior and failure patterns.

Research Objectives and Scope

The objectives of this experimental study were to investigate the behavior of the cast-in-place closure pour slab and evaluate the feasibility of its design details. Specifically, to determine if the cast-in-place slab responds the same as a conventional monolithic deck. The closure pour detail differs from a continuous deck; the reinforcing bars are not continuous across the closure pour, and there is a cold joint at each side of

the closure pour. The effects of these details are the focus of the research work described herein.

LITERATURE REVIEW

Jointless Bridges

Jointless deck bridges were initially designed to resolve problems associated with expansion joints. Presently, jointless bridges are being constructed all over the world and in a majority of the American states, and their performance is largely reported as good. The emergence of this design was seen in several states around the 1970s to 1980s (Wasserman 1987; Burke 1994; Hambly 1997; Alampalli and Yannotti 1998; Van Lund and Brecto 1999; Kunin and Alampalli 2000; Hussain and Bagnariol 2000).

Although there is a general positive attitude towards jointless deck bridges, there are a few limitations that have been observed from in-service bridges. Foremost, jointless deck bridges are still prone to the same inherent construction problems such as early-age transverse deck cracking, weather related troubles, drainage at abutments, and poor or unsupervised construction (Burke 1999; Kunin and Alampalli 2000). The most commonly noted problems in jointless deck bridges are approach slab settlement and minor cracking at pier supports (Alampalli and Yannoti 1998; Burke 1999, Kunin and Alampalli 2000). Field evaluations conducted on these bridges found that approach slabs deteriorated faster than the deck or abutment (Alampalli and Yannotti 1998; Kunin and Alampalli 2000). However, these limitations are preferable to the maintenance problems of jointed bridges.

Modular Precast Deck Connection

A precast deck panel is a section of deck slab whose width is the full width of the bridge and length, in the direction of traffic, is a fraction of the span length. They are typically fabricated off-site and transported to the bridge site by crane. Modular construction of precast deck panels has been used in many states for deck replacement and bridge rehabilitation. Generally, these bridges are jointed with shear keys and topped with waterproofing and/or an asphalt wearing surface. Cracking at the transverse joint (shear key) is the most common problem reported (Issa et al. 1995c; Culmo 2000). To combat transverse cracking, some DOT's are using longitudinal post-tensioning to reduce the tensile forces in the deck. Although this delays crack initiation and improves joint stress distribution, spalling and leakage have still been seen at the closed joint (Issa et al. 1995c, Issa et al. 1998; Issa et al. 2000; Shim and Chang 2003).

The Federal Highway Administration (FHWA) published a report discussing modular precast deck panel connections (Martin and Osborn 1983). This study found several instances of closure pour use in bridges to connect precast elements. A 1973 publication by the United States Steel Company suggests the use of a transverse pour strip between precast deck panels laid perpendicular to girders. One bridge constructed in this manner was still performing adequately and had no leakage problems when evaluated for the FHWA report. Alabama has a bridge that utilizes a small closure pour between precast slab panels at the bridge ends and is still functioning well after many years (Culmo 2000).

The FHWA report also studied longitudinal and transverse connection practices for jointless bridges constructed with precast deck panels. Some systems in use include transverse bolts or tie rods, weld plates, and transverse post-tensioning. A Canadian design was found that employed hooked reinforcing bars in a grout key to attach adjacent precast box beams longitudinally. The conclusions of the FHWA research stated that the best method of longitudinal connection is 4 in. or more of cast-in-place reinforced concrete.

In 1998, Caner and Zia reported an analysis on a transverse link slab that connects two simply supported bridge spans. In this study, a partially de-bonded concrete and steel girder bridge specimen was investigated. De-bonding of the girders and deck at the link slab reduces the stiffness and consequently the stress in the link slab. It was found that the transverse link slab acted more like a beam in bending than a tension member. Failure of the steel girder section was initiated by yielding of the girders, followed by yielding of the reinforcing bars and ultimately, crushing of the concrete at the bottom surface of the link slab.

Summary

The literature reviewed suggested the following points with regard to the behavior of cast-in-place closure pour connections between steel beam precast modular units.

- The transverse joint over an interior support has been shown experimentally to behave like a beam in flexure, not a tensile member.

- Cracking at the supports and abutment of a jointless deck bridge is to be expected and is most often not problematic.

LABORATORY TESTING

Testing Overview

The goal of this test program was to study experimentally the behavior of the closure pour connections proposed for use by TxDOT. Both transverse and longitudinal closure pours were tested and data acquisition included specimen strains, crack monitoring, and specimen strengths. Testing mimicked service load conditions in the closure pours which were determined from a parallel computer FE model. Steel tub-girders were not included in test specimens, but their presence was accounted for in the support and loading setup.

Seventeen specimens were constructed and tested: six containing transverse closure pours and eleven containing longitudinal closure pours. A relatively narrow strip was taken out of the bridge deck to test, and the strip included a section of closure pour and portions of the precast deck units as shown in Fig. 5. The forms for each specimen were divided into three sections that represented the three divisions of the actual bridge: two exterior sections from the precast deck slabs and an interior section simulating the closure pour slab. Throughout the testing program, specimens were occasionally altered to understand better the governing failure mechanisms and details; thus there was some deviation in the details of the various beams. Specimen labels followed a basic numbering system with a T or L prefix denoting a transverse or longitudinal closure pour, respectively. The first transverse specimen is labeled T1 and the last T6.

Similarly, the longitudinal specimens are labeled L1 through L11. Numbering does not designate the chronological order of testing.

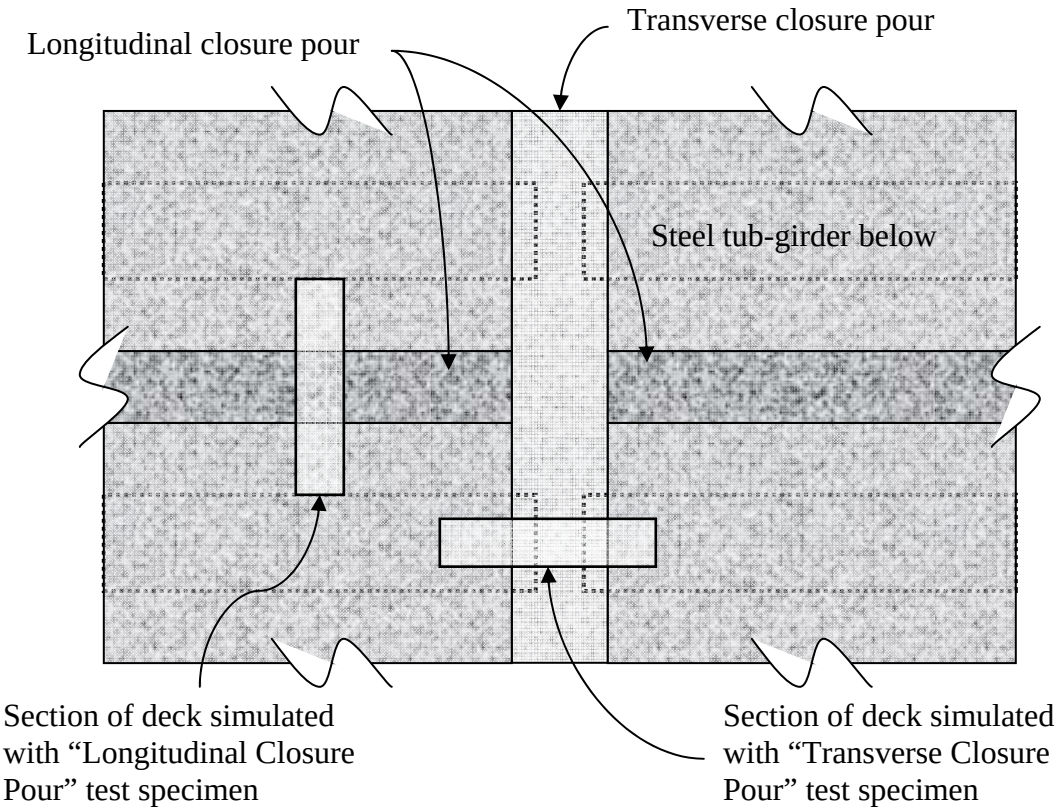

Fig. 5. Plan View of Bridge showing orientation of laboratory beam strips

Specimen Descriptions

Transverse Closure Pour

Transverse closure pours extend across the bridge over pier supports to connect adjacent bridge spans. Tested specimens were beams that represent a longitudinal strip across the transverse bridge closure pour and included portions of the precast panel deck

and cast-in-place slab as shown in Fig. 5. The basic dimensions of all transverse specimens are shown in Fig. 6, and the slab reinforcing details for the beams are described in Fig. 7, Fig. 8 and Table 1. Beam width was chosen to allow multiple bar repetitions in the beam, and beam length was chosen to permit any possible loading setup. In actual construction, the transverse closure pour is formed on a 1 in. preformed bituminous fiber material pad to protect the concrete deck from steel girder end rotations bearing against the concrete. This pad was not used or needed in testing, but specimens were built with the closure pour concrete depth reduced by 1 in. as seen in Fig. 6.

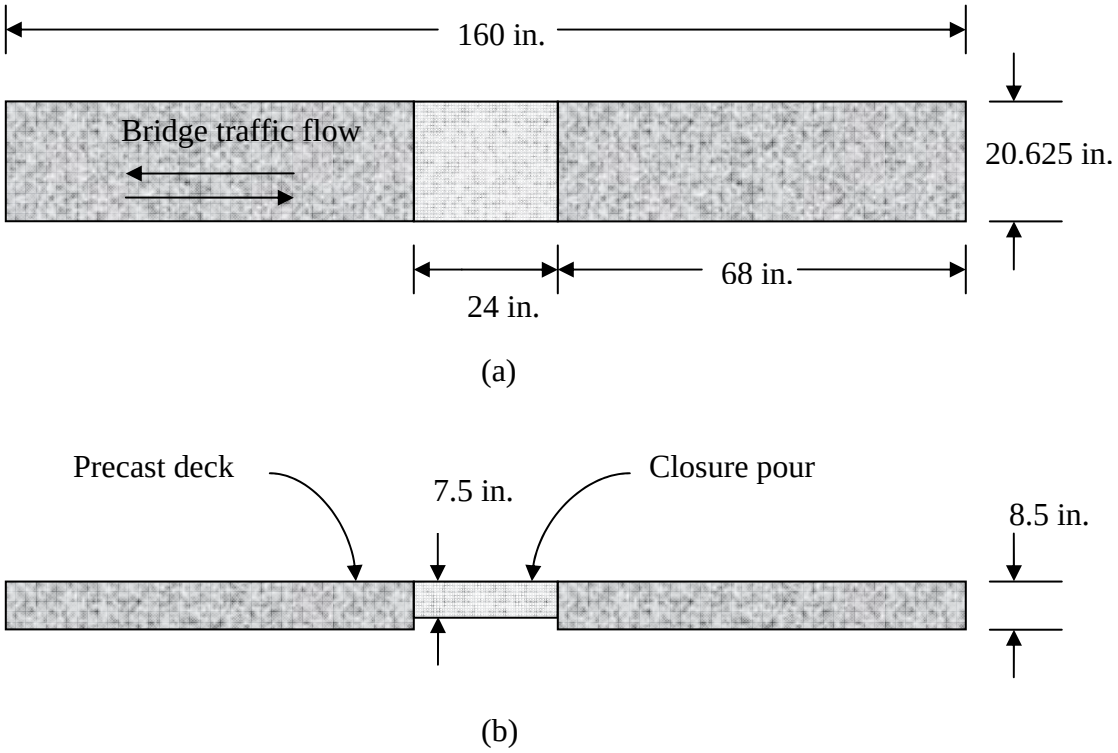

Fig. 6. Dimensions and orientation of transverse test specimen: (a) plan view; (b) elevation view

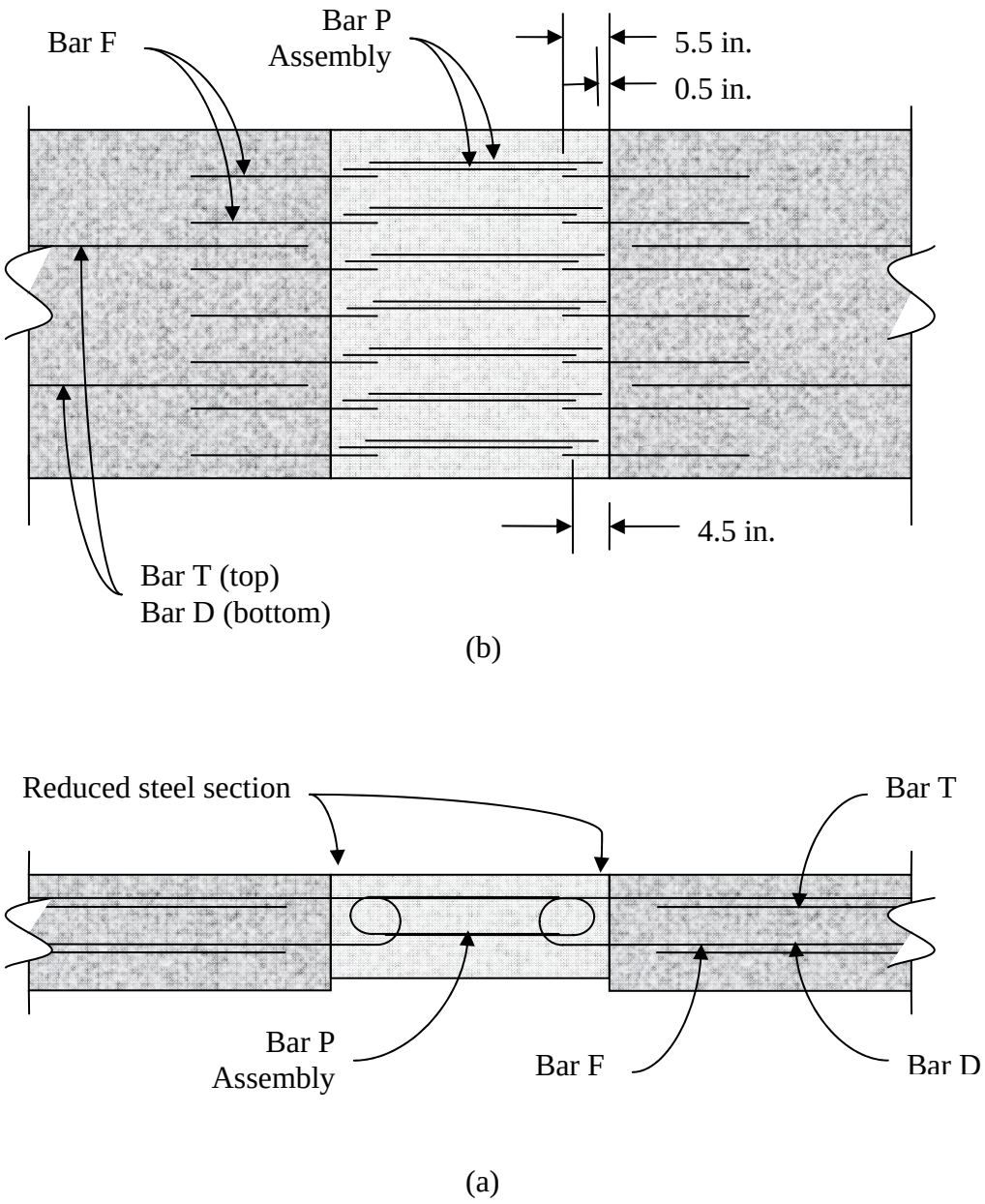

Fig. 7. Reinforcing pattern for transverse test specimens: (a) plan view; (b) elevation view

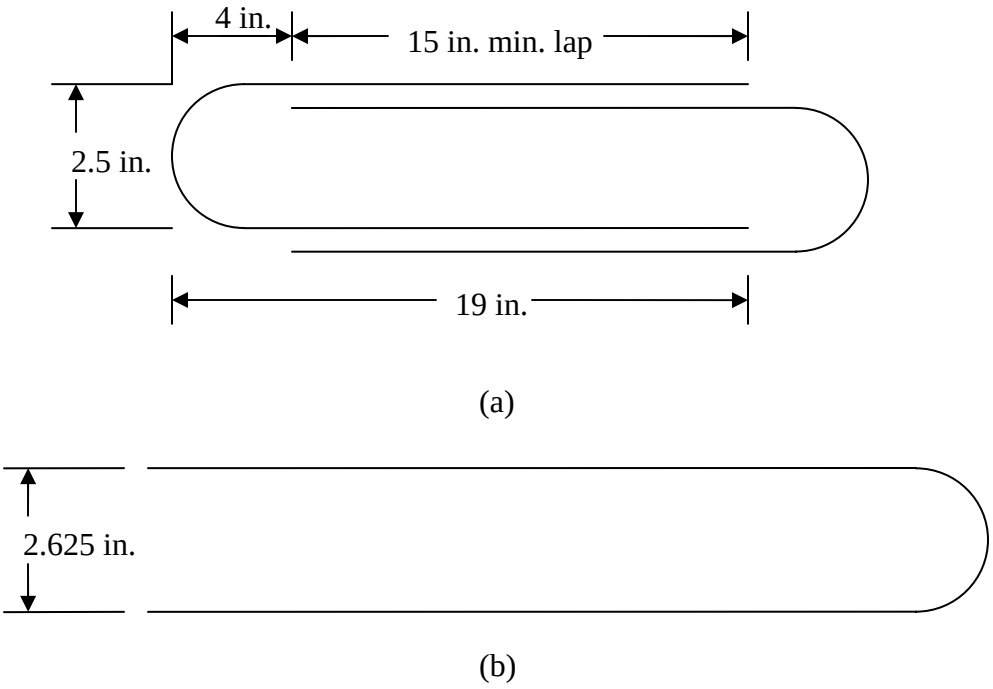

Fig. 8. Geometry of transverse hoop bars: (a) bar P assembly; (b) bar F

Table 1. Spacing, Cover, and Size of Transverse Specimen Reinforcing Steel

Bar	Size	Spacing (in.)	Top Clear Cover (in.)	Bottom Clear Cover (in.)
F	No. 3	3	2.625	1.5
P	No. 3	3	2.625	1.625
T	No. 4	9	3.125	N/A
D	No. 5	9	N/A	2.125

Both epoxy-coated and plain reinforcing bars, as noted in Table 2, were used in the six transverse specimens. Specimens T3 and T6 were cast with uncoated rebar to test the effect of the concrete-to-steel bond on the failure of the beams. Specimen T6 also acted as control specimen because the beam was cast monolithically and the rebar detailing was changed from the hook system shown in Fig. 7 to a system of straight bars shown in Fig. 9. The straight bars are continuous through the closure pour with the same bar size and spacing as the precast panel deck reinforcing, Bar F shown in Fig. 7. This specimen provided a basis for isolating the possible detrimental effects resulting from the closure pour cold joints and a reinforcing detail that terminates bars within the closure pour.

Table 2. Construction Variations in Transverse Specimens

Specimen Label	Rebar Coating	Closure Pour	Rebar Pattern
T1	Epoxy	Yes	Fig. 7
T2	Epoxy	Yes	Fig. 7
T3	None	Yes	Fig. 7
T4	Epoxy	Yes	Fig. 7
T5	Epoxy	Yes	Fig. 7
T6	None	No	Control (Fig. 9)

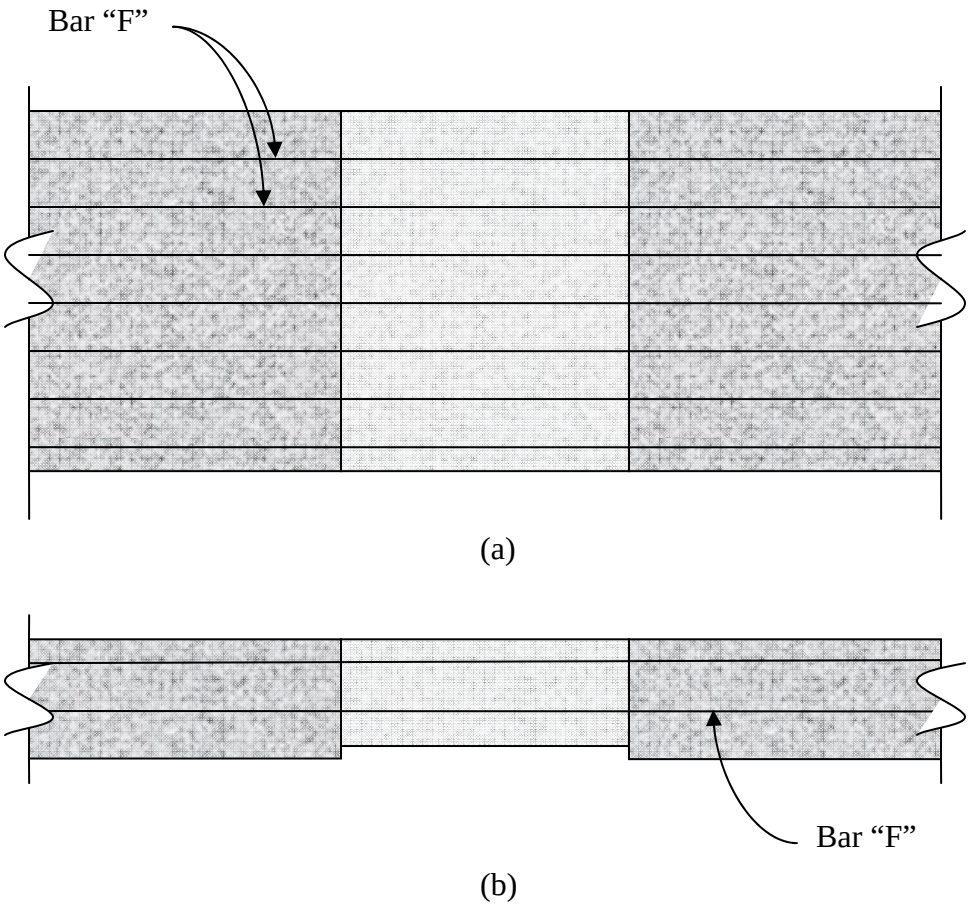

Fig. 9. Reinforcing pattern for transverse control test specimen: (a) plan view; (b) elevation view

Longitudinal Closure Pour

Longitudinal closure pours run in the direction of traffic to connect transverse edges of adjacent pre-cast unit decks. Tested specimens were representative beam strips from a transverse section of the longitudinal closure pour with portions of the precast

decks included as described in Fig. 5. Dimensions of the longitudinal specimen are given in Fig. 10, and the reinforcing pattern is shown in Fig. 11.

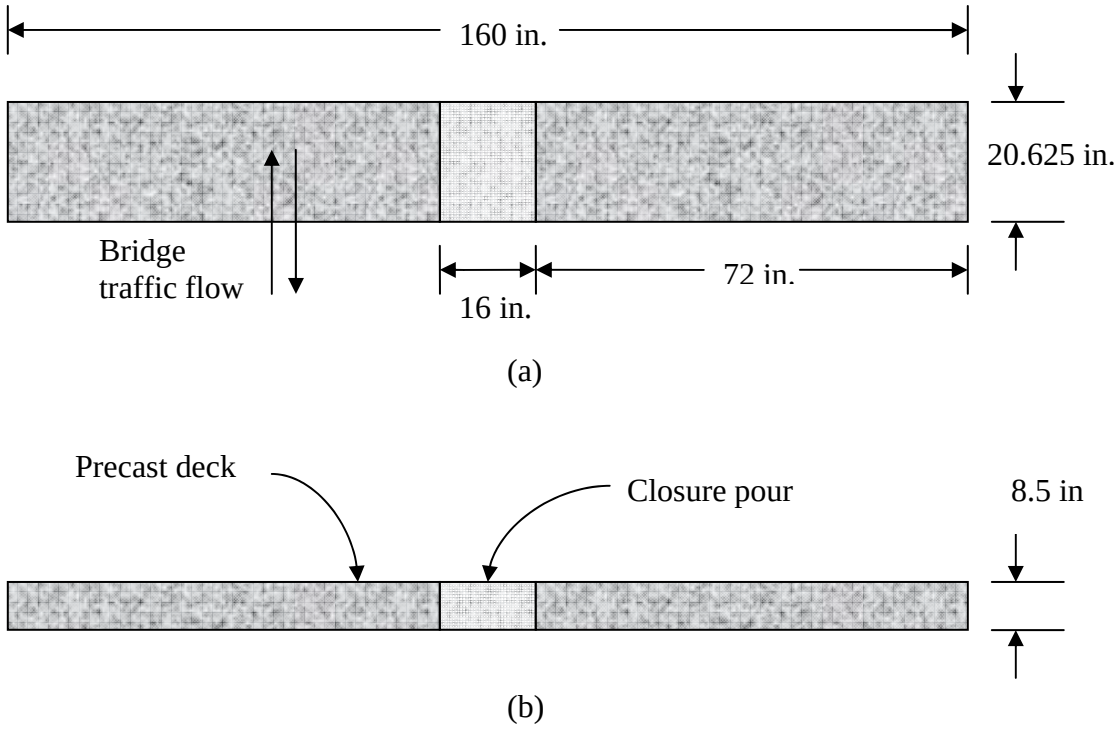

Fig. 10. Dimensions and orientation of longitudinal test specimen: (a) plan view; (b) elevation view

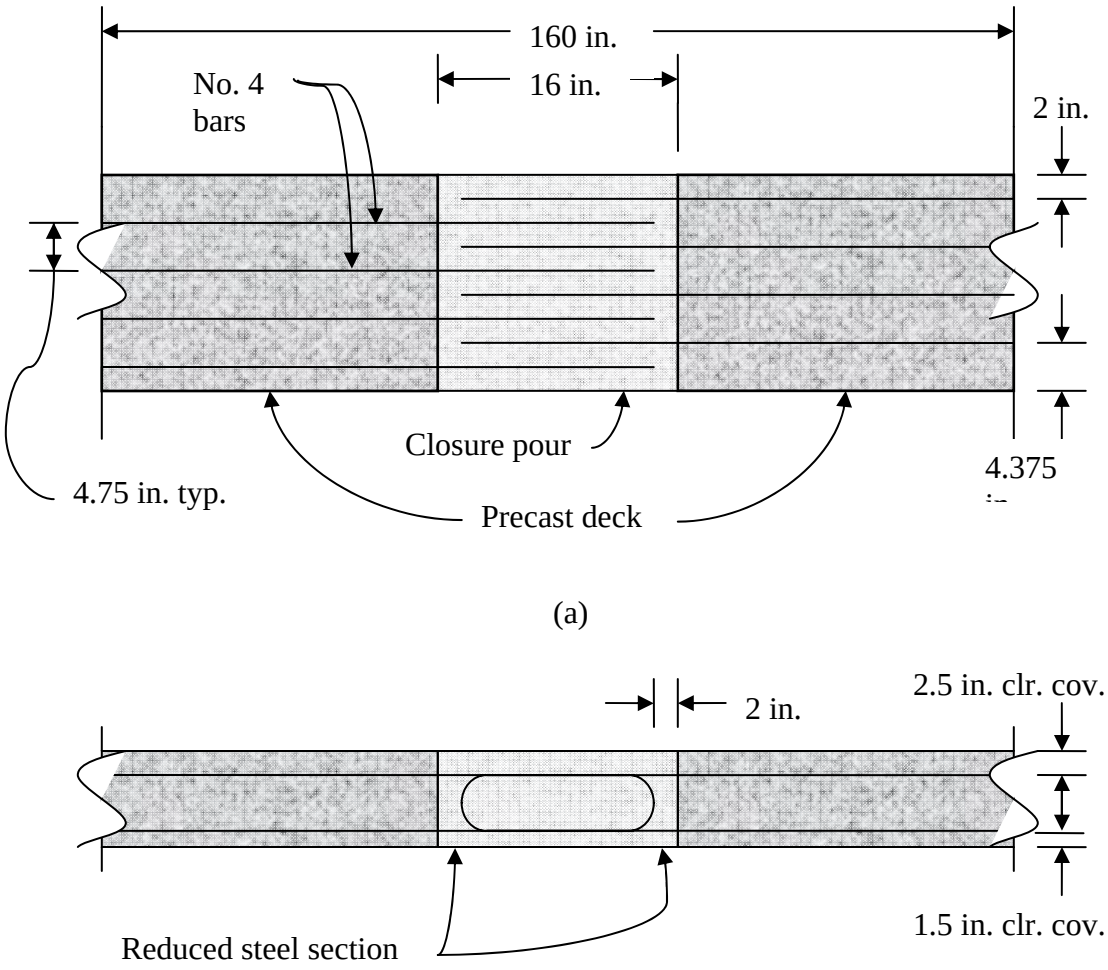

Fig. 11. Reinforcing pattern for longitudinal test specimens: (a) plan view; (b) elevation view

A preliminary design using No. 5 bars was modeled by specimens L1 through L7. These bars were changed to No. 4 bars in the remaining specimens. Data for L1 – L7 is provided in Appendix E. To determine if the presence of the closure pours was a

major factor in producing the observed failure pattern, L5 was cast without a closure pour (i.e., a monolithic pour) but included the reinforcing pattern of the other specimens. Subsequently, L7 was cast without a closure pour and without specified hooks. In L7, the precast deck reinforcing was made continuous through the closure pour with straight bars similar to Fig. 12 with spacing and bar size matching the previous beams. L5 and L7 were considered control specimens to which other beams with No. 5 bars were compared.

Specimen L1 – L9, labeled Type 1 for their smaller cross-sectional width, showed signs of adverse edge effects during testing, so two additional beams (L10 and L11) were fabricated with an increased side cover to eliminate this problem. In addition, beam length was increased to 168 in. and transverse bars were added to the closure pour to better simulate actual bridge reinforcing. These two beams are labeled Type 2 and are shown in Fig. 13. Table 3 lists the construction and reinforcing variations in L1 – L11.

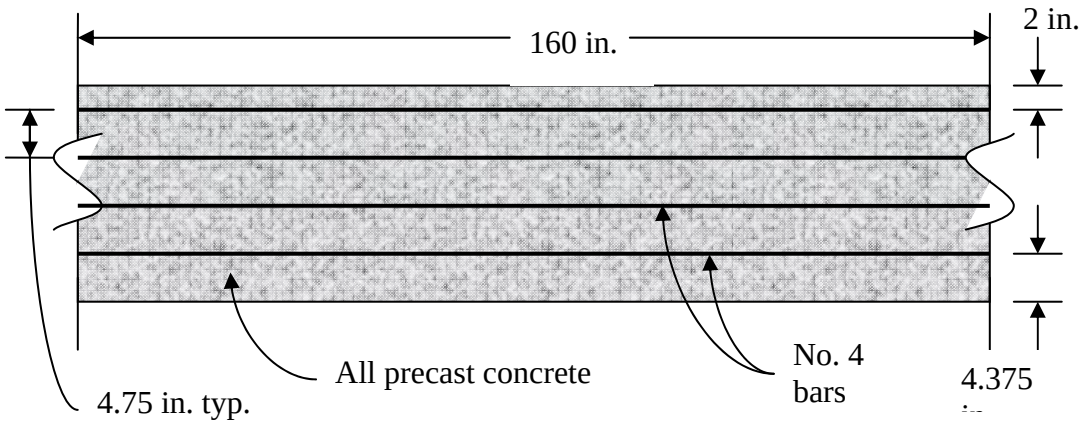

Fig. 12. Reinforcing pattern for longitudinal control test specimens – plan view

Table 3. Construction Variations in Longitudinal Specimens

Specimen Label	Rebar Coating	Bar Size	Closure Pour	Transverse Bars	Beam Width (in.)	Rebar Pattern	Beam Type
L1	Epoxy	No. 5	Yes	No	20.625	Fig. 11	1
L2	Epoxy	No. 5	Yes	No	20.625	Fig. 11	1
L3	Epoxy	No. 5	Yes	No	20.625	Fig. 11	1
L4	None	No. 5	Yes	No	20.625	Fig. 11	1
L5	None	No. 5	No	No	20.625	Fig. 11	1
L6	None	No. 5	Yes	No	20.625	Fig. 11	1
L7	None	No. 5	No	No	20.625	Fig. 12	1
L8	Epoxy	No. 4	Yes	No	20.625	Fig. 11	1
L9	Epoxy	No. 4	Yes	No	20.625	Fig. 11	1
L10	Epoxy	No. 4	Yes	Yes	34	Fig. 11	2
L11	Epoxy	No. 4	Yes	Yes	34	Fig. 11	2

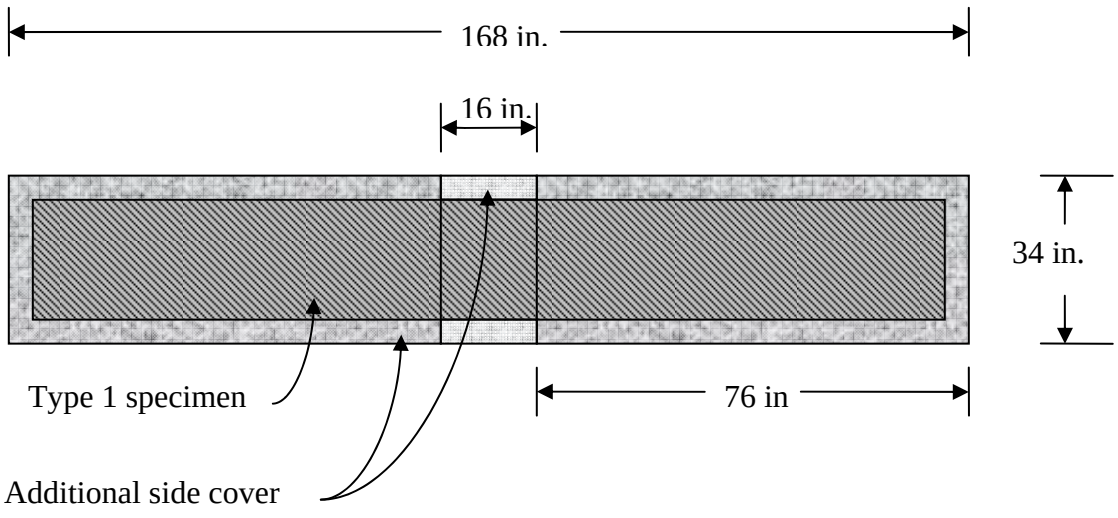

Fig. 13. Dimensions of variation for Type 2 longitudinal specimens – plan view

Specimen Construction

Three reusable plywood forms were constructed and used to fabricate all specimens except the longitudinal Type 2 specimens that had a wider cross-section and extended length. Fig. 14 shows a Type 1 form prior to installation of the reinforcing steel. A transverse bulkhead was used to separate the precast and cast-in-place beam sections and was removed for the placement of the closure pour after the precast sections had cured. Type 2 specimens were designed with an increased width in an attempt to reduce edge effects, and two new forms were constructed to adjust for the new section. Fig. 15 is a photograph of a Type 2 form after steel installation.

Fig. 14. Type 1 form prior to steel installation (20.625 in. width)

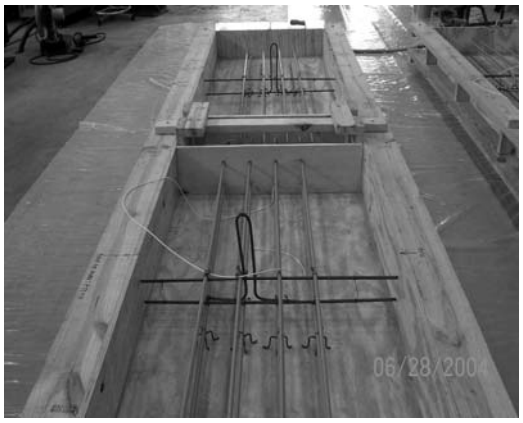

Fig. 15. Type 2 form after steel installation (34 in. width)

Before steel placement, rebar was instrumented with strain gages. Bar ridges were ground down to prepare the surface for gage installation, and gages were bonded to the prep site and sealed with an air-curing silicone rubber. After curing of the protective rubber coating, the reinforcing steel was installed into the forms. To allow for two separate pours, the rebar was passed through holes in a wood bulkhead so that only the specified steel was extending from the precast section into the closure pour as shown in Fig. 16 and Fig. 17.

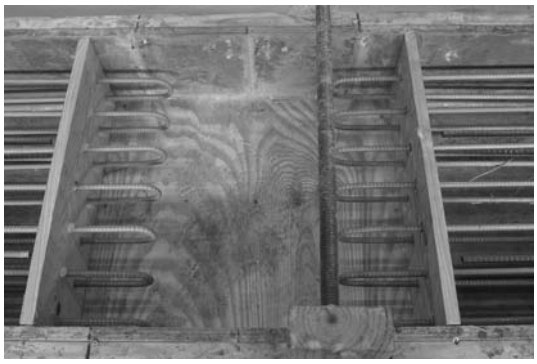

Fig. 16. Transverse closure pour section during steel installation

Fig. 17. Longitudinal closure pour section after steel installation

Once all steel was instrumented and tied into place, the concrete was placed. A vibrator was used to remove air voids and the concrete surface was smoothed out with hand trowels. Each precast section was cast simultaneously with a wood partition blocking out the closure pour section. Following 7-day compression cylinder tests that revealed strengths exceeding the specified 28-day concrete strength of 4000 psi, the bulkheads were removed and the closure pour concrete was placed. Fig. 18 shows a transverse specimen prior to casting of the closure pour section.

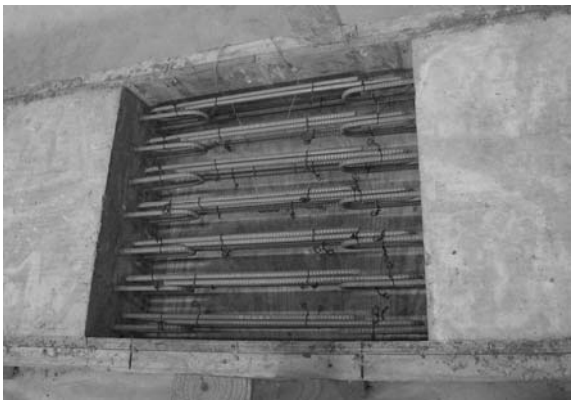

Fig. 18. Transverse specimen prior to placing of closure pour concrete

After 7 days, the closure pour concrete had surpassed the 28-day strength and forms were stripped in preparation for installation of concrete surface strain gages. These gages were designed to capture the surface strains at failure locations to compare with theory. To ensure proper adhesion of the gage to the concrete surface, the concrete was prepared by grinding it to a smooth finish. Next, a 5-minute epoxy was applied to the area to fill voids and allowed to dry overnight. Once cured, the epoxy was ground off leaving a void free concrete surface for good strain gage adhesion. When all surface gages were mounted to the specimen and epoxy had cured, the beam was moved to the testing area and lifted onto its support system and linear variable displacement transducers (LVDT) were installed.

Specimen Instrumentation

Steel Strain Gages

Multiple strain gages were affixed to reinforcing steel for data acquisition during testing. Vishay Micro-Measurements, 0.25 in. (6 mm) gage length strain gages (Type CEA-06-250UW-120) were used for the reinforcing steel strain readings in specimens L1 through L6. After these six specimens, strain gages were changed to Type FLA-6-11-1L manufactured by Tokyo Sokki Kenkyujo Company. Placement of the gages was based on the predicted beam failure location and areas of particular interest. As experimentation progressed, sites and numbers of strain gages were changed based on test results and observations. Chosen strain gage locations are discussed in the Experimental Results section.

Two epoxy glues were used during testing to affix strain gages to steel reinforcement. The first strain gage adhesive tried was RP-2 manufactured by Tokyo Sokki Kenkyujo Company. This epoxy was used on specimens L1 though L7 and T1 through T3. For the last seven specimens (T4, T5, T6, L8 – L11), Vishay Micro-Measurements M-Bond AE-10 strain gage adhesive was used.

Concrete Strain Gages

Gages mounted on the surface of the concrete specimens were 2.5 in. (60 mm) gage length, Type PL-60-11, manufactured by Tokyo Sokki Kenkyujo Company. This gage performed well during testing and was used on all beam specimens. Concrete strain gage locations will be discussed in the following section.

Linear Variable Displacement Transducer

One LVDT was attached to each side of each specimen to measure vertical deflections during testing. RDP Group, Type ACT1000A, LVDTs were used for all tests. The corresponding transducer amplifier was RDP Electronics, Ltd., Type S7AC and Model 8.

Specimen Testing

Transverse Closure Pour

All transverse specimens were loaded to failure under static negative flexural loading in a 4-pt bend test as shown in Fig. 19, creating a pure moment in the closure pour zone. Caner and Zia (1998), as well as FE analysis of typical bridges, indicated that both shear and axial forces in the closure pour region are small (Brush N.C., Sharpe, G.P., James, R., Jones, H. Unpublished document). Thus, a pure bending loading arrangement was used. Beam supports were placed flush with the interface of the closure pour and precast sections, at the location of girder end diaphragms in the bridge. Fig. 20 is a photograph of a transverse specimen during testing. One LVDT was placed on each side of the beam at the centerline of the closure pour to measure vertical beam deflection.

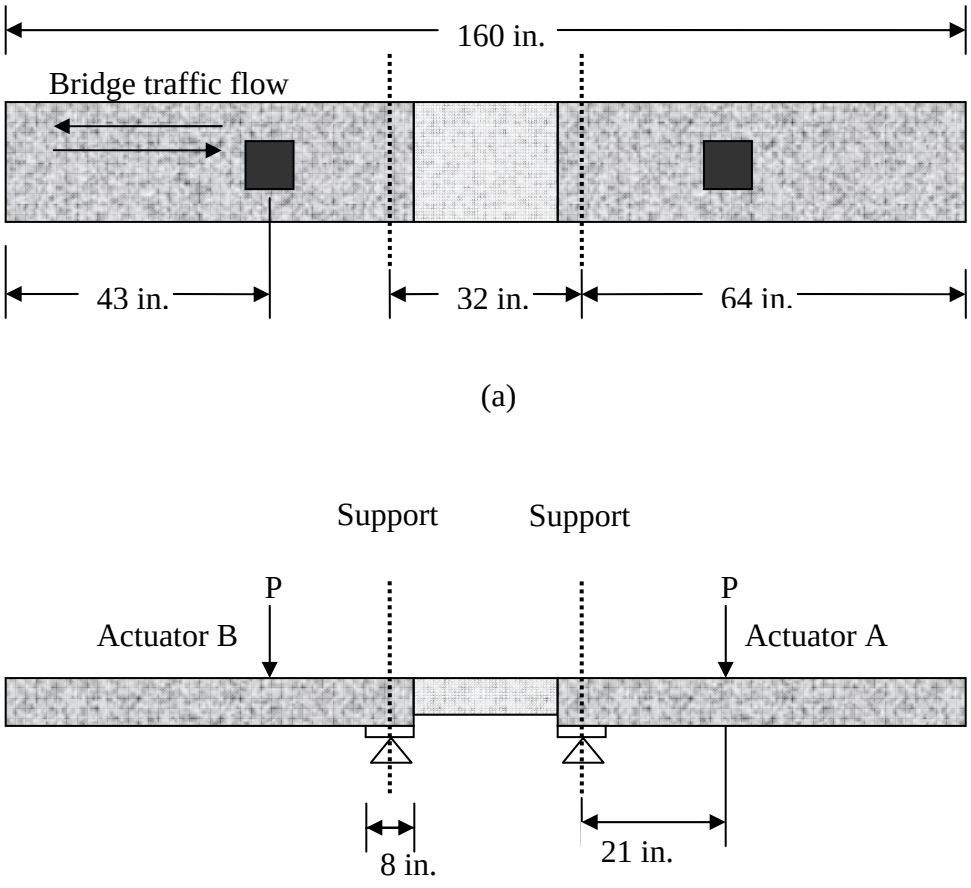

Fig. 19. Negative moment test setup for transverse specimens: (a) plan view; (b) elevation view

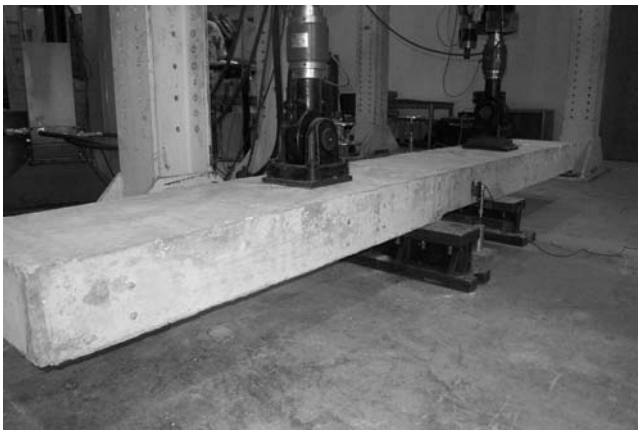

Fig. 20. Transverse specimen during testing

Negative flexure in the transverse closure pour produces topside cracks in the deck that could cause leakage problems at the joint. Therefore, cracks were visually monitored and measured during testing using rulers designed to measure crack widths.

Longitudinal Closure Pour

Longitudinal beams were tested to ultimate capacity under a static 3-point positive moment loading with the exception of L8 and L9 as discussed later. The two closure pour faces are labeled as joint 1 and joint 2 as shown in Fig. 21. Supports were offset to achieve both a moment and shear at joint 2 of the closure pour. Initially, a concentrated load was to be applied to the specimen inside the closure pour next to joint 2. With this scenario, the support setup yields the service moment-to-shear (M/V) ratio found in the congruent FE analysis (Brush N.C., Sharpe, G.P., James, R., Jones, H. Unpublished document). It was subsequently decided to reproduce a real tire patch to

better represent actual loadings. As discussed further in the results section, changes in M/V ratio due to support location movements was not significant to the resulting failure because joint 1 was the actual failure location, not joint 2.

Loading simulated an AASHTO HS-25 tire patch flush with joint 2 which was identified by the FE analysis as the controlling truck location. Maximum positive transverse moment in the longitudinal closure pour occurs when two HS-25 trucks are located at mid-span of the bridge on both sides of the interior closure pour. Laboratory testing simulated one of these trucks' wheel patch inline with closure pour joint 2 (see Fig. 21). AASHTO design gives the dimensions of the tire patch as 22 5/8 in. perpendicular to traffic flow and 9 in. parallel with traffic. The load distributor used during testing had dimensions of 22 in. by 9 in. and resulted in an actuator centerline 5 in. offset from the joint 1 face and 11 in. offset from joint 2. Throughout this report, the centerline of the load will be represented in graphics as a solid 5-point star. Fig. 22 is a photograph of the longitudinal loading setup.

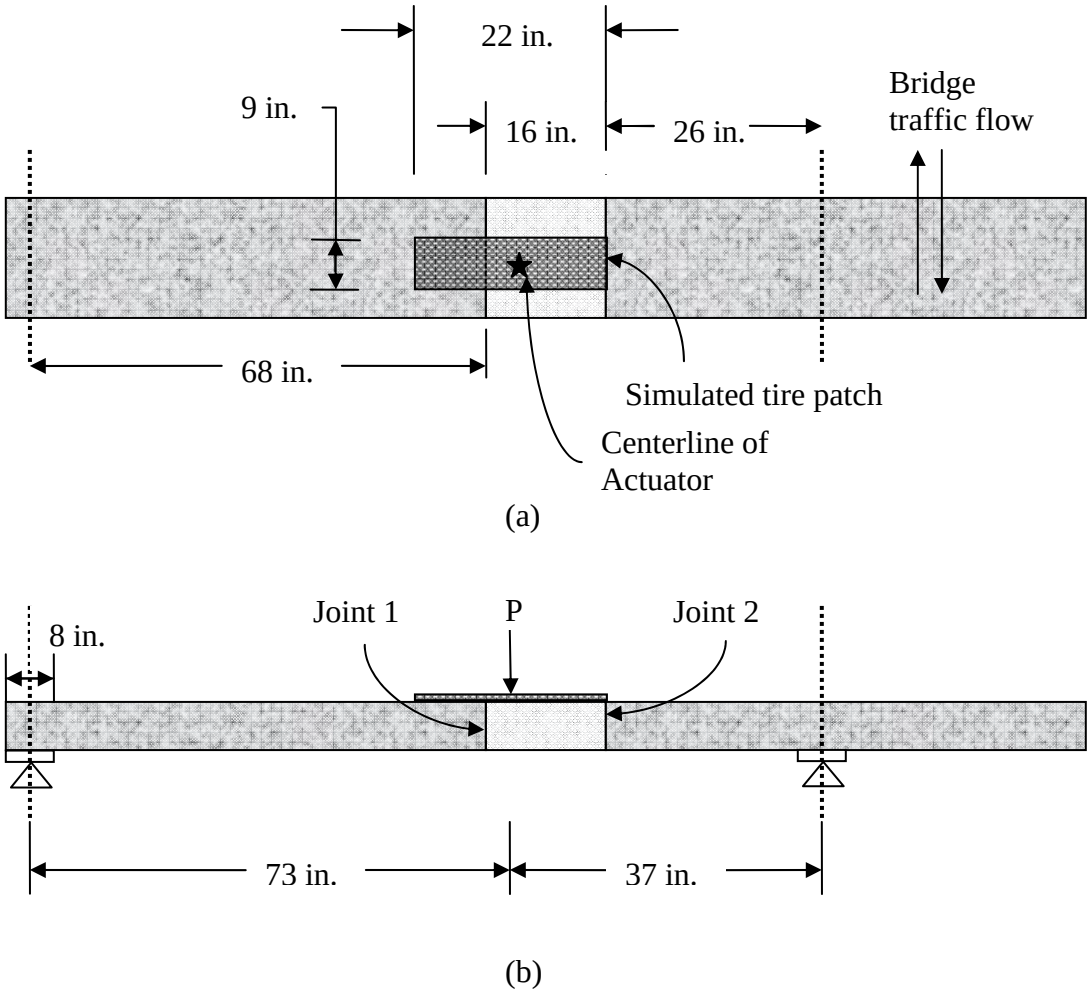

Fig. 21. Positive moment test setup for longitudinal specimens: (a) plan view; (b) elevation view

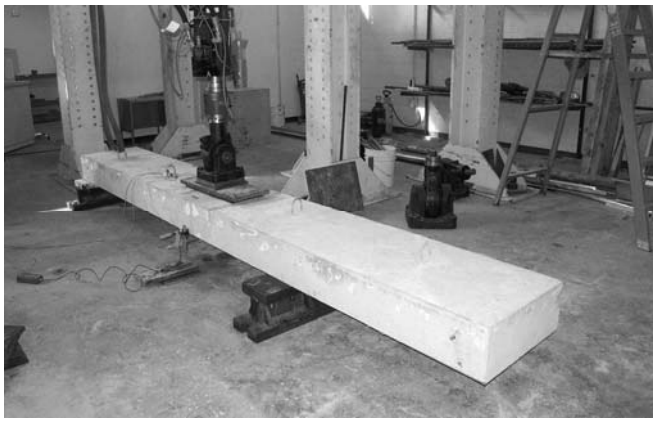

Fig. 22. Longitudinal specimen during testing

Specimen L8 and L9 were loaded differently. As determined by a FE model, one truck location pattern produced a small negative moment in the closure pour (Brush N.C., Sharpe, G.P., James, R., Jones, H. Unpublished document). Therefore, specimen L8 was initially loaded in negative flexure to the calculated FE model service load moment to determine if cracking would occur at the closure pour. The beam was then reloaded in the typical positive moment to failure. The negative moment test setup for L8 is identical to the transverse specimen test illustrated earlier and shown in Fig. 19. L9 was tested with pure flexure in the closure pour using the support setup shown in Fig. 23. This loading was chosen to determine the flexural capacity without shear in the joint. A photograph of the L9 testing is provided in Fig. 24.

Supports for L10 and L11 were in slightly different locations than for L1 – L7 due to the increased specimen length from 160 in. to 168 in. The loading setup variations for Type 2 beams are given in Appendix F, Fig. 78 and Fig. 79.

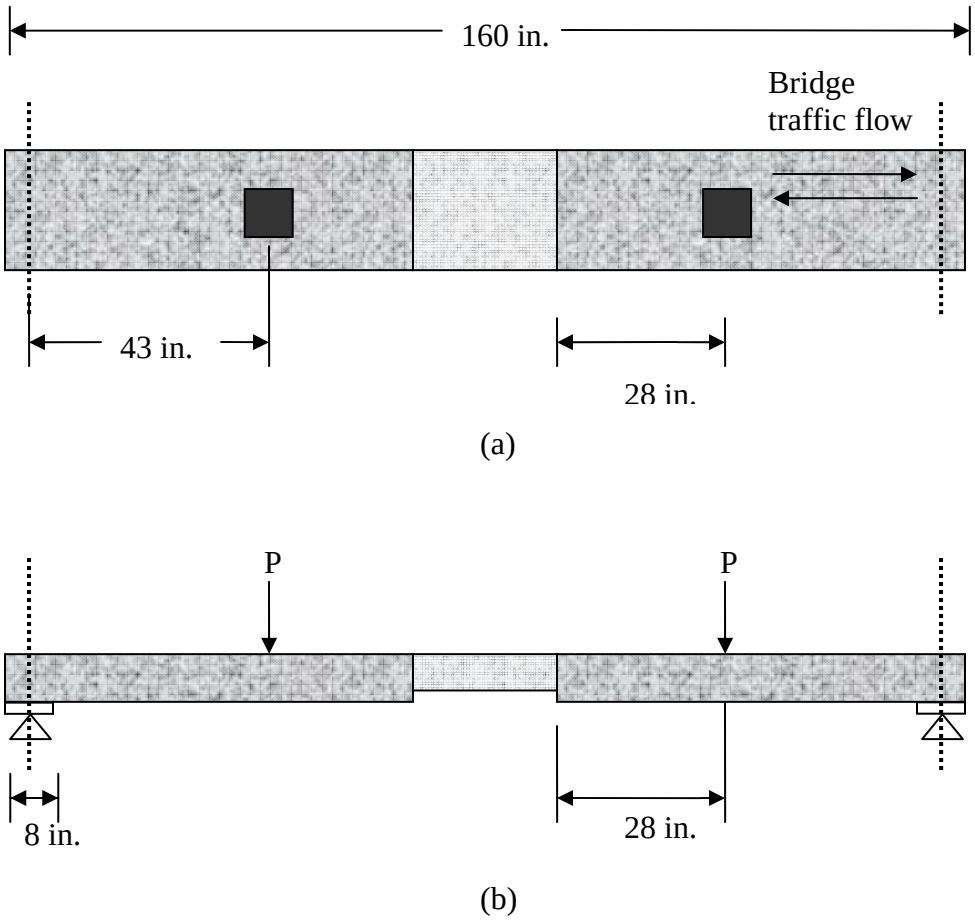

Fig. 23. Pure positive flexure test setup for longitudinal specimen L9: (a) plan view; (b) elevation view

Fig. 24. L9 during testing setup preparation

Specimen Concrete

TXDOT Class S Concrete

Specified concrete was TxDOT Class S, which is generally used for bridge decks, topping slabs, and bridge superstructures. Both the precast and closure pour segments of the beams were poured with Class S concrete. Details of the concrete mix are given in Table 4.

Compression Cylinders

To establish the progress of curing concrete and the strength of beams during testing, multiple compression cylinders were molded with each pour. ASTM C 39/C 39M – 99 was followed in the casting and testing of the cylinders throughout experimentation. Cylinders had a nominal radius of 6 in. and nominal height of 12 in. Length measurements were repeated 4 times along different quadrants of the cross-

section, and the diameter was measured twice with perpendicular lines on the circular cross-section at both the top and bottom of the cylinder. All tested specimens were within ASTM tolerances.

Concrete compression cylinders were tested at 7 days to ensure that 70% of the specified minimum strength (2800 psi) had been reached following guidelines from TxDOT Item 421.9. At 7 days, every cylinder tested above the 28-day compressive strength requirement. Appendix C provides the details of each concrete pour, including 7-day cylinder strengths and concrete strength at testing.

Table 4. TxDOT Class S Concrete Specifications

Cement per C.Y. Minimum. (sacks)	6.5
Minimum Compressive Strength (f'c) 28 day (psi)	4000
Minimum Flexural Strength 7 day (psi)	570
Maximum Water Cement Ratio (Gal/sack)	5.0
Coarse Aggregate Grade (No.)	2-3-4-5
Desired Slump (in.)	3
Maximum Slump (in.)	4

Testing Machinery

All tests were run with MTS machines. One or two 50 k hydraulic actuators, Model 204.71, were used to apply load to each specimen. These actuators had a 6 in. total stroke. The load cell used in conjunction with the actuators was a 55 k capacity MTS, Model 661.23A-01, load cell. Actuators were driven with a MTS 410

Digital Function Generator and a MTS 464 Data Display was used to monitor applied loads. Fig. 25 is a photograph of the function generator. Fig. 26 is a photograph of the 500 k MTS Model 311.41 machine used in. compression cylinder testing. The actuator has a 6 in. total stroke.

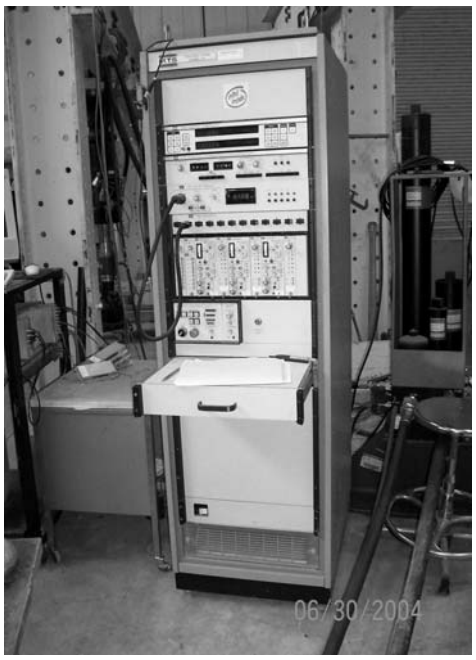

Fig. 25. MTS Digital Function Generator and Data Display

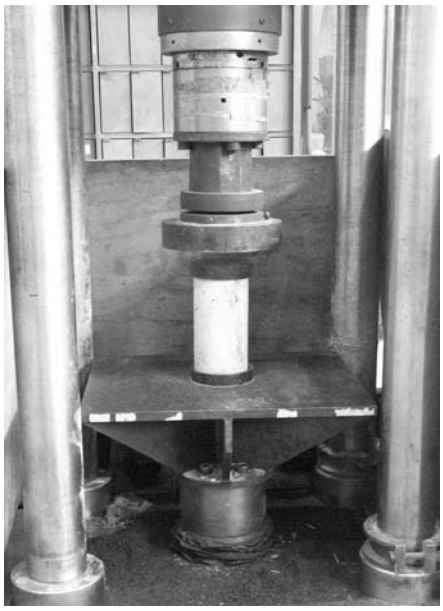

Fig. 26. MTS load frame for compression cylinder tests

Graphic Data Acquisition

Video and photography was utilized for observations following testing. Two video cameras were placed approximately 3 feet from the closure pour to capture crack propagation and beam failure. Digital photos were taken throughout testing to document beam behavior, cracks, and to photograph pertinent reference items, such as gage locations, rebar orientation, and support setups.

EXPERIMENTAL RESULTS

Overview

Data was analyzed during and after beam testing, including strain in the concrete and reinforcing, percentage of theoretical moment capacity reached, and cracking and failure patterns. Strain values were compared between specimens and to theory and based on the acquired strains, a better understanding of the mechanisms occurring during failure was reached. Evaluation of the measured capacity versus theory determines the effects of closure pour presence. Failure patterns and crack monitoring aid in identification of limiting attributes of the proposed design.

Reinforcing Steel Yield Strength

Yield strength of the reinforcing in L1 – L7 was tested with a MTS Axial Precision load frame (Model 312.31S) and ASTM standard clip gage extensometer. Based on the results of these test, L1 – L7 was determined to have 72 ksi yield strength as shown in Fig. 27. All other specimens' reinforcing was not tested but was assumed to be 72 ksi in calculations. The corresponding yield strain for 72 ksi steel is approximately 2500 microstrain.

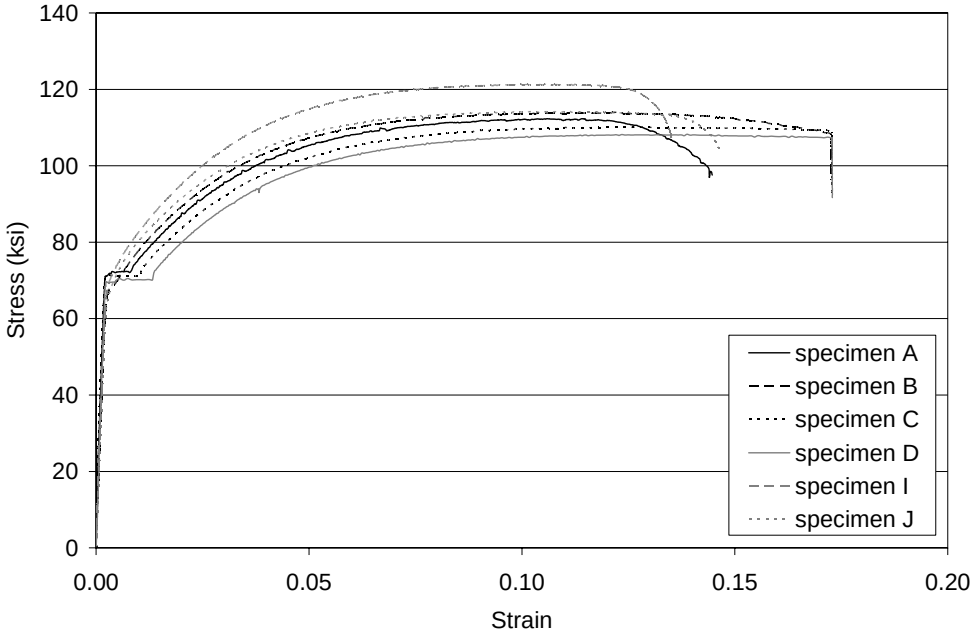

Fig. 27. Yielding strength for reinforcing steel in L1 – L7

Theoretical Beam Capacity

Measured beam capacity was compared to theoretical nominal flexural strength using a basic reinforced concrete approach. Assumptions included the following:

1. Concrete in the tension zone was neglected and the tension steel was assumed to take the total tensile force.
2. A linear strain distribution based on Bernoulli's "plane sections remain plane" hypothesis was used.
3. The concrete compressive stress distribution was idealized by the Whitney stress block.

4. Strain in the rebar and surrounding concrete was assumed to be the same value.
5. The theoretical maximum compressive concrete strain was 3000 microstrain.

Equilibrium of the beam section is satisfied by equating the horizontal compressive and tensile forces in the concrete and steel and by forcing the internal bending moment to zero. Results from one sample beam capacity calculation are provided in Appendix B.

Theoretical Beam Cracking

The tested cracking load was compared to theoretical cracking based on a transformed gross moment of inertia. The center-of-gravity axis was obtained using the first moment of area equation and taking the moment about the extreme top section fiber. The resulting equation for the center of gravity is

$$\bar{y} = \frac{(\frac{bh^2}{2}) + (n-1)A_s d}{bh + (n-1)A_s} \quad (1)$$

$$n = \frac{E_s}{E_c} \quad (2)$$

in which b = section width; h = section height; n = modular ratio; A_s = area of steel; and E_s and E_s = steel and concrete modulus of elasticity. The transformed section is

$$I_{gt} = I_g + \sum d^2 A \quad (3)$$

where I_g = gross moment of inertia; d = distance to section from axis of rotation; and A = section area. For an elastic and homogeneous member, the classical flexural equation for stress is designated by

$$\sigma = \frac{M\overline{y}}{I} \tag{4}$$

By substituting cracked properties and rearranging, the cracking moment was calculated by

$$M_{cr} = \frac{f_r I_{gt}}{\bar{y}} \tag{5}$$

$$f_r = 7.5\sqrt{f'_c\ (psi)} \tag{6}$$

where f_r = concrete modulus of rupture (psi). The rupture stress was used because the initiation of cracking begins when the concrete reaches this stress value. The resulting cracking moment is theoretically when cracking will initiate in tested specimens. This value was compared against observed cracking in beams and is discussed further in the following sections.

Transverse Specimen Data Results

Transverse Specimen Strain Gage Locations

All six transverse specimens were equipped with rebar and concrete surface strain gages, and Appendix A gives the gage positions for each beam. Concrete gages were placed in multiple positions around the closure pour and varied between specimens.

A grid of three transverse locations (1, 2, or 3) and five longitudinal positions (a, b, c, d, and e), depicted in Fig. 28, make up the possible concrete strain gage positions.

The intersection of two gridlines designates the gage label and the centerline of the gage. Longitudinal positions ‘a’ and ‘e’ represent gages flush with the closure pour construction joint and extending into the closure pour. Transverse position 1 and 3 are 3 in. from the beam edge. Position 2 and ‘c’ are along two of the closure pour centerlines. Gage labeling consists of the letter C, for concrete gage, followed by the transverse and longitudinal position number. Hence, a gage on the centerline of the closure pour, in both directions, would be identified as gage C2c.

Six longitudinal positions, placed on the innermost rebar, were chosen for the reinforcing steel gages as shown in Fig. 29. Steel gages are labeled with an R prefix and the position number. Observations and results will refer to this labeling system. Individual specimen gage locations are provided in Appendix A and Table 5 lists working gages for each transverse specimen.

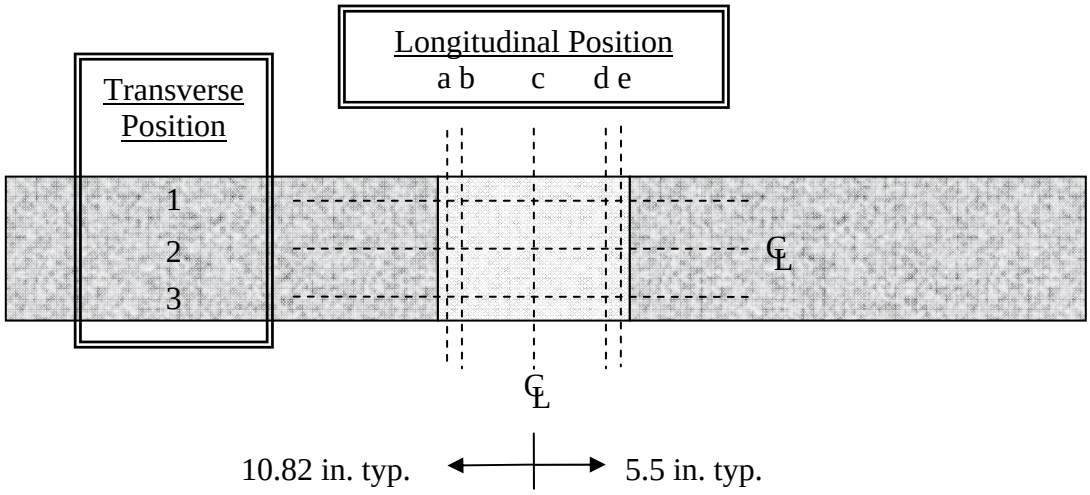

Fig. 28. Position labels for concrete strain gages on transverse specimens

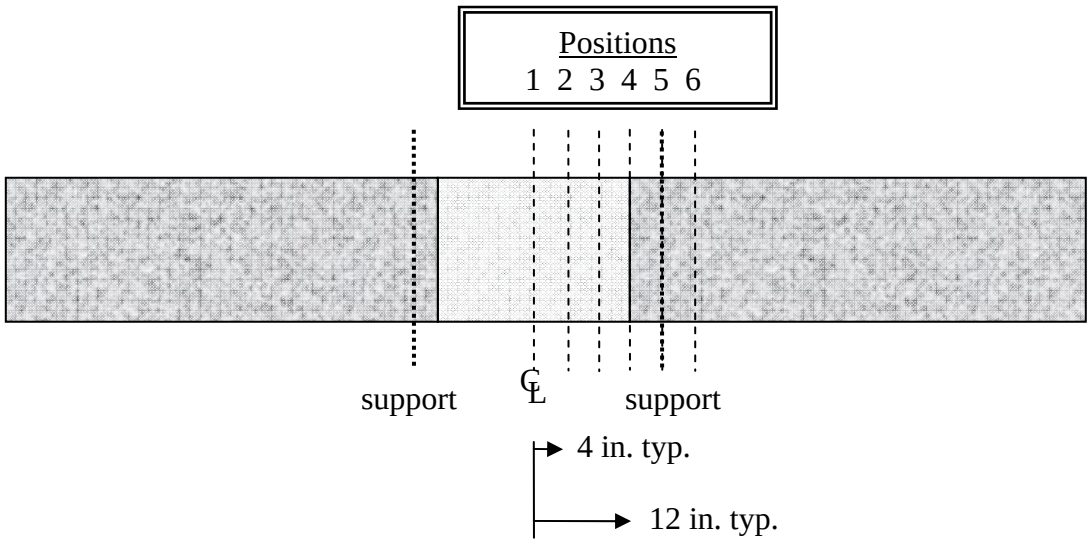

Fig. 29. Position labels for rebar strain gages on transverse specimens

Table 5. Valid Steel Strain Gages for Transverse Specimens

Specimen Label	Strain Gage Location					
	1	2	3	4	5	6
T1	x	x	x			x
T2	x	x	x	x		x
T3	x	x	x	x	x	x
T4			x	x		x
T5		x	x		x	x
T6	x	x	x	x		

x denotes valid strain gage data for this position

Measured Concrete Properties

Following the completion of each beam test, four compression cylinders were tested to determine the specimen's concrete strength during testing. Two specimens from the precast section and two from the closure pour batch were tested and then averaged to determine the compressive strengths to be used in calculations. Calculated strengths for the transverse specimens are provided in Table 6. Individual cylinder strengths are given in Appendix C, Table 15. T6 was monolithic so it does not have data on closure pour concrete strength.

Table 6. Transverse Beam Concrete Strengths

Specimen Label	Precast Concrete Strength[1] (psi)	Closure Pour Concrete Strength[1] (psi)
T1	9316	6099
T2	8964	5791
T3	4685	6580
T4	4823	6512
T5	4870	6625
T6	6475	N/A

[1]strength determined the day of testing

Data Analysis

Documentation of transverse testing included flexural capacity, strain readings, vertical deflections, and crack patterns and growth. Measured strengths for transverse specimens are given in Table 7 and theoretical capacities are provided in Table 8. Theoretical strengths were determined from the compressive strengths in Table 6. Fig. 30 graphically represents the difference between theory and tested strengths. Based on the locations of the failure described later in this section, the amount of steel reinforcing used in capacity calculations was based on the seven bars that pass through the closure pour cold joints labeled in Fig. 7 as Bar F.

Table 7. Tested Failure Load and Moment for Transverse Specimens

Specimen Label	Failure Load (kip)	Failure Moment[1] (k-in)	Failure Moment per unit width (k-in)
T1	12.8	269	13.1
T2	12.4	259	12.6
T3	13.7	287	13.9
T4	14.4	302	14.6
T5	14.0	293	14.2
T6	12.6	301	14.6

[1]Bending moment at section where flexural failure occurred

Table 8. Theoretical Capacity and Failure Load for Transverse Specimens

Specimen Label	Moment Capacity (k-in)	Moment Capacity per unit width (k-in/in)	Theoretical Failure Load (kip)
T1	314	15.2	15.0
T2	310	15.0	14.8
T3	321	15.6	15.3
T4	320	15.5	15.2
T5	322	15.6	15.3
T6	320	15.5	15.2

T1 – T5 averaged 89% of theoretical capacity, and the monolithic control specimen, T6, reached 94% of calculated strength. Longitudinal specimens (discussed in the next section) showed this same low capacity trend, and based on the findings from the longitudinal specimens, the decreased capacities in the transverse specimens are attributed to edge effects and inadequate rebar confinement from side cover. No transverse specimens were tested to confirm this assumption.

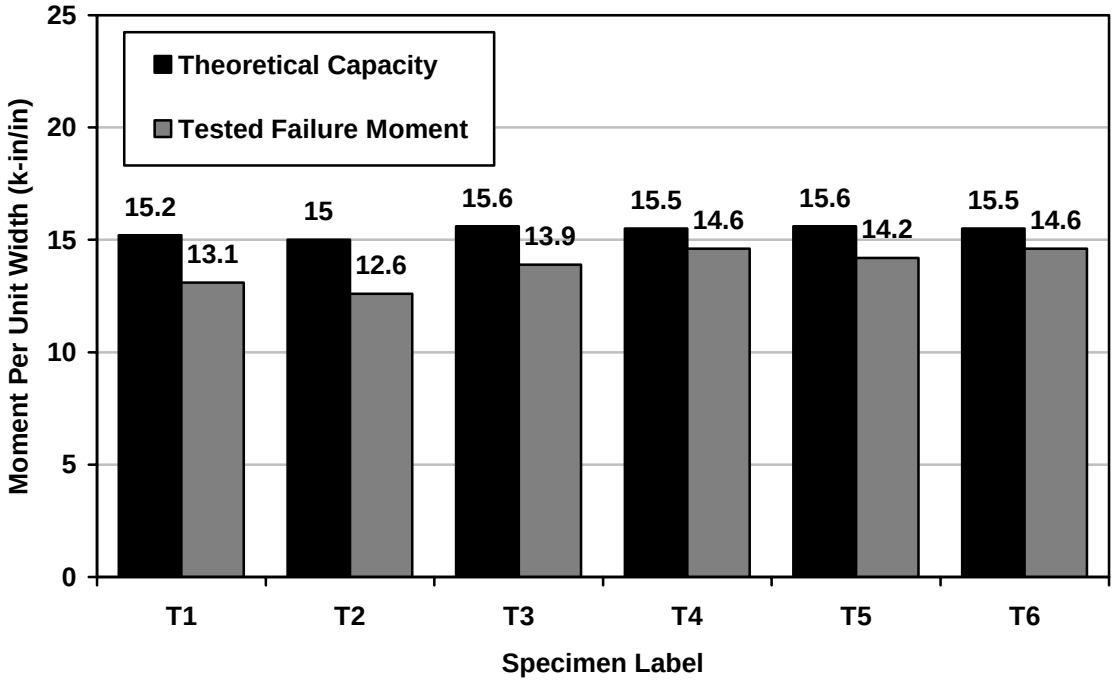

Fig. 30. Theoretical and tested moment capacity obtained in specimen T1 – T6

Failure patterns were typically the same for all specimens. Closure pour construction joints were the first to begin cracking and then either one or two cracks in the closure pour would initiate. Fig. 31 shows the average locations of these two crack patterns. Either one crack formed around the centerline of the closure pour (crack a in Fig. 31) or two formed near the quarter points (crack b in Fig. 31). These cracks are normal flexural cracks and do not cause failure in the beam. Immediately preceding failure, another crack forms approximately 4.5 in. away from the closure pour face and causes failure. T3, T4, and T5 failed at the crack denoted “Failure crack 1” in Fig. 31,

and T1, T2, and T9 failed on the opposite side of the closure pour, at the location labeled "Failure crack 2" in Fig. 31. The control specimen, T6, failed from a flexural crack located approximately 9 in. offset from the beam centerline.

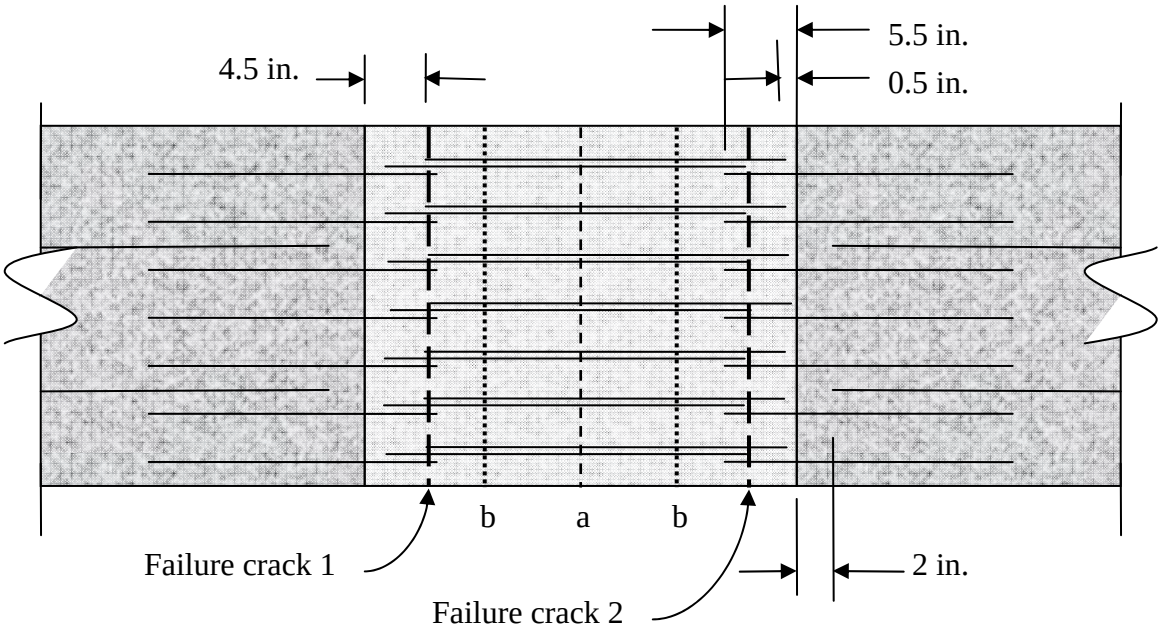

Fig. 31. Typical crack locations for transverse specimens

Closure pour joint cracks grew to approximately 0.035 in. prior to failure, and the cracks in the closure pour that did not cause failure reached roughly 0.02 in. as shown in Fig. 32 though Fig. 37. Theoretical cracking for T1 – T6 was calculated as approximately 5.6 k. Cracks at the two cold joints began cracking almost immediately (0 – 1 k) while the closure pour flexural cracks formed around 2 – 4 k.

There is a constant moment across the closure pour and failure was expected at the joint face due to the reduced steel at that locations (see Fig. 7). However, the failure crack occurs at a site of rebar discontinuity where there is more reinforcing than at the closure pour face. One of the hairpins (bar P in Fig. 7) ends 4.5 in. inside the closure pour joint at the same location of the typical failure crack. It is believed that the hairpins that are solely inside the closure pour produce a prying action which ultimately causes the sudden crack and failure. Transverse reinforcing was not installed in these specimens and, if present, may have reduced this phenomenon and improved the closure pour capacity.

Steel strain gages did not consistently give valid data due to multiple gage failures. For this reason, it was not possible to determine the strain profile and corresponding behavior in the transverse closure pour. Graphs of the strain readings are provided in Appendix D, Fig. 65 through Fig. 69.

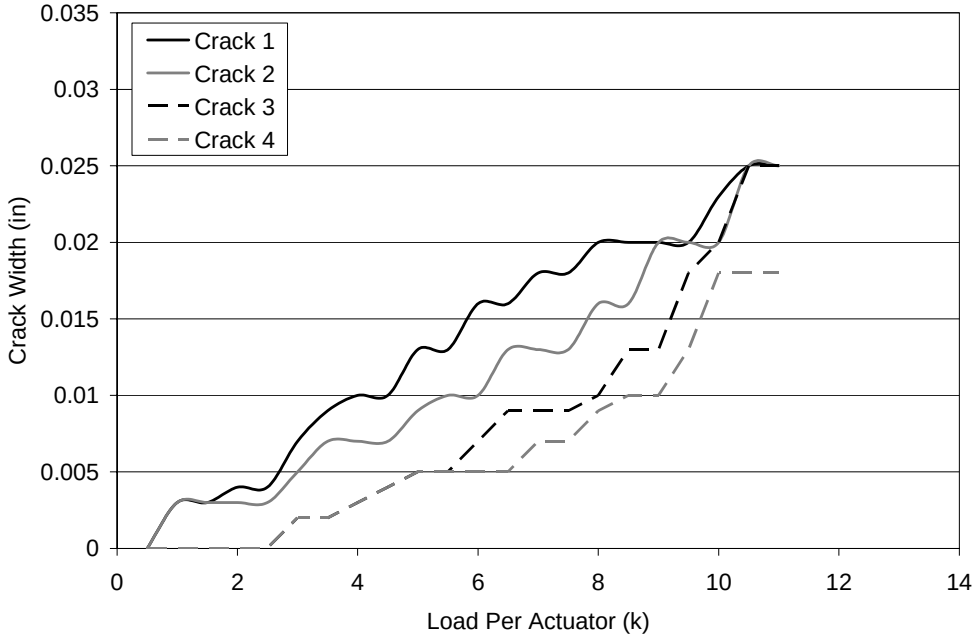

Fig. 32. Measured crack widths in T3

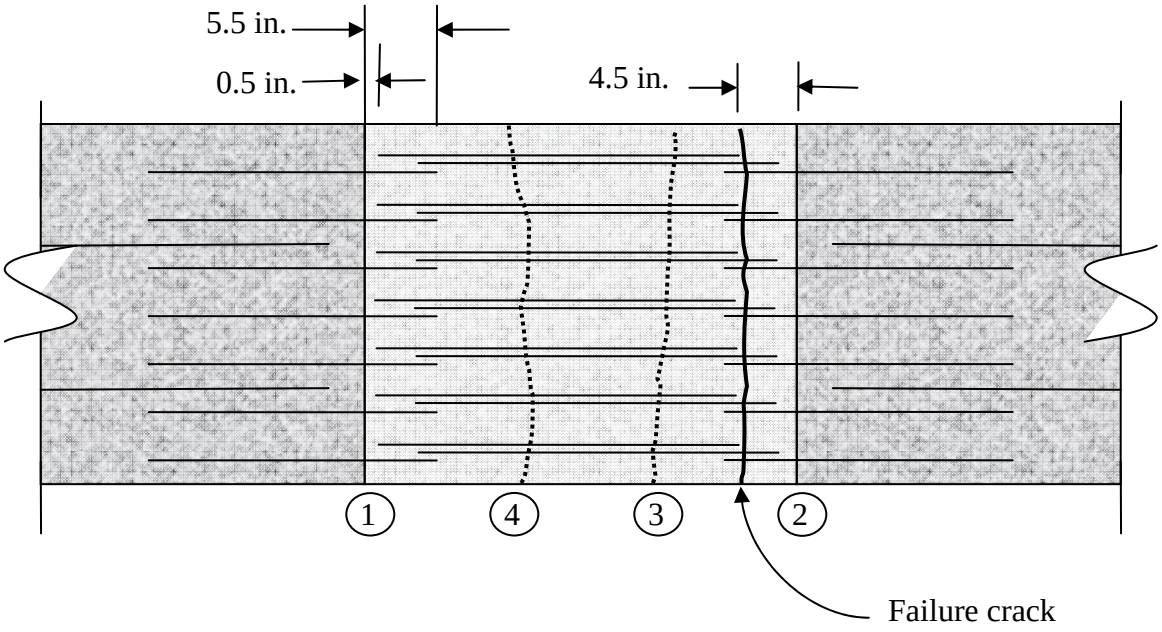

Fig. 33. T3 closure pour cracks

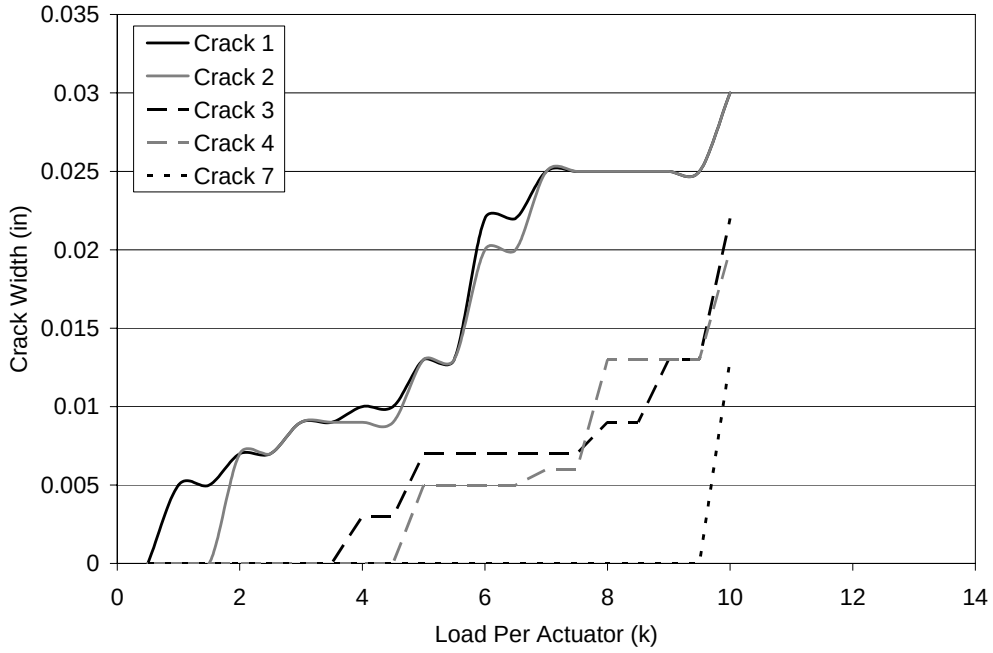

Fig. 34. Measured crack widths in T4

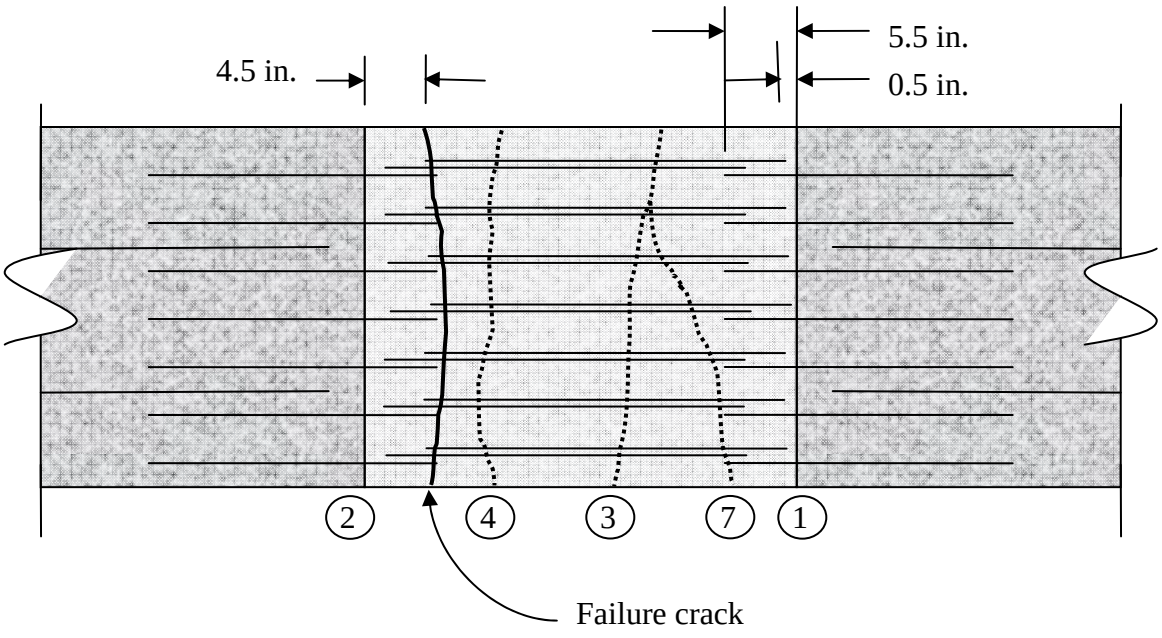

Fig. 35. T4 closure pour cracks

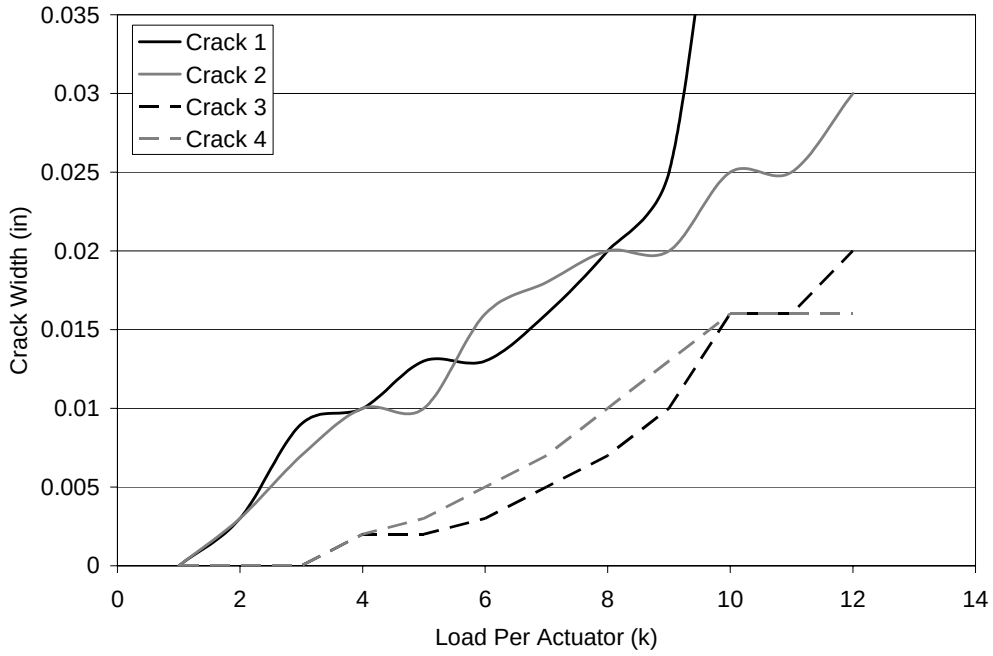

Fig. 36. Measured crack widths in T5

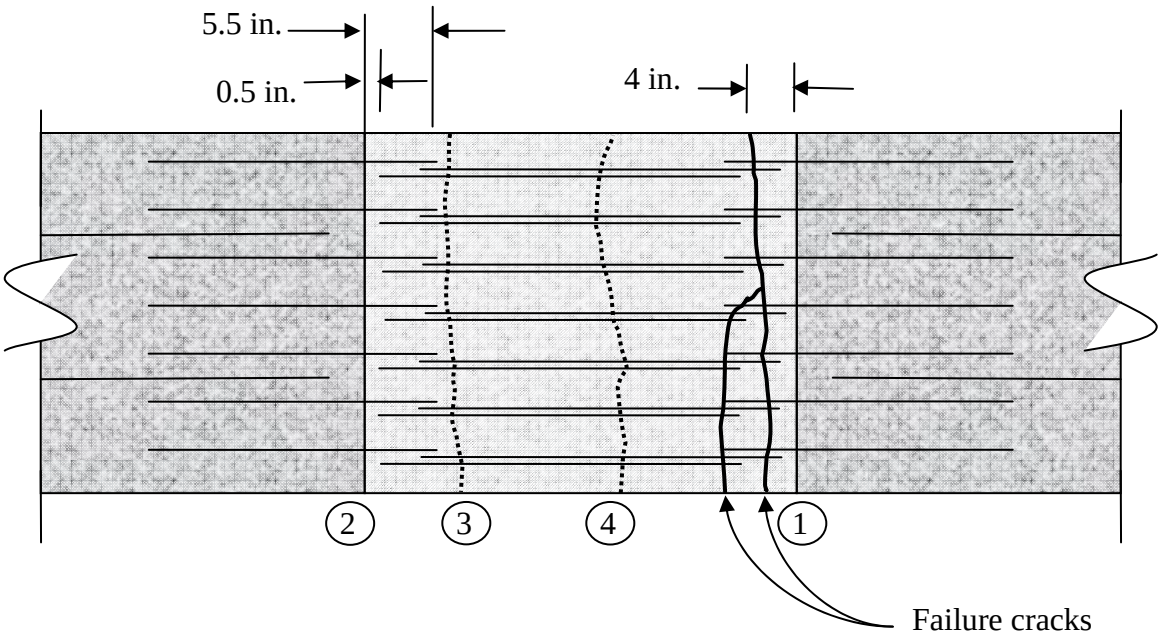

Fig. 37. T5 closure pour cracks

Longitudinal Specimen Data Results

Longitudinal Specimen Type 1 Strain Gage Locations

Longitudinal specimens were instrumented with strain gages at locations which varied slightly throughout the project. Fig. 38 and Fig. 39 give the position labeling system for concrete and reinforcing steel gages, respectively. Results and prepared data refer to these labeling systems.

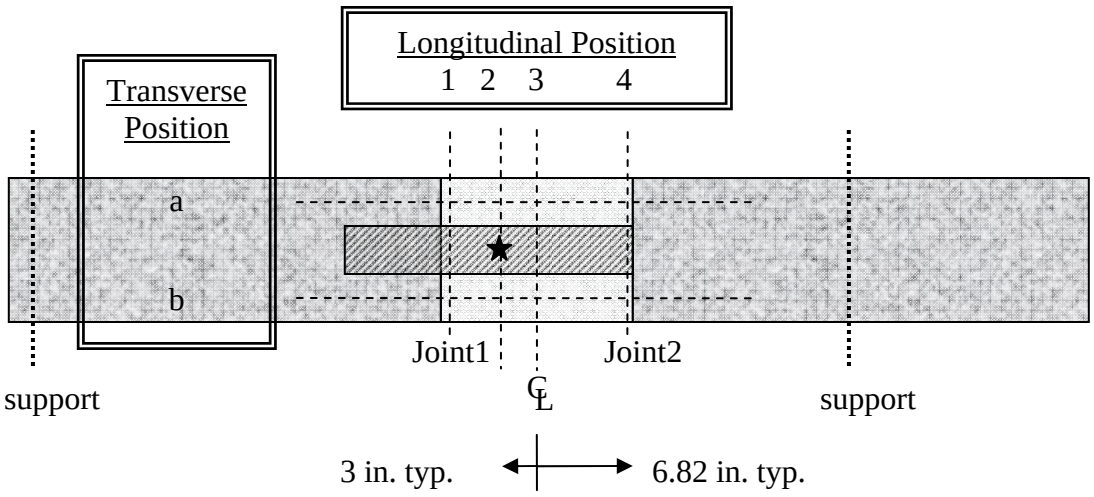

Fig. 38. Type 1 and Type 2 position labels for concrete strain gages

Four longitudinal (1, 2, 3, and 4) and two transverse (a and b) positions were used for concrete surface gages. Longitudinal positions are located at joint 1, the actuator centerline, closure pour centerline, and joint 2. Both transverse positions are 3 in. from the edge of the beam and 2.8 in. from the side of the load pad. Labeling of these gages consists of the letter C denoting a concrete gage followed by two characters

that represent the longitudinal and transverse location. For example, a C2b gage is located at the intersection of the longitudinal position 2 and transverse position ‘b’. C2b is inline with the actuator centerline and 3 in. from the edge of the beam.

Concrete surface gages on Type 1 beams were located at the centerline of the tire patch (position 2 in Fig. 38) except for L1, L8, and L9. Concrete strain gages in L1 were adhered incorrectly at 1 in. off from the actuator centerline and are 4 in. (instead of 5 in.) from the joint 1 face as depicted in Fig. 56. L8 and L9 gages were placed on one side of the tire patch and located at position 1 and 4 as shown in Fig. 61 and Fig. 62.

Nine longitudinal rebar strain gage positions for Type 1 beams (L1 – L9) are shown in Fig. 39. Strain gages are designated by the prefix R for rebar and the position number given in Fig. 39. Hence, R7 is a rebar strain gage at position 7 which is located at joint 2. Position 3 and 7 represent gages installed flush with the closure pour cold joint and extending away from the closure pour. A few beams were instrumented with gages at all locations shown, although most had gages at only some of the sites. The gage locations are the same for all beams except as noted in Fig. 56 through Fig. 62. Due to multiple factors, some strain gages did not work properly during testing. Functioning gage positions for each longitudinal beam are given in Table 9.

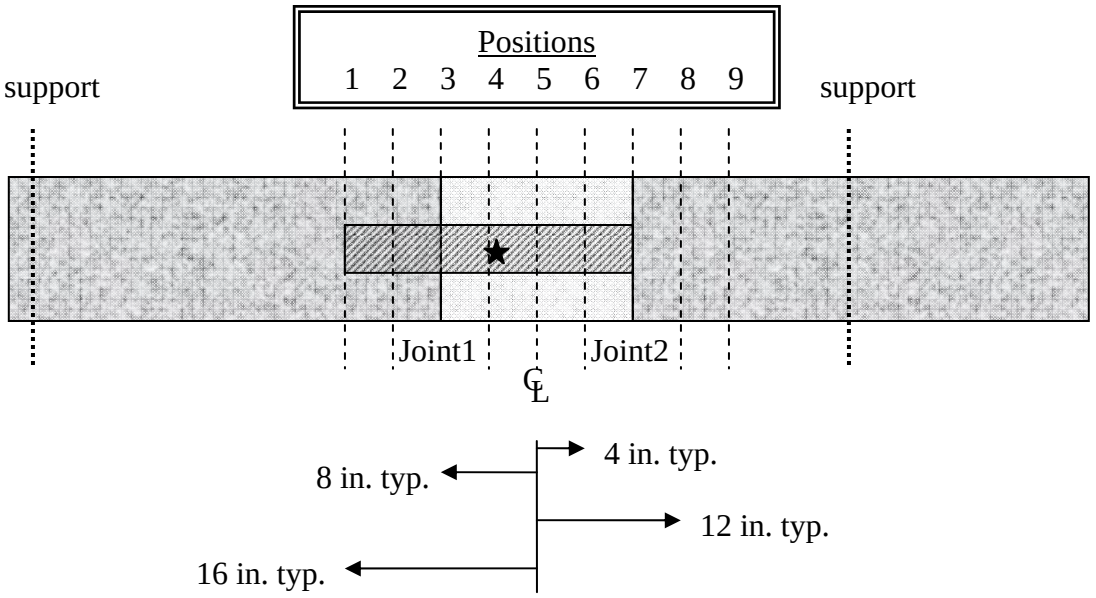

Fig. 39. Type 1 position labels for rebar strain gages

Table 9. Valid Steel Strain Gages for Longitudinal Specimens

Specimen Label	Strain Gage Location								
	1	2	3	4	5	6	7	8	9
L1									
L2						x		x	
L3						x			
L4					x	x	x	x	x
L5					x	x	x	x	x
L6					x	x	x	x	x
L7					x	x	x	x	
L8	x	x	x		x				
L9	x	x	x	x	x	x	x	x	x
L10		x	x	x	x		x	x	
L11		x	x	x	x	x	x	x	

x denotes valid strain gage data for this position

Longitudinal Specimen Type 2 Strain Gage Locations

The rebar in Type 2 longitudinal specimens were instrumented extensively with strain gages in an attempt to better characterize behavior and to ensure a constant strain across the beam width during loading. The labeling system is shown in Fig. 40. Longitudinal positions are the same as Type 1 specimens except position 1 and 9 are removed. Rebar passing through joint 1 is lettered ‘a’ through ‘d’ and rebar passing through joint 2 is lettered ‘e’ through ‘h’. Labels include the prefix R for rebar gage, the longitudinal location, and the bar name. For instance, R5c is at position 5 on the closure pour centerline and adhered to rebar ‘c’ which passes through joint 1. Concrete surface gages use the numbering system described for Type 1 beams and shown in Fig. 38.

Measured Concrete Properties

Concrete compressive strength was determined by averaging the strengths of two concrete cylinders for each concrete pour. Computed strengths are provided in Table 10. Table 18 in Appendix C gives individual cylinder strengths.

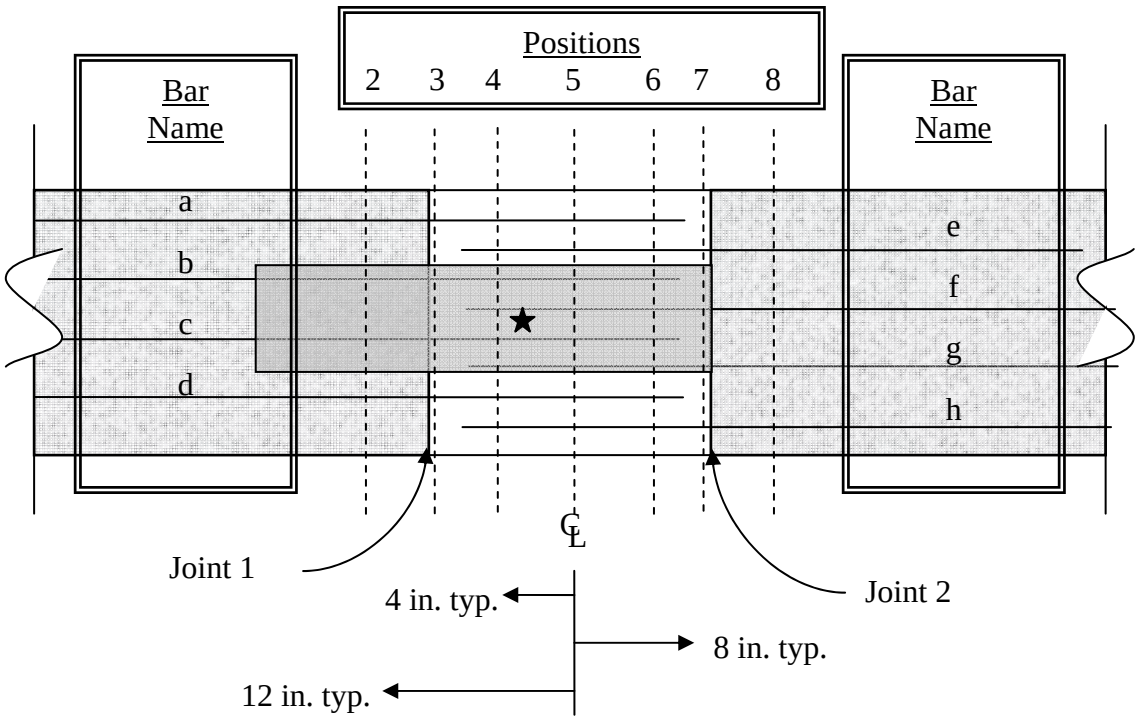

Fig. 40. Type 2 position labels for rebar strain gages

Table 10. Longitudinal Beam Concrete Strengths for L8 – L11

Specimen Label	Precast Concrete Strength[1] (psi)	Closure Pour Concrete Strength[1] (psi)
L8	6827	5780
L9	7150	5990
L10	6646	5486
L11	6456	4974

[1]strength determined the day of testing

Data Analysis

Specimens L1 – L7

The first seven longitudinal specimens were constructed with No. 5 bars and testing data for L1 – L7 is provided in Appendix E. No. 4 bars were used for specimens L8 – L11 and are discussed in the next section.

L1 – L3 used epoxy-coated reinforcing bars. L4 – L7 had uncoated bars to determine if epoxy-coated rebar had any adverse effects on the performance of the joint. No identifiable differences in performance were observed between specimens with coated and uncoated rebar.

Due to a tested moment capacity less than theory in the first three specimens, L5 was cast monolithically without a closure pour and the same rebar as other specimens to determine if the presence of the closure pour construction joint or the rebar detailing was the primary cause of the observed failure pattern. Fig. 41 is a photograph of specimen L1 which had a closure pour section. The two main failures occurred at the closure pour joint and a few inches inside the joint at the location of rebar discontinuity (see Fig. 11). Fig. 42 is a photograph of monolithic (no closure pour) specimen L5 which cracked in nearly the same manner as L1 except that the cracking was cleaner and more distinctly followed the orientation of the outermost rebar hoop. From this test, it was concluded that the controlling factor in the failure pattern is the reinforcing steel discontinuity location.

Although large cracks formed at both joint 1 and 2, actual failure took place at joint 1 in every beam. This was determined from the location of concrete crushing, a beam hinge observed at joint 1, and the concrete strain readings.

Fig. 41. Failure pattern of L1 with closure pour

Fig. 42. Failure pattern of monolithic specimen L5

In theoretical flexural capacity calculation, it was assumed that a maximum compressive strain of 3000 microstrain is produced at the extreme compression fiber. Therefore, strain values of 3000 microstrain are expected at the location of failure. Concrete strains did not reach 3000 microstrain in specimens L1 – L7 as shown in Fig. 76 and Fig. 77. However, gages were located at the centerline of the load pad, while the failure location was closer to the closure pour cold joints. In L8 – L11, gages were placed at the failure location to determine the correct strain in the concrete at failure and the findings are discussed in the next section. Concrete surface strains below 3000 microstrain may indicate more complex failure mechanisms than accounted for in the utilized reinforced concrete theory.

Edge effects were observed in L1 – L7 and contributed to the premature failure of the specimens with regard to calculated moment capacities. Edge effects are here defined as the outermost rebar pulling away from the section, aggravating cracking, and helping to initiate failure as the crack moves around the 180 degree bend in the bar. Since specimen beam strips were taken from the interior of the bridge and actually have concrete on both sides strip, this could not happen in an actual bridge. L10 – L11 were constructed with a larger concrete side cover in an attempt to reduce these test effects.

Specimens L8 – L11

L8 – L11 were fabricated with No. 4 bars and are the basis for determination of the adequacy of the longitudinal closure pour design. Tested failure loads and moments are given in Table 11 and Table 13, and corresponding beam capacities are provided in

Table 12 and Table 14. Capacities were determined from the compressive strengths provided in Table 10. Fig. 43 compares the experimental versus theoretical capacity for L8 – L11.

Table 11. Tested Failure Load and Moment for L8 and L9

Specimen Label	Failure Load (kip)	Failure Moment at Joint 1 (k-in)	Failure Moment per unit width at Joint 1 (k-in)
L8	20.6	451	21.9
L9[1]	9.0	360	17.5

[1]L9 was loaded in pure flexure

Table 12. Theoretical Capacity and Failure Load for L8-L9

Specimen Label	Moment Capacity (k-in)	Moment Capacity per unit width (k-in/in)	Failure Load to Cause Failure at Joint 1 (kip)
L8	474	23.0	21.7
L9[1]	476	23.1	11.9

[1]L9 was loaded in pure flexure

Table 13. Tested Failure Load and Moment for L10 – L11 (extended width)

Specimen Label	Failure Load (kip)	Failure Moment at Joint 1 (k-in)	Failure Moment per unit width at Joint 1 (k-in)
L10	24.1	583	17.2
L11	24.2	546	16.1

Table 14. Theoretical Capacity and Failure Load for L10 – L11 (extended width)

Specimen Label	Moment Capacity (k-in)	Moment Capacity per unit width (k-in/in)	Failure Load to Cause Failure at Joint 1 (kip)
L10	496	14.6	20.5
L11	493	14.5	21.8

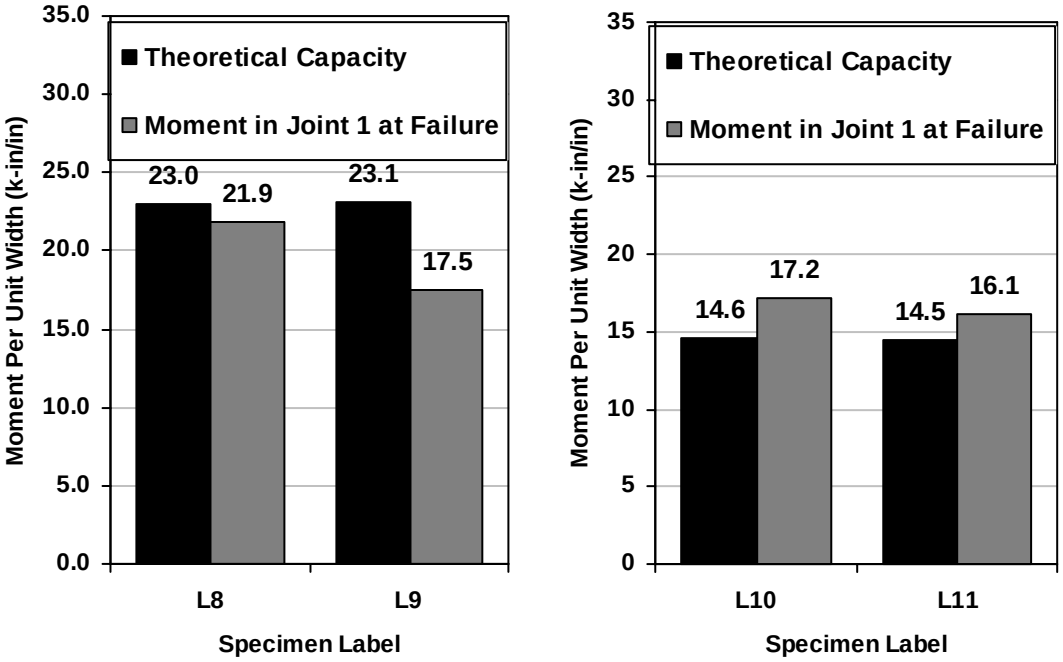

Fig. 43. Theoretical and tested moment capacity obtained in L8 – L10

L8 and L9 did not reach theoretical capacity and this appeared to be due to beam edge effects as discussed earlier. L10 and L11, which had greater side cover, exceeded theoretical capacity by 11% and 18%, respectively. This supports the idea that edge

effects played a factor in all previous longitudinal and transverse specimens' premature failures.

L8 was initially loaded in negative flexure to simulate a negative moment in the longitudinal closure pour. Maximum load for this test was either 3 k (equivalent moment is 3 k-in/in) as determined by the FE analysis or when cracking was observed in the beams, whichever came first. Theoretically, cracking would have begun at 7.1 k (7.3 k-in/in) which is higher than the suggested service load, so L8 was not expected to crack under a 3 k load. Loading the specimen with 3 k produced small cracks at the joint faces, but no substantial cracking was observed. Following this test, L9 was loaded in pure positive flexure to determine the flexural capacity of the section in the absence of shear force. L9 had an unexpected and unusually low capacity, which could not be attributed to any observed factors.

Failure in L1 – L7 consistently occurred at joint 1, so the concrete surface gages for L8 – L11 were located at this position to capture strain readings prior to crushing of the concrete. A surface mounted strain gage was placed on the concrete at joint 1, the closure pour centerline, and joint 2 for L8 and L9 to help verify that failure was occurring at joint 1. Fig. 44 shows that longitudinal gage position 1 in L8, which is at joint 1, reached maximum compressive strains and joint 2 (position 3) and the closure pour centerline (position 4) did not. Although L9 failed prematurely and strain readings were lower than L8, the trend is similar to L8 and joint 1 still has a higher strain at failure.

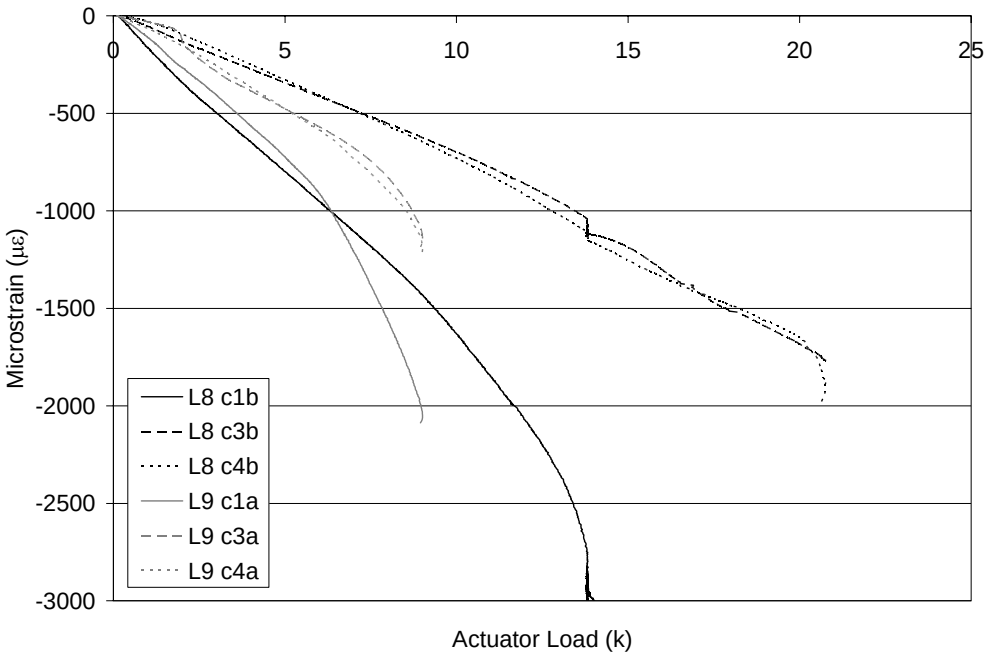

Fig. 44. Measured concrete strain in L8 and L9

Fig. 45 gives the strain readings for L10 and L11. Discrepancies between L10 and L11 strain readings were due to the slight differences in support locations which resulted in different applied moments for a given load. The additional side cover on these specimens provided better rebar confinement and consequently yielded higher concrete strain values. Similar to L8, the position 1 gages in these beams reached 3000 microstrain and the other gage positions did not. This confirms that joint 1 is the failure location even though joint 2 had been loaded with the specified M/V ratio. The high moment at joint 1 was more critical than the combination of shear and moment at joint 2.

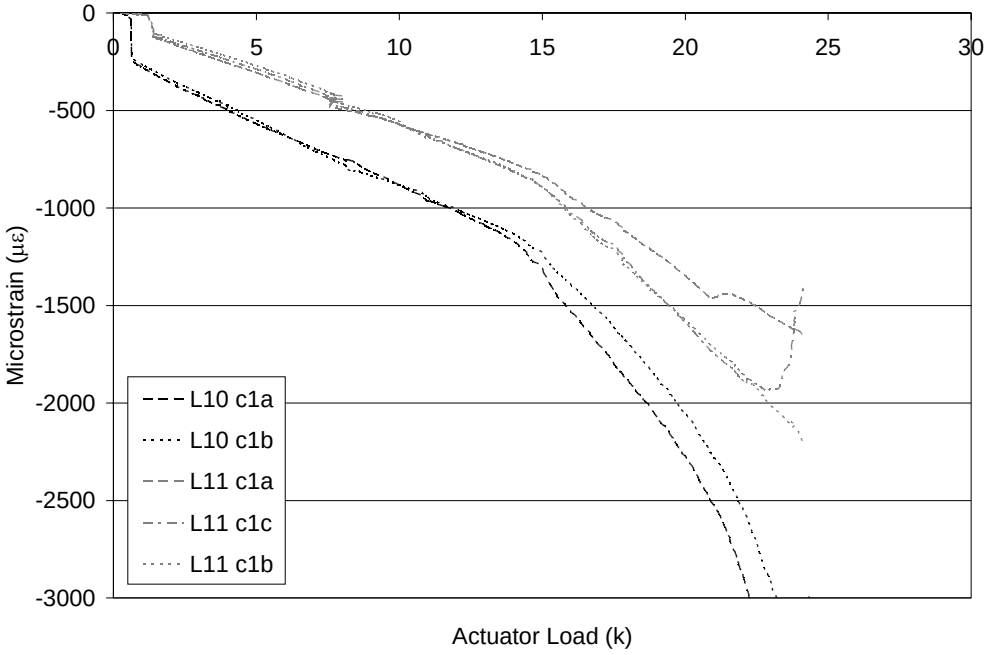

Fig. 45. Measured concrete strain at gage position 1 in specimen L8 – L11

Steel strain readings were taken at multiple longitudinal locations along the specimens to capture the behavior of the closure pour and adjacent precast concrete. Appendix F provides graphs of steel strains at each gage position. Fig. 46 and Fig. 47 illustrate strain profiles longitudinally along the beam for L10 and L11. Each data point represents the strain at a gage position for a given actuator load. Reinforcing bars yield throughout the section, with highest strains readings at the gages flush with the closure pour joints. The gage flush with joint 1 averaged strain readings over 0.24 in, which does not include the maximum moment location that is 1.4 in. inside joint 1. Therefore, it is likely that the highest strain was occurring between gage locations at the site of maximum applied moment.

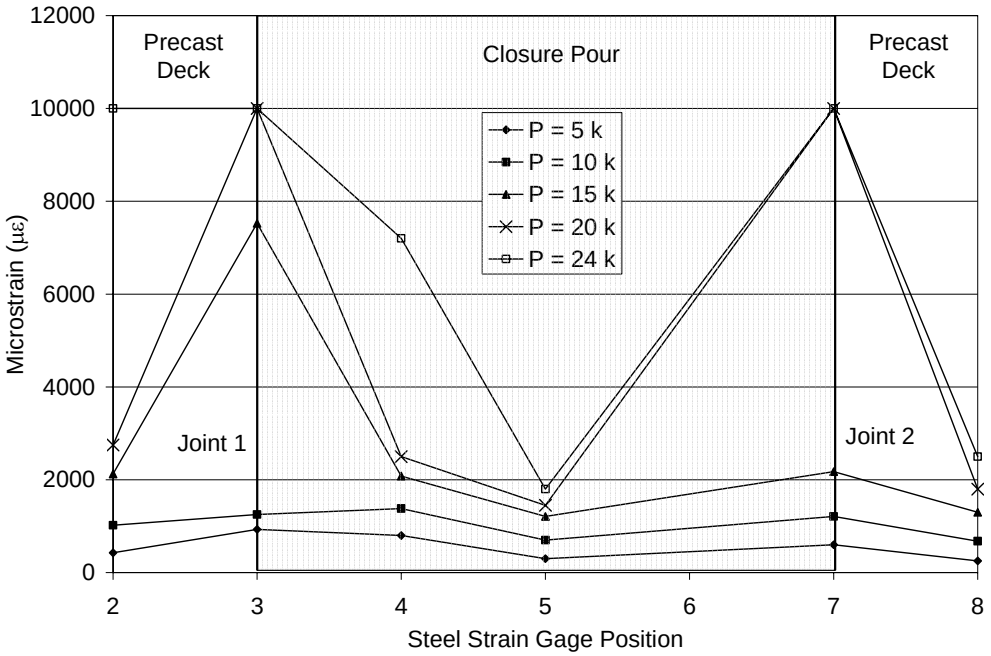

Fig. 46. Steel strain profile longitudinally along beam for L10

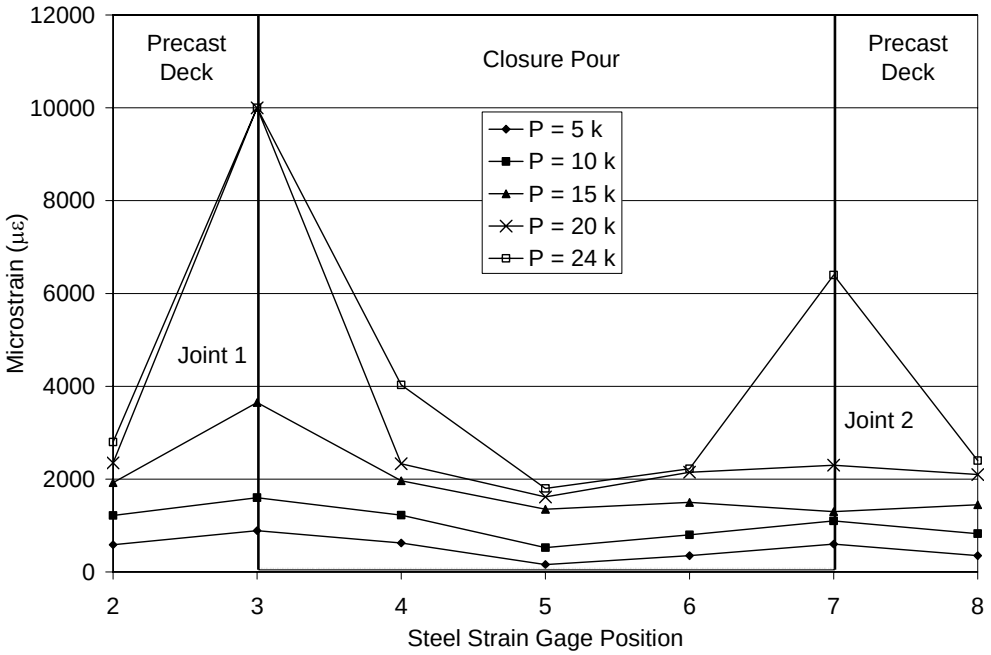

Fig. 47. Steel strain profile longitudinally along beam for L11

Cracking on both sides of the specimen was located within the reduced steel section (shown in Fig. 11) of the closure pour so only eight bars resist tension forces instead of sixteen like the center of the closure pour where the bars overlap. Maximum moment in the beams was located 1.4 in. inside joint 1 which is also within this reduced steel section. Therefore, all calculated beam capacities represent the 2 in. section between the reinforcing hoop ends and the closure pour face.

Crack patterns were similar in all longitudinal specimens as described in the previous section for beams L1 – L7. Two major failure initiating cracks typically occurred: one at the joint face and one following the outside reinforcing hoop as shown in Fig. 41 and Fig. 42. In a monolithic section, the failure would occur within the 0.6 in. between the maximum moment and rebar discontinuity location. It was observed after failure that the interface of the closure pour and precast concrete was smooth, as shown in Fig. 48, indicating a bond failure between the two concrete surfaces. The presence of the closure pour introduced a weak section with a poor bond at the joint between the two concrete sections. This is believed to have caused failure in the lower moment region of the reduced steel section of the closure pour.

Fig. 48. Poor bond between closure pour and precast concrete

An LVDT was attached on each side of a specimen at the centerline of the load pad to monitor symmetry of the loading and to capture the vertical displacement behavior. Beam deflections shown in Fig. 49 reveal a ductile behavior. Ductility allows possible or imminent failures to be recognized through large deflections in the beam. L8 and L9, which had a smaller beam width, had less ductility than L10 and L11. This is due to the lack of sufficient side cover in L8 and L9 and a consequential premature failure of rebar pulling out from the beam sides before capacity and full ductility could be reached. The increased beam width in L10 and L11 appears to have limited this adverse behavior and specimens had increased deflection before failure.

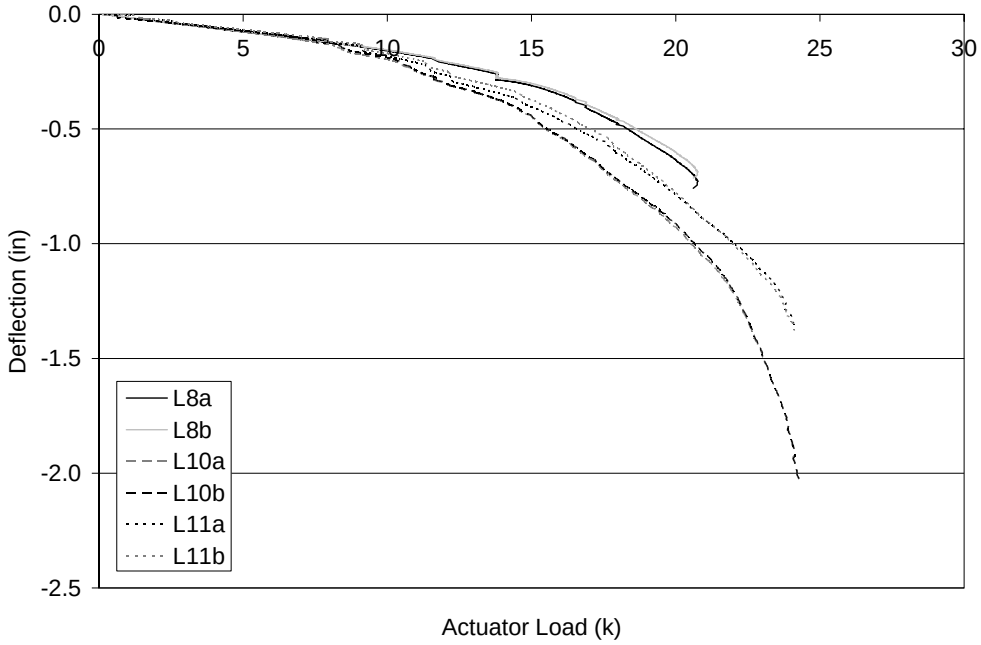

Fig. 49. Beam deflection at the centerline of actuator load for L8, L10, and L11

SUMMARY AND CONCLUSIONS

Summary

Overview

Jointless bridges are a common method used to improve bridge performance by eliminating movable joints in the bridge deck that lead to degradation of the bridge substructure and reinforcing. To construct a jointless deck, the deck is typically cast with one pour, approach slab to approach slab, on top of placed girders. To reduce formwork and traffic disturbance, TxDOT proposes a construction method using prefabricated girder and deck units that are connected on-site with cast-in-place closure pour slabs. The objective of this experimental study was to determine if the closure pour slab section behaved similar to a typical monolithic section of a jointless bridge.

Specimens were beam strips taken from the bridge deck that included the closure pour and portions of the prefabricated deck unit. Six transverse and eleven longitudinal closure pour beams were statically loaded to failure. Specimens T1 – T6 included a portion of the transverse closure pour and were loaded in pure negative flexure. Specimens L1 – L11 included a portion of the longitudinal closure pour and were loaded to achieve a combined shear and positive flexure at joint 2. The beam flexural capacities, failure locations, rebar and concrete strains, and cracking patterns were documented to compare to reinforced concrete theory. All data was analyzed in an attempt to capture the behavior and failure of the beam strip specimens.

Longitudinal Closure Pour

Eleven longitudinal closure pour specimens were tested in this study. Seven specimens had No. 5 bars and four specimens had No. 4 bars. Two out of the eleven specimens had increased rebar side cover. Other variations in beams included coating, the absence of a closure pour, straight and hooked closure pour rebar, and flexural loading setups.

Beam edge effects played a major role in the percent of theoretical capacity reached during testing. Once edge effects were reduced with a wider beam cross-section in L10 and L11, the capacity of the specimens exceeded theoretical moment capacity by 11% and 18%, respectively. The premature failures resulting from edge effects also affected the concrete surface strain readings. Prior to the testing of the wider beam sections, the concrete strain at failure was below 3000 microstrain. After the removal of the edge effects, strain readings at the failure location reached expected maximum concrete strains.

Crack propagation of the longitudinal closure pour was not monitored closely like the transverse closure pour specimens since cracking would be on the underside of the deck and is less of a concern than top surface crack formation.

The two controlling factors in the pattern of cracking and failure appear to be the rebar discontinuities in the closure pour reinforcing and the presence of the closure pour cold joint. At 2 in. away from the closure pour construction joint, the reinforcing is reduced from 16 – No. 4 bars to 8 – No. 4 bars (see Fig. 11) which reduces the section's flexural capacity. This discontinuity occurred near the maximum applied moment and

was the location of failure. The closure pour cold joint also introduces a weak section due to the poor bond between the precast and cast-in-place concrete.

Transverse Closure Pour

Six transverse closure pour specimens were tested. Measured moment capacities for these beams were lower than calculated theoretical strengths, including the control specimen that was monolithically poured with straight rebar. Based on the longitudinal closure pour findings, the low strengths are partially attributed to edge effects. Side cover was not sufficient to confine the reinforcing bars and this allowed the outermost bars to be pulled out and away from the beam before the section's capacity was reached. In addition, the hairpin bars in the closure pour produce a prying action within the closure pour causing the sudden initiation and failure of a non-flexural crack at the location of the hairpin rebar ends. Precast deck reinforcing is stopped in the same approximate location. The combined effect of the hairpin prying, rebar discontinuity and a reduced cross-sectional steel area generates a weak deck section 4.5 in. away from the transverse closure pour cold joint.

Cracking was monitored for the transverse closure pour specimens since cracks occur at the top of the bridge deck and may lead to leakage and corrosion. A small crack was observed at the cold joints at a very low load due to a weak interface bond. Flexural cracks in the closure pour initiated at a lower load than theory, but were not the location of failure. Immediately preceding failure, another crack initiated and failed at approximately 4.5 in. from the cold joint.

Conclusions

Overview

The results of this study have aided in understanding the behavior of closure pour slabs in comparison to a monolithic deck. However, due to unexpected results found in this experimental research, more testing and analysis is recommended to fully capture the behavior of the proposed closure pour construction method. This section lists final conclusions from the research described in this report along with recommendations for future research.

Experimental Research Conclusions

1. Specimens with adequate rebar side cover reach expected theoretical beam capacity. However, crack and failure patterns were unexpected and the basic theories used herein may not apply if the failure mechanisms are found to be more complex.
2. The closure pour cold joint has a poor bond and introduces a weak section in the deck. This may affect the type of bridge failure (i.e. punching shear).
3. The location of discontinuity in closure pour reinforcing should be carefully specified to lessen the effects of the reduction in cross-sectional steel.

Recommendations for Future Work

1. The transverse closure pour hairpin detail may cause unexpected failures due to the observed prying action. Possible alterations to the design or changes to rebar discontinuity locations should be studied.
2. Closure pour presence may introduce another mode of bridge failure other than punching shear that is typically seen in bridges. A slab specimen is scheduled in the continuation of this project to address this issue. The slab specimen will also further reduce any edge effects.
3. The longitudinal closure pour at the bridge approach slabs was not tested in this research and should be studied to ensure expected behavior.
4. The location on the bridge deck where a transverse and longitudinal closure pour slab meet may also play a key role in the performance and failure of the bridge. A slab specimen including the intersection of closure pours could be tested to determine the behavior at this bridge location.

REFERENCES

Alampalli, S., and Yannotti, A. P. (1998). "In-service performance of integral bridges and jointless decks." *TRB*, 1624, 1-7.

Burke, M.P. Jr. (1993). "Integral bridges: attributes and limitations," *TRB*, 1393, 1-8.

Burke, M. P. Jr. (1994). "Semi-integral bridges: movements and forces." *TRB*, 1460, 1-7.

Burke, M. P. Jr. (1999). "Cracking of concrete decks and other problems with integral-type bridges." *TRB*, 1688, 131-138.

Caner, A., and Zia, P. (1998). "Behavior and design of link slabs for jointless bridge decks." *PCI Journal*, 43(3), 68-80.

Culmo, M. P. (2000). "Rapid bridge deck replacement with full-depth precast concrete slabs." *TRB*, 1712, 139-146.

Hambly, E. C. (1997). "Integral bridges." *Proceedings of the Institute of Civil Engineers, Transport*, 123(1), 30-38.

Husain, I., and Bagnariol, D. (2000). "Design and performance of jointless bridges in Ontario." *TRB*, 1696, 109-121.

Issa, M. A., Yousif, A. A., and Issa, M. A. (2000). "Experimental behavior of full-depth precast concrete panels for bridge rehabilitation." *ACI Struct. Journal*, 97(3), 397-407.

Issa, M. A., Yousif, A. A., Issa, M. A., Kaspar, I. I., and Khayyat, S. Y. (1998). "Analysis of full depth precast concrete bridge panels." *PCI Journal*, 43(1), 74-85.

Issa, M. A., Yousif, A. A., Kaspar, I.I., and Khayyat, S. Y. (1995c). "Field performance of full-depth precast panels for bridge deck reconstruction." *PCI Journal*, 40(3), 82-108.

Kunin, J., and Alampalli, S. (2000). "Integral abutment bridges: current practice in United States and Canada." *ASCE J. Perf. Constr. Facil.*, 14(3), 104-111.

Martin, L. D., and Osborn, A. E. N. (1983). "Connections for Modular Precast Concrete Bridge Decks," Publ. No. FHWA-RD-82-106, U.S. Department of Transportation, Washington, D.C.

Shim, C. -S., and Chang, S. -P. (2003). "Cracking of continuous composite beams with precast panels." *J. Constr. Steel Research*, 59, 201-214.

Thippeswamy, H.K., GangaRao, H.V.S., and Franco, J.M. (2002). "Performance evaluation of jointless bridges," *ASCE J. Bridge Eng.*, 7(5), 276-289.

Van Lund, J. A., and Brecto, B. B. (1999). "Jointless bridges and bridge deck joints in Washington State." *TRB*, 1688, 116-123.

Wasserman, E. P. (1987). "Jointless bridge decks." *Eng. J. AISC*, 24(3), 93-100.

APPENDIX A

SPECIMEN STRAIN GAGE LOCATIONS

A.1 Transverse Specimen Strain Gage Locations

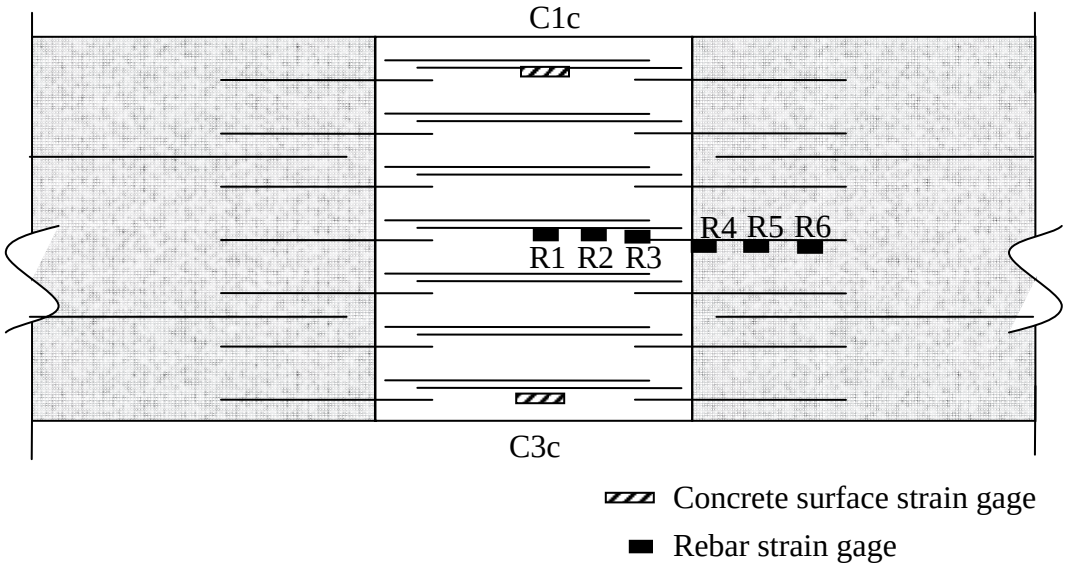

Fig. 50. T1 strain gage locations

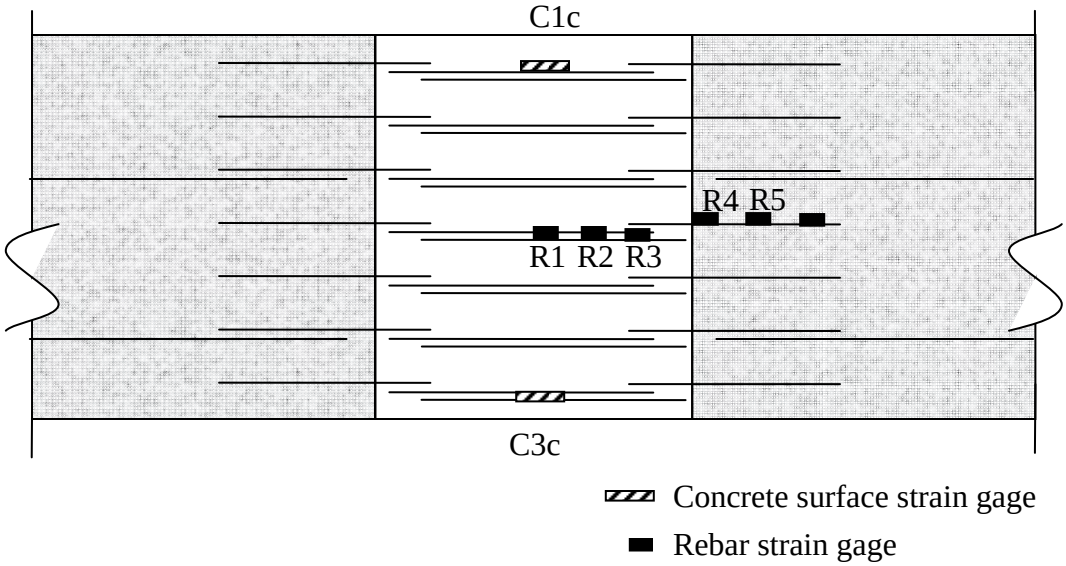

Fig. 51. T2 strain gage locations

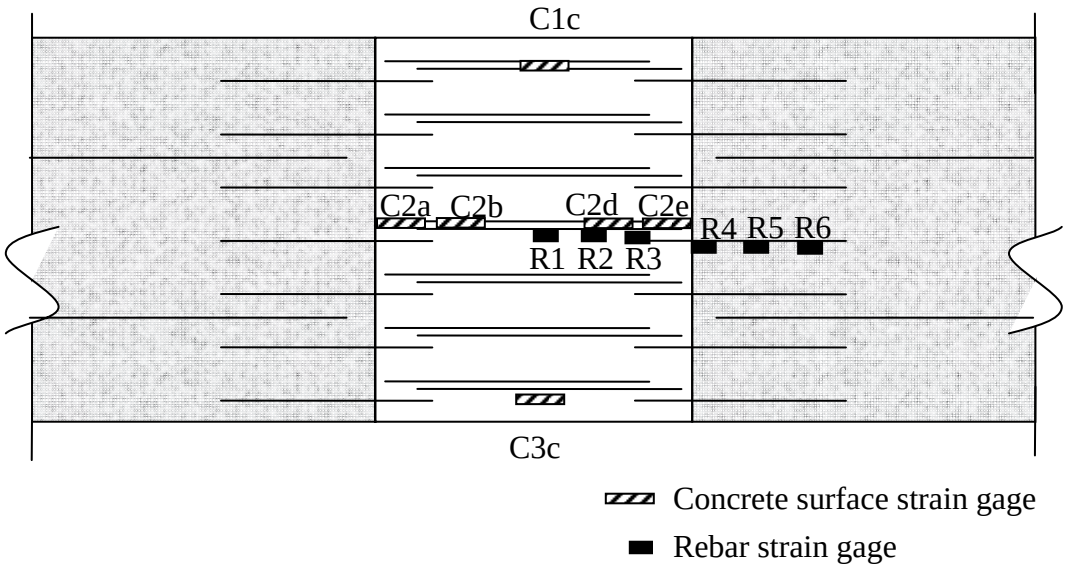

Fig. 52. T3 strain gage locations

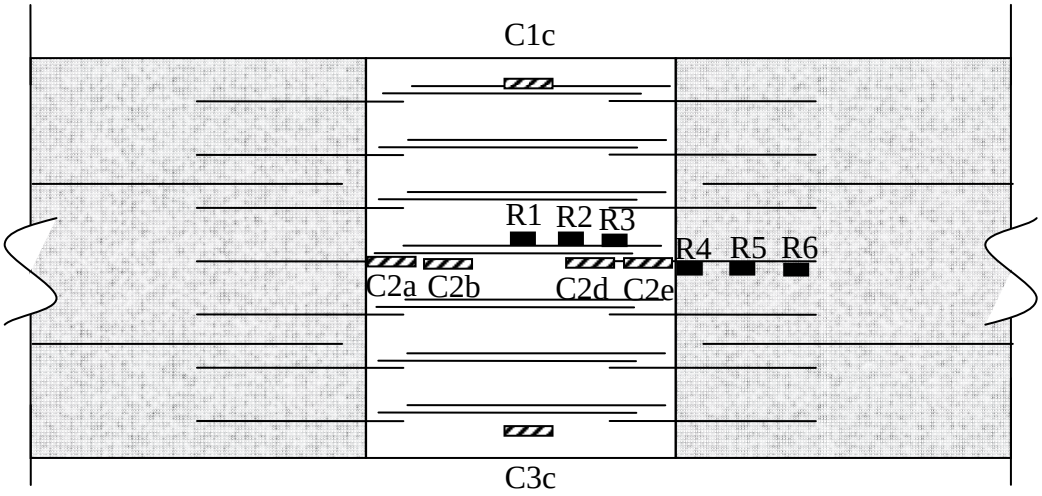

Fig. 53. T4 strain gage locations

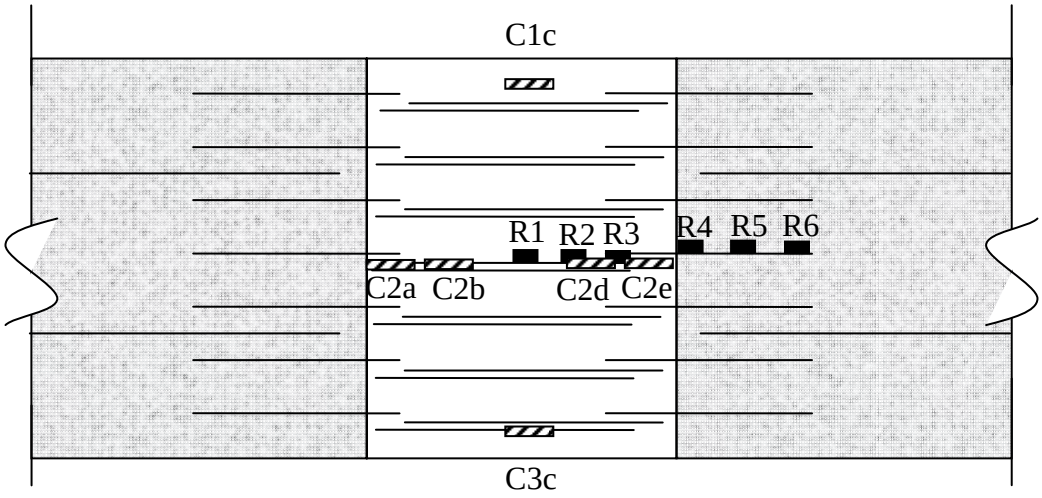

Fig. 54. T5 strain gage locations

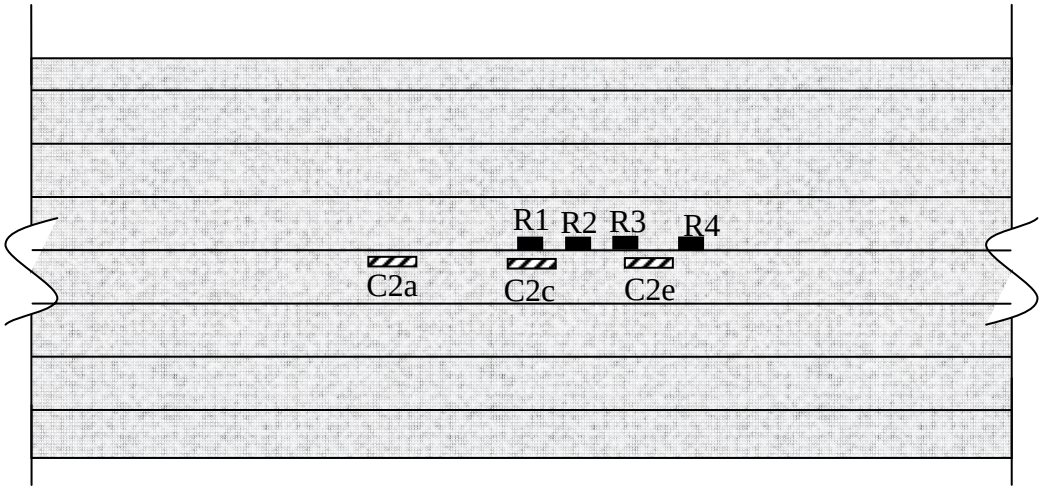

Fig. 55. T6 strain gage locations

A.2 Longitudinal Specimen Strain Gage Locations

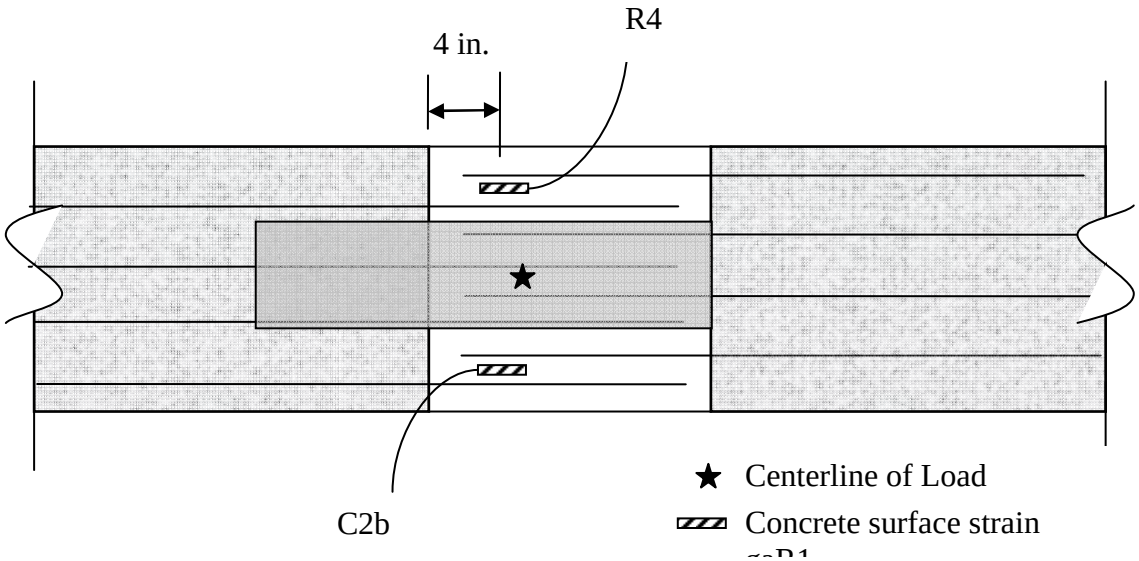

Fig. 56. L1 strain gage locations

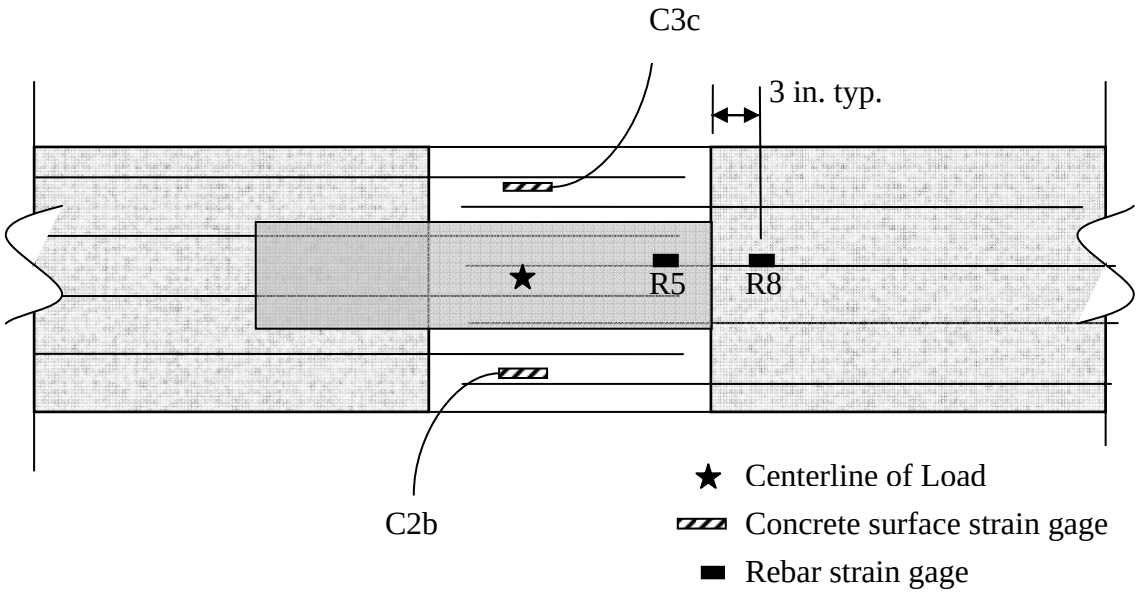

Fig. 57. L2 strain gage locations

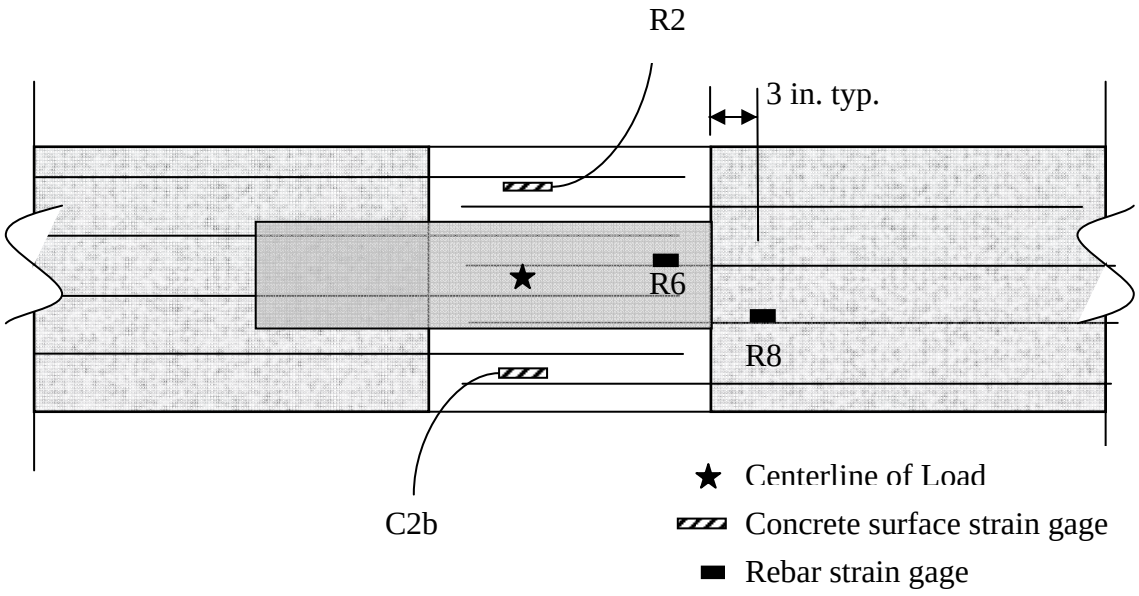

Fig. 58. L3 strain gage locations

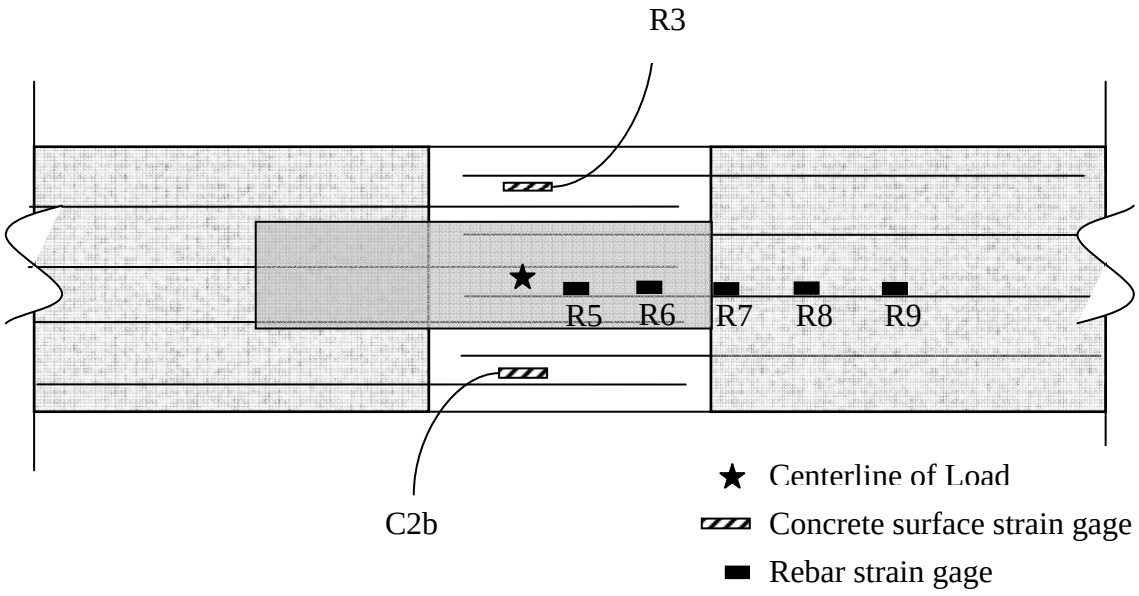

Fig. 59. L4, L5, L6 strain gage locations

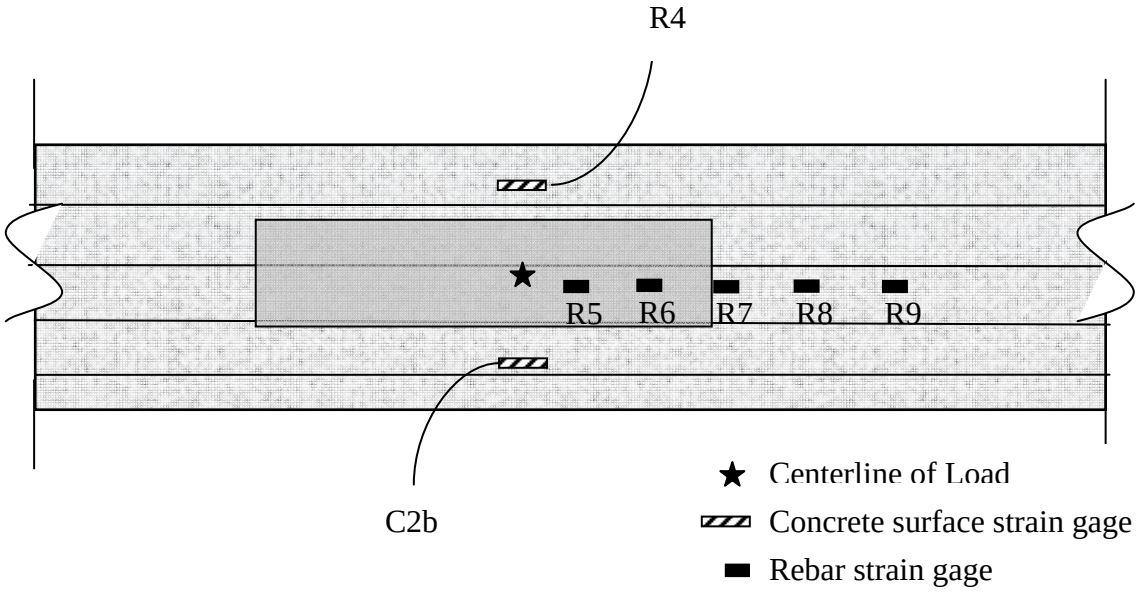

Fig. 60. L7 strain gage locations (control specimen)

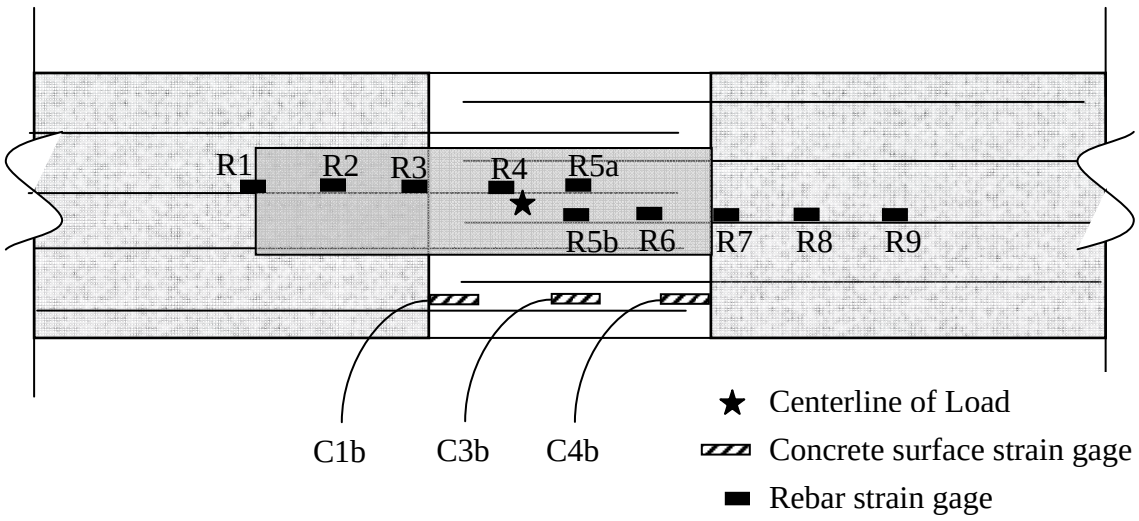

Fig. 61. L8 strain gage locations

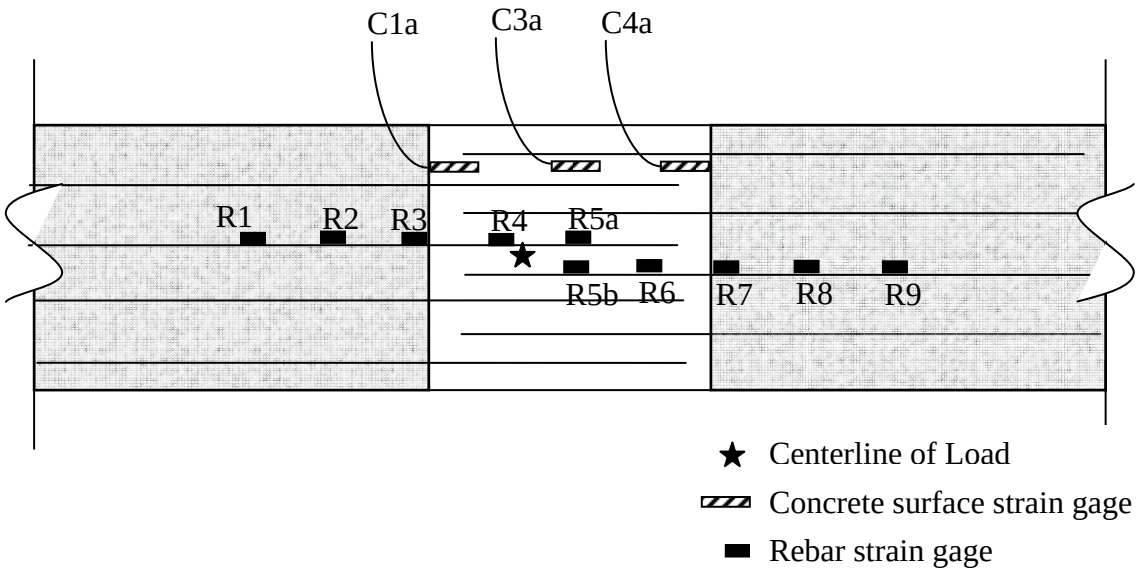

Fig. 62. L9 strain gage locations

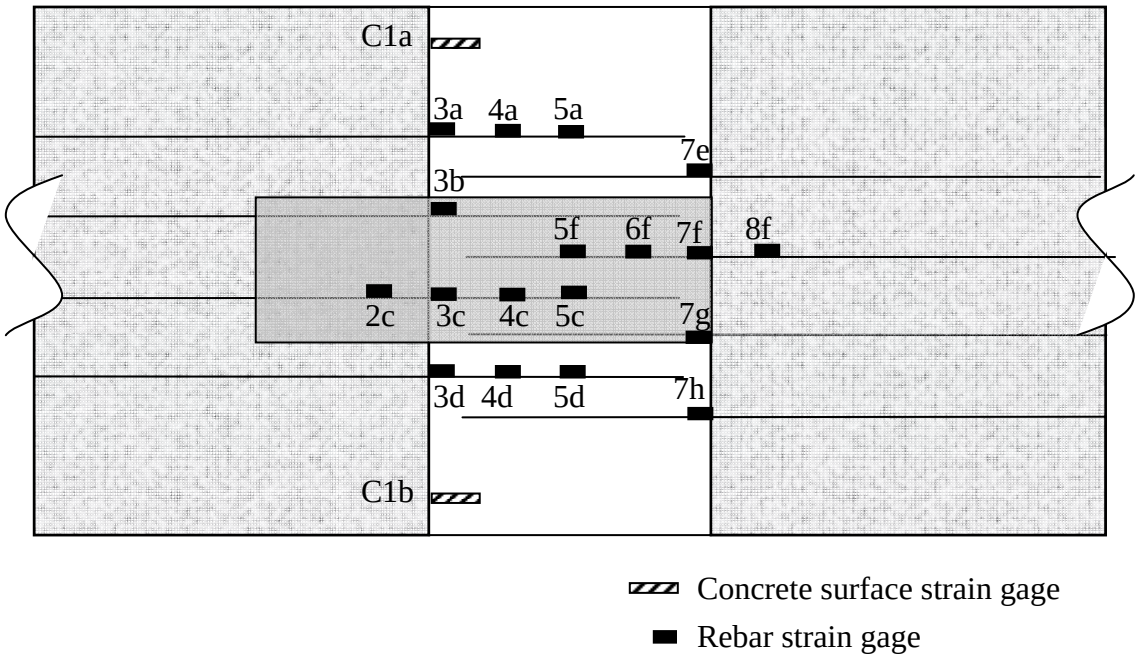

Fig. 63. L10 strain gage locations

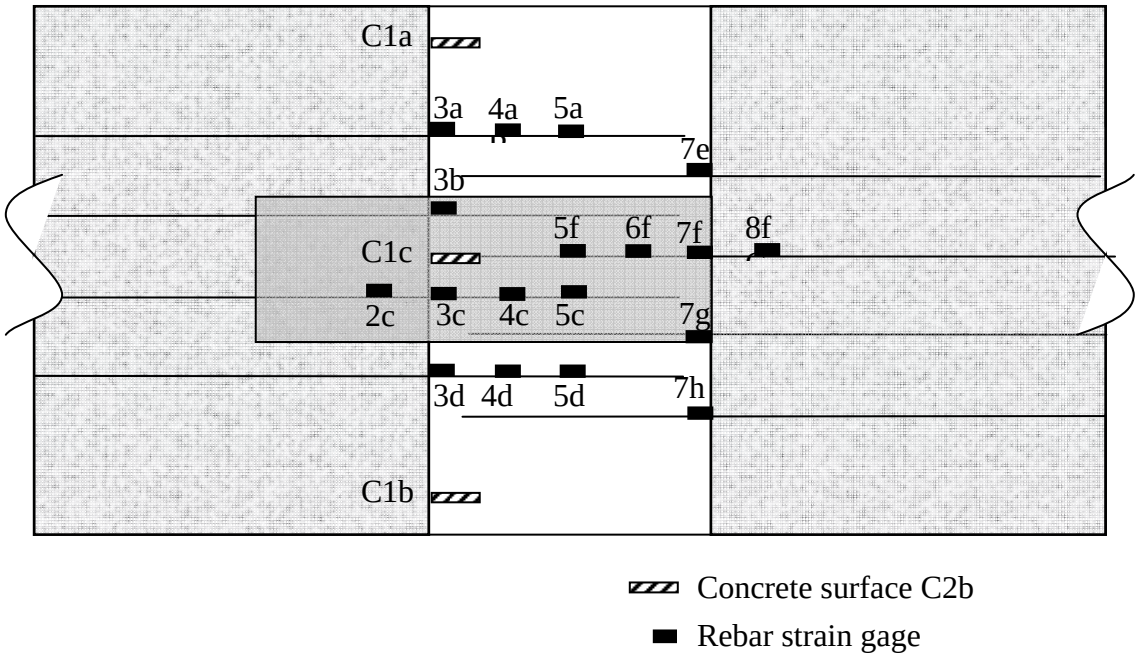

Fig. 64. L11 strain gage locations

APPENDIX B

EXAMPLE BEAM CALCULATION FOR L3

Assumptions:

Neutral axis is above compression steel
Compression steel does not yield
Tension steel does yield

	Compression steel (A's)	Tension Steel As	
ACI Bar Number	5	5	
Number of Bars in cross section	4	4	
Bar diameter (in)	0.625	0.625	
Bar area (in2)	0.31	0.31	
Beam section height	8.5		in
Beam section width	20.625		in
Compression steel clear cover	2.5		in
Tension steel clear cover	1.5		in
Concrete compressive strength	8.075		ksi
Steel yield strength	72		ksi
depth from extreme compression fiber to A's	2.8125		in
depth from extreme compression fiber to As	6.6875		in
ACI factor $\beta 1$	0.65		
Steel yield strain	0.00248		

Solving quadratic equation from equilibrium to determine neutral axis location

quadratic coefficient 'a'	92.0	
quadratic coefficient 'b'	18.4	
quadratic coefficient 'c'	-300.3	
neutral axis from extreme compression fiber	1.71	in
equivalent Whitney stress block depth	1.11	in
Strain in A's	0.001936533	
Strain in As	0.008737978	
Compressive force in Concrete	157.3	k
Tensile force in A's	88.35729338	k
Tensile force in As	68.9	k
Nominal moment	697.36	k-in
Actuator load to produce above moment in joint 1	31.90	k-in
Actuator load to produce above moment in joint 2	40.42	k-in

APPENDIX C

CONCRETE PROPERTIES

C.1 Transverse Specimen Concrete Properties

Table 15. Individual Compression Cylinder Strengths for Transverse Specimens

Specimen Label	Precast Cylinder 1 Strength (psi) and Failure Pattern	Precast Cylinder 1 Strength (psi) and Failure Type	Closure Pour Cylinder 1 Strength (psi) and Failure Type	Closure Pour Cylinder 1 Strength (psi) and Failure Type
T1	9227 shear	9405 shear	6334 shear	5863 columnar
T2	8909 shear	9019 shatter	6000 cone	5582 columnar
T3	4780 shear	4590 shear	6580 shear	6580 shear
T4	4925 shear	4720 shear	6505 columnar	6520 columnar
T5	4590 shear	5150 columnar	6680 shear	6570 shear
T6	6600 shear	6350 shear	N/A	N/A

Table 16. Slump and Average Precast Concrete Strength for Transverse Specimens

Specimen Label	Final Slump (in.)	Errors in Testing and Concrete	Average 7-day strength (pis)	Average Strength at Test (psi)	Concrete Age at Test (days)
T1	2.5	1” initial slump; added water	7150	9316	45
T2	2.5	1” initial slump; added water	7150	8964	30
T3	4	No initial slump; added water	3398	4685	64
T4	4	No initial slump; added water	3398	4823	71
T5	4	No initial slump; added water	3398	4870	83
T6	3.5	1.5” initial slump; added water	6141	6475	14

Table 17. Slump and Average Closure Pour Strength for Transverse Specimens

Specimen Label	Final Slump (in.)	Errors in Testing and Concrete	Average 7-day strength (pis)	Average Strength at Test (psi)	Concrete Age at Test (days)
T1	3.5	No initial slump; added water	4775	6099	34
T2	3.5	No initial slump; added water	4775	5791	19
T3	3.5	None	5823	6580	49
T4	3.5	None	5823	6512	56
T5	3.5	None	5823	6625	68
T6	N/A	N/A	N/A	N/A	N/A

C.2 Longitudinal Specimen Concrete Properties

Concrete properties for specimens L1 – L7 can be found in Appendix E.

Table 18. Individual Compression Cylinder Strengths for Longitudinal Specimens

Specimen Label	Precast Cylinder 1 Strength (psi) and Failure Pattern	Precast Cylinder 1 Strength (psi) and Failure Type	Closure Pour Cylinder 1 Strength (psi) and Failure Type	Closure Pour Cylinder 1 Strength (psi) and Failure Type
L8	6730 shear	6826 shear	6118 columnar	5440 shear
L9	7700 shear	6600 shear	5815 shatter	6160 shear
L10	6663 shear	6628 columnar	5157 columnar	5486 shear
L11	6456 shear	None	4988 shear	4960 shear

Table 19. Slump and Average Precast Concrete Strength for Longitudinal Specimens

Specimen Label	Final Slump (in.)	Errors in Testing and Concrete	Average 7-day strength (pis)	Average Strength at Test (psi)	Concrete Age at Test (days)
L8	3.5	1.5” initial slump; added water	6141	6827	31
L9	3.5	1.5” initial slump; added water	6141	7150	36
L10	4.5	no 7day cylinders	N/A	6646	22
L11	4.5	no 7day cylinders	N/A	6456	17

Table 20. Slump and Average Closure Pour Strength for Longitudinal Specimens

Specimen Label	Final Slump (in.)	Errors in Testing and Concrete	Average 7-day strength (pis)	Average Strength at Test (psi)	Concrete Age at Test (days)
L8	4.5	1” initial slump; added water	4396	5780	24
L9	4.5	1” initial slump; added water	4396	5990	29
L10	5.5	2” initial slump; added water	4933	5486	12
L11	5.5	2” initial slump; added water	4933	4974	7

APPENDIX D

SPECIMEN T1 – T6 STRAIN DATA

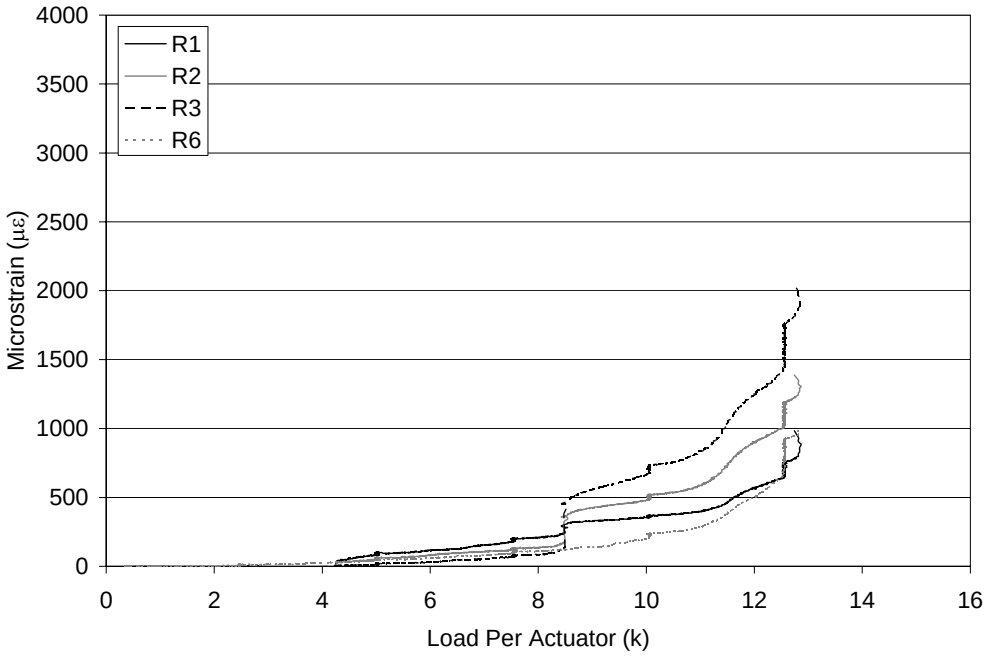

Fig. 65. Measured reinforcing strain for T1

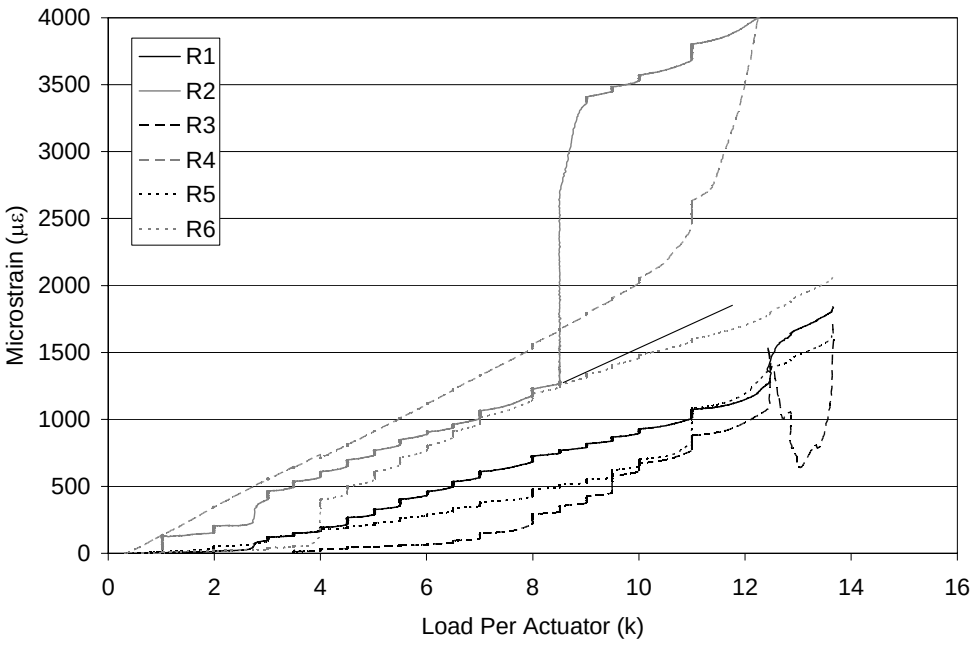

Fig. 66. Measured reinforcing strain for T3

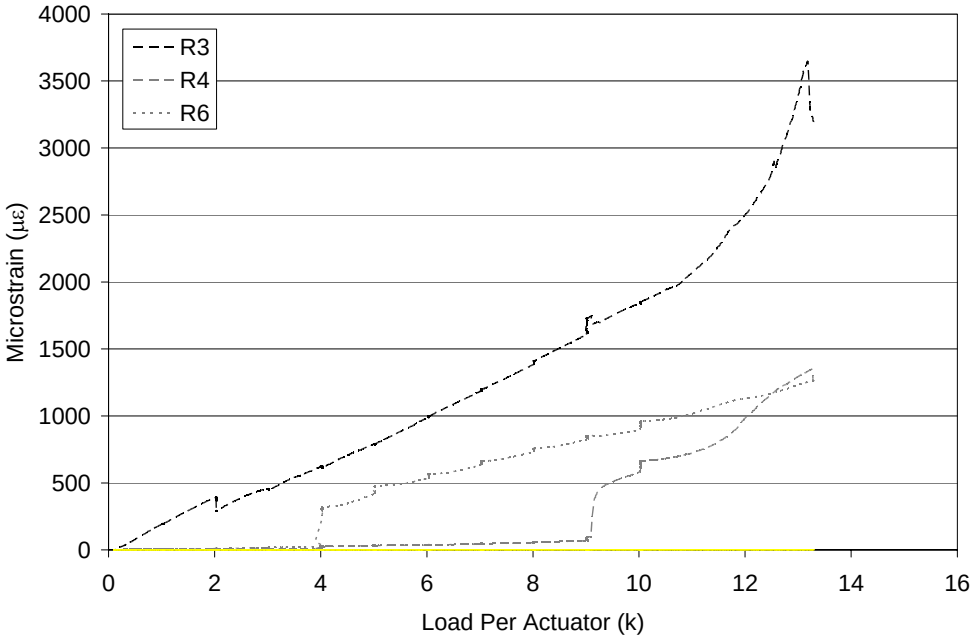

Fig. 67. Measured reinforcing strain for T4

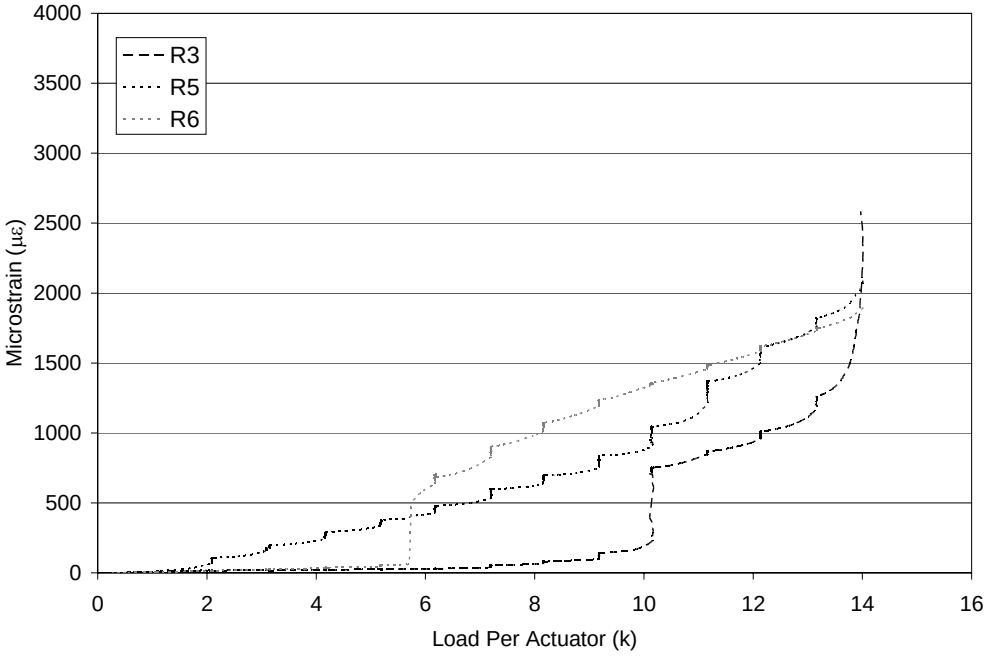

Fig. 68. Measure reinforcing strain for T5

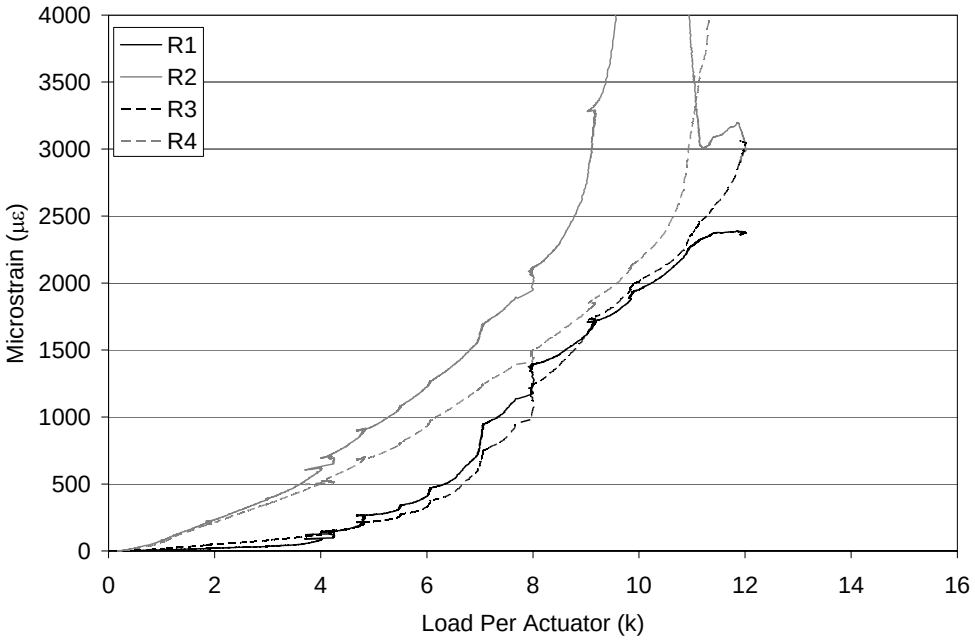

Fig. 69. Measured reinforcing strain for T6 (control specimen)

APPENDIX E

SPECIMEN L1 – L7 DATA

Table 21. Individual Compression Cylinder Strengths for L1 – L7

Specimen Label	Precast Cylinder 1 Strength (psi) and Failure Pattern	Precast Cylinder 1 Strength (psi) and Failure Type	Closure Pour Cylinder 1 Strength (psi) and Failure Type	Closure Pour Cylinder 1 Strength (psi) and Failure Type
L1	8087 cone & shear	7650 shear	7915 shear	7291 cone & shear
L2	7980 cone & shear	8040 shear	8490 shear	7570 cone & shear
L3	8320 shatter	None	8430 columnar	7720 shear
L4	8327 cone	8068 cone & shear	5628 shatter	5564 shear
L5	8217 cone & shear	8034 shatter	N/A	N/A
L6	8212 shatter	8555 columnar	5937 shear	6115 cone
L7	8330 cone & shear	8490 shear	N/A	N/A

Table 22. Slump and Average Precast Concrete Strength for L1 – L7

Specimen Label	Slump (in.)	Errors in Testing and Concrete	Average 7 day strength (pis)	Average Strength at Test (psi)	Concrete Age at Test (days)
L1	3	7-day cylinder tested at 8 days	6125	7869	35
L2	3	7-day cylinder tested at 8 days	6125	8010	49
L3	3	7-day cylinder tested at 8 days	6125	8320	55
L4	3	None	7118	8198	16
L5	3	None	7118	8125	14
L6	3	None	7118	8384	20
L7	2.5	1” initial slump; added water	7150	8410	15

Table 23. Slump and Average Closure Pour Concrete Strength for L1 – L7

Specimen Label	Slump (in.)	Errors in Testing and Concrete	Average 7 day strength (pis)	Average Strength at Test (psi)	Concrete Age at Test (days)
L1	3.5	None	6520	7603	22
L2	3.5	None	6520	8030	36
L3	3.5	None	6520	8075	42
L4	4	None	5318	5596	9
L5	N/A	N/A	N/A	N/A	N/A
L6	4	None	5318	6026	13
L7	N/A	N/A	N/A	N/A	N/A

Table 24. Precast Concrete and Closure Pour Strength at Testing for L1 – L7

Specimen Label	Precast Concrete Strength* (psi)	Closure Pour Concrete Strength* (psi)
L1	7869	7603
L2	8010	8030
L3	8320	8075
L4	8198	5596
L5	8125	N/A
L6	8384	6026
L7	8410	N/A

Table 25. Theoretical Capacity and Theoretical Failure Load for L1-L7

Specimen Label	Moment Capacity (k-in)	Moment Capacity per unit width (k-in/in)	Failure Load to Cause Failure at Joint 1 (kip)	Failure Load to Cause Failure at Joint 2 (kip)
L1	688	33	31.5	39.9
L2	696	34	31.8	40.3
L3	697	34	31.9	40.4
L4	639	31	29.2	37.0
L5	699	34	32.0	40.5
L6	651	32	29.8	37.7
L7	707	34	N/A	N/A

Table 26. Tested Failure Load and Moment for L1 – L7

Specimen Label	Failure Load (kip)	Failure Moment at Joint 1 (k-in)	Failure Moment at Joint 2 (k-in)	Failure Moment at Joint 1 per unit width (k-in)	Failure Moment at Joint 2 per unit width (k-in)
L1	23.4	512	404	25	20
L2	24.8	542	427	26	21
L3	26.1	571	450	28	22
L4	22.2	485	383	24	19
L5	24.9	544	430	26	21
L6	20.1	439	347	21	17
L7	36.1	790	623	38	30

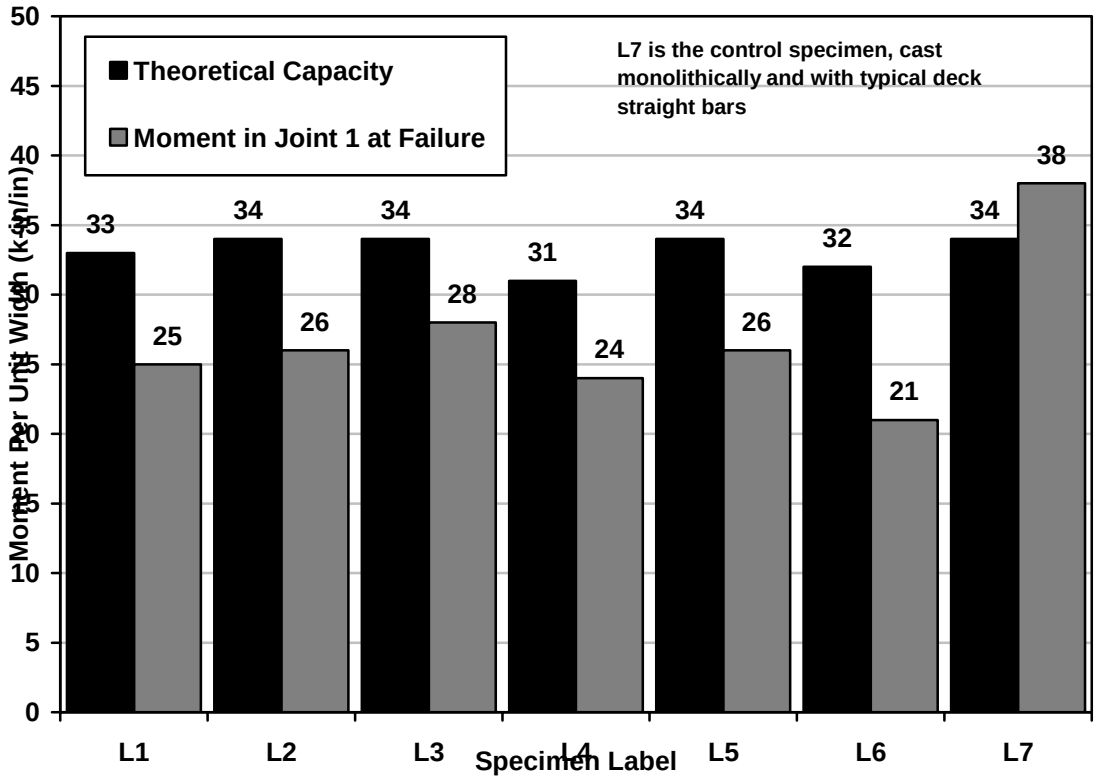

Fig. 70. Percent of theoretical capacity obtained in L1 – L7

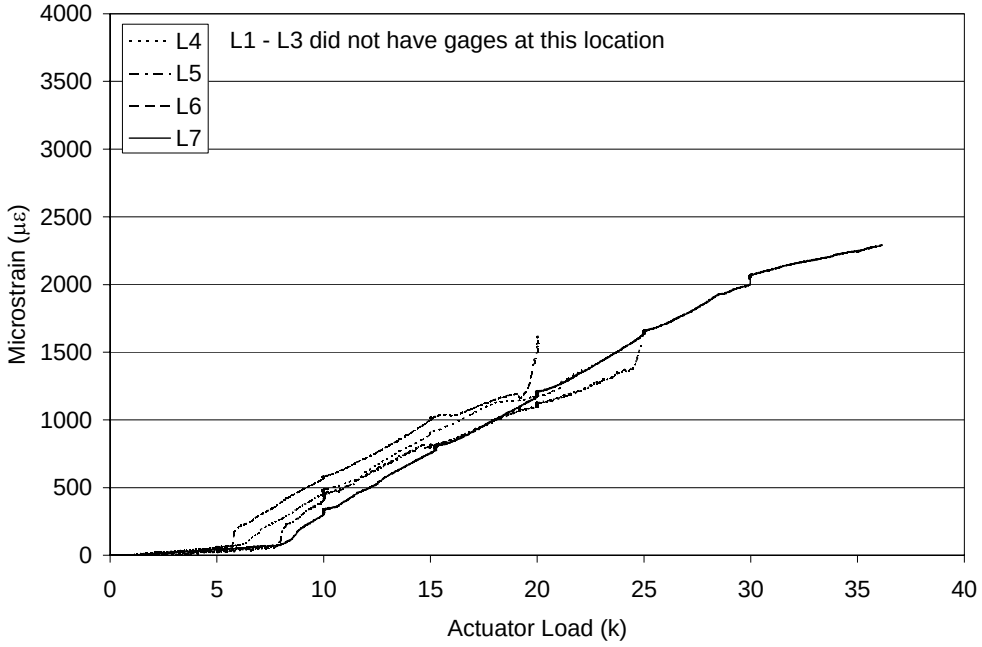

Fig. 71. Measured reinforcing strain at gage position 5 in L1 – L7

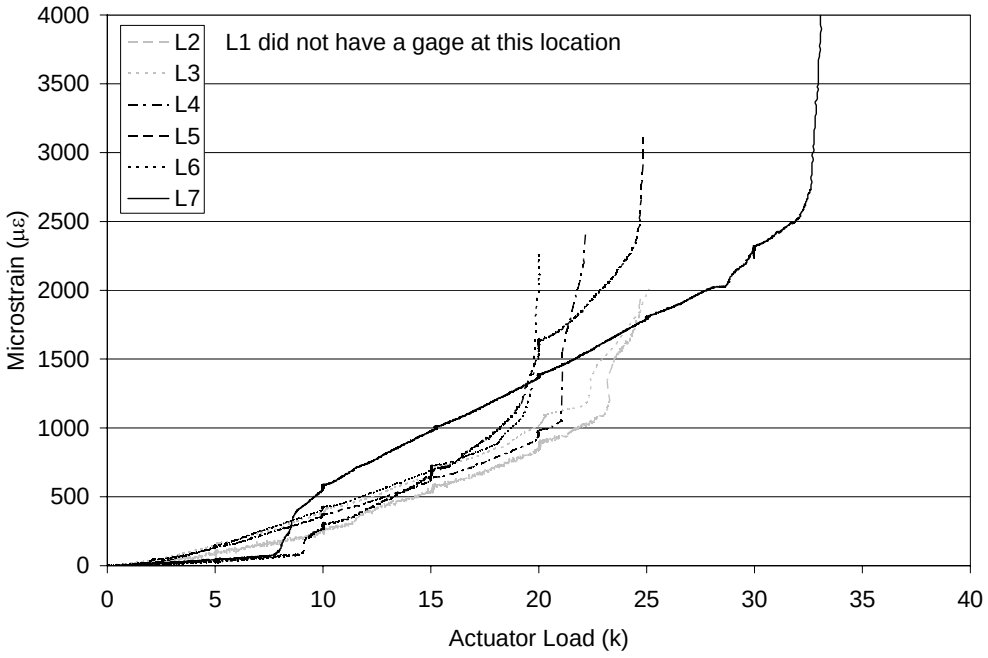

Fig. 72. Measured reinforcing strain at gage position 6 in L1 – L7

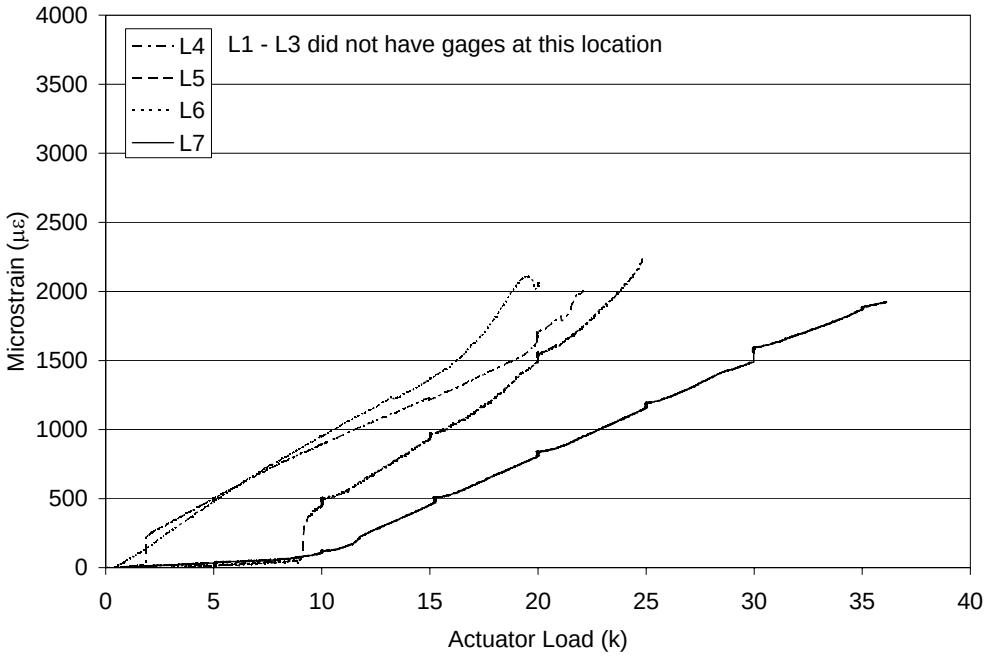

Fig. 73. Measured reinforcing strain at gage position 7 in L1 – L7

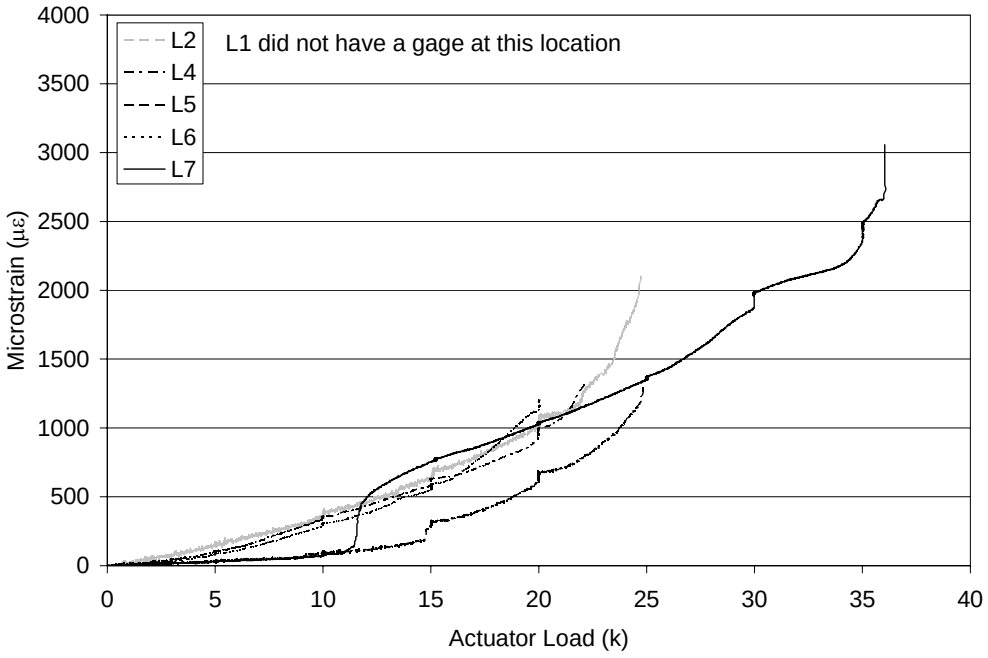

Fig. 74. Measured reinforcing strain at gage position 8 in L1 – L7

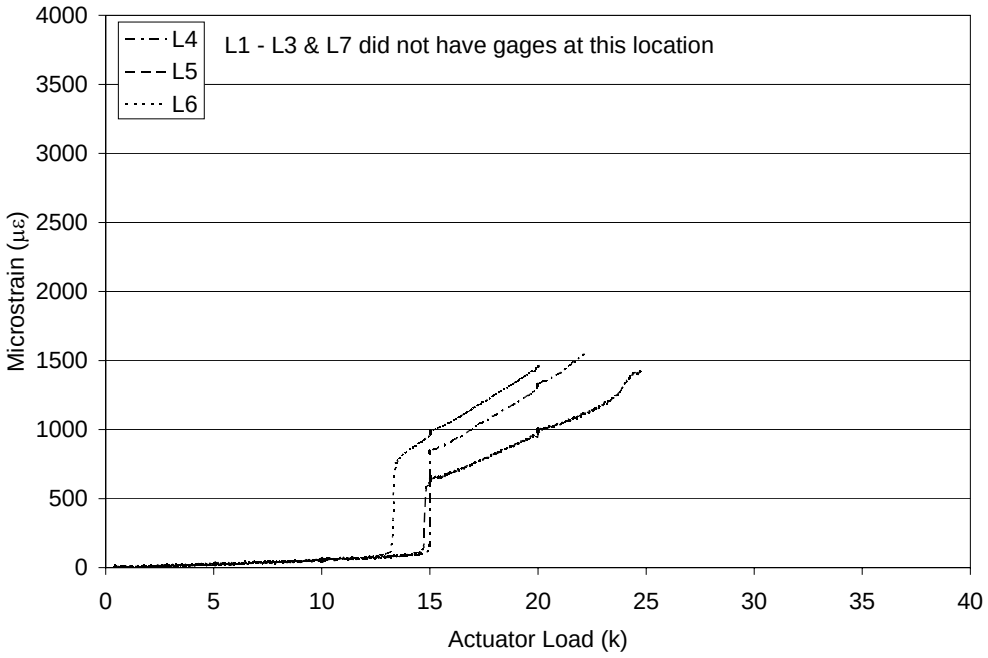

Fig. 75. Measured reinforcing strain at gage position 9 in L1 – L7

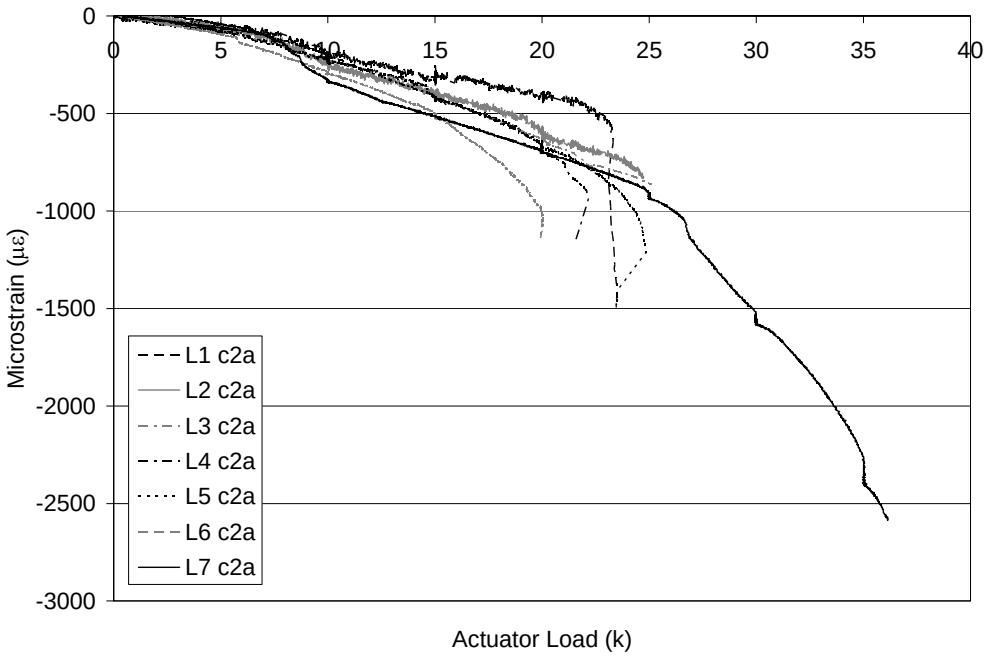

Fig. 76. Measured concrete strain at gage position 2a in L1 – L7

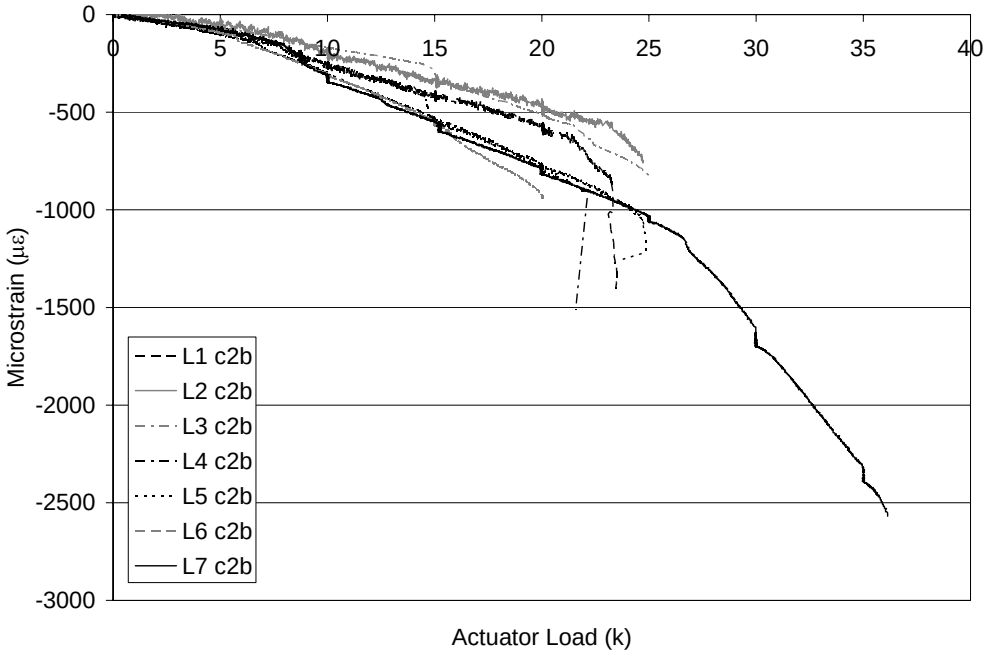

Fig. 77. Measured concrete strain at gage position 2b in L1 – L7

APPENDIX F

ADDITIONAL DATA FOR L8 – L11

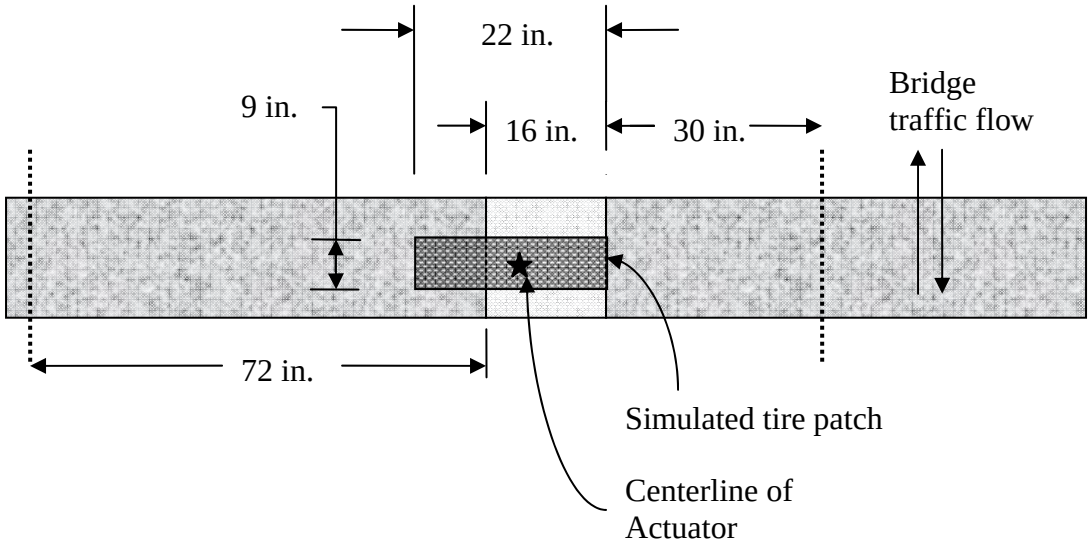

(a)

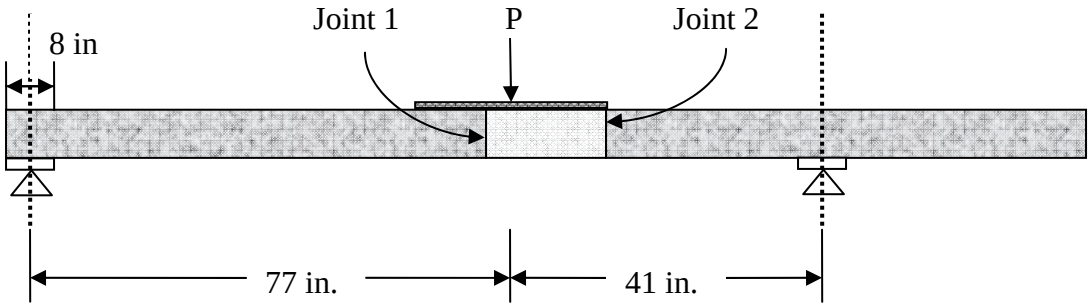

(b)

Fig. 78. Positive moment test setup for L10: (a) plan view; (b) elevation view

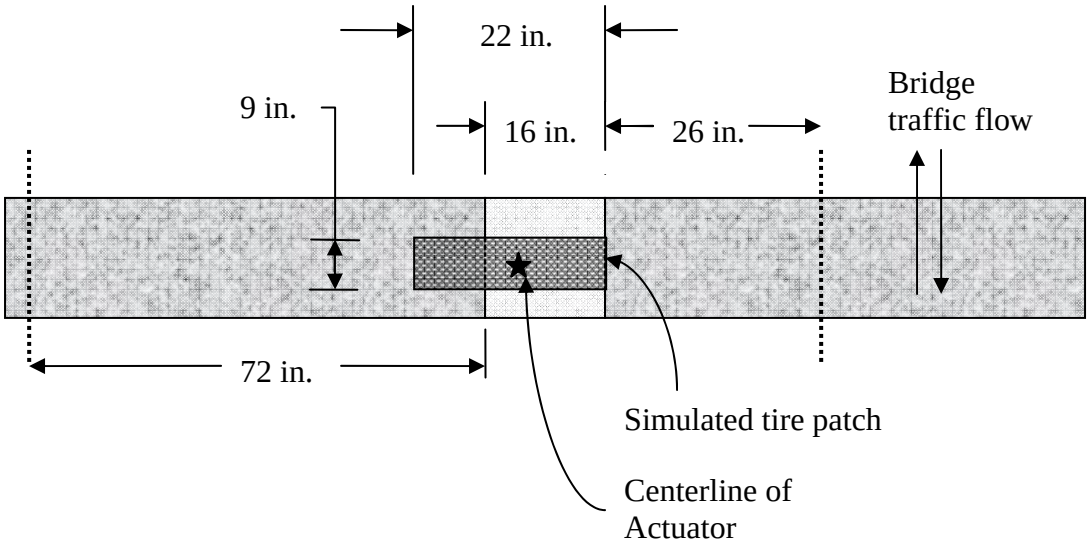

(a)

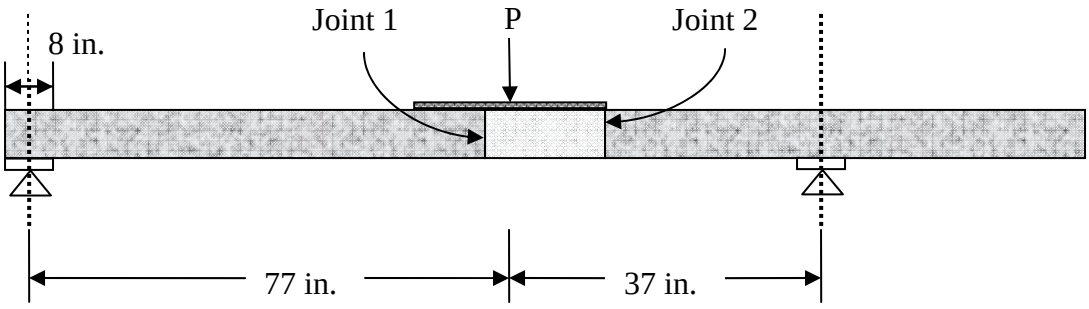

(b)

Fig. 79. Positive moment test setup for L11: (a) plan view; (b) elevation view

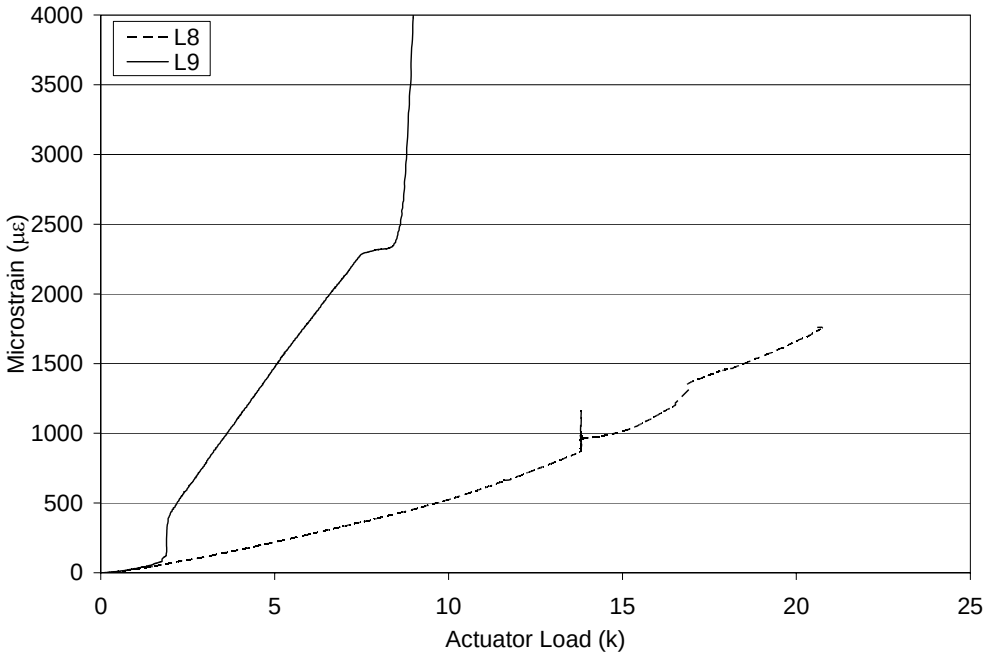

Fig. 80. Measured reinforcing strain at gage position 1 in L8 – L9

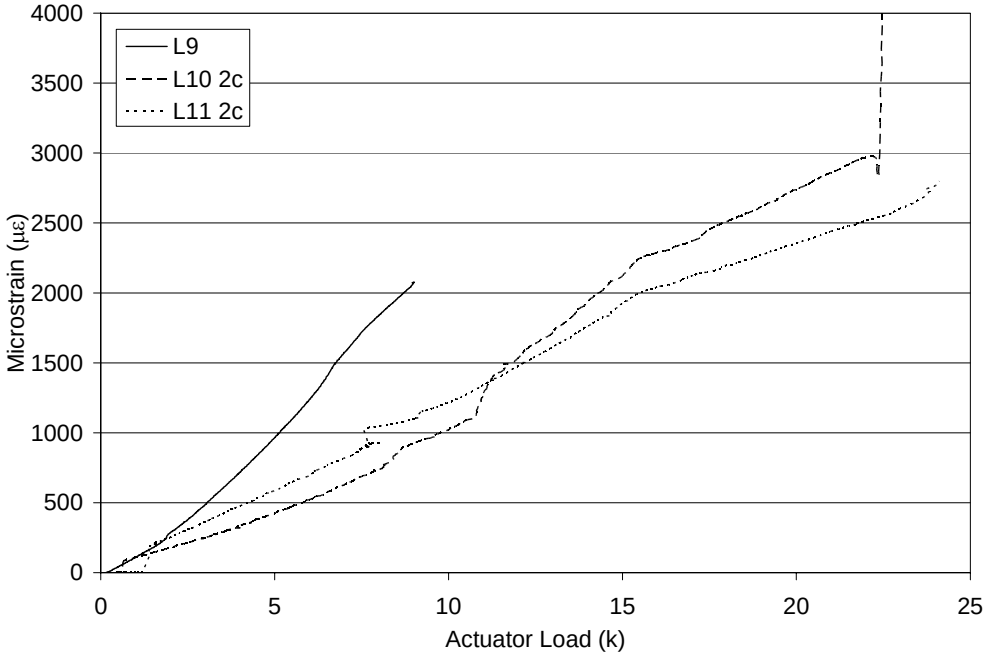

Fig. 81. Measured reinforcing strain at gage position 2 in L9 – L11

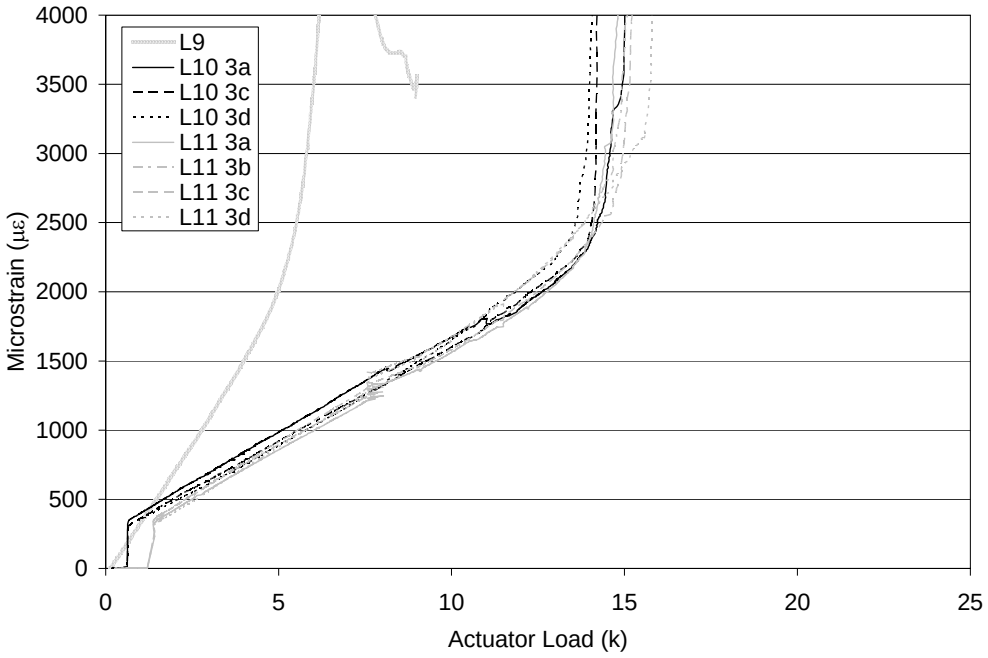

Fig. 82. Measured reinforcing strain at gage position 3 in L9 – L11

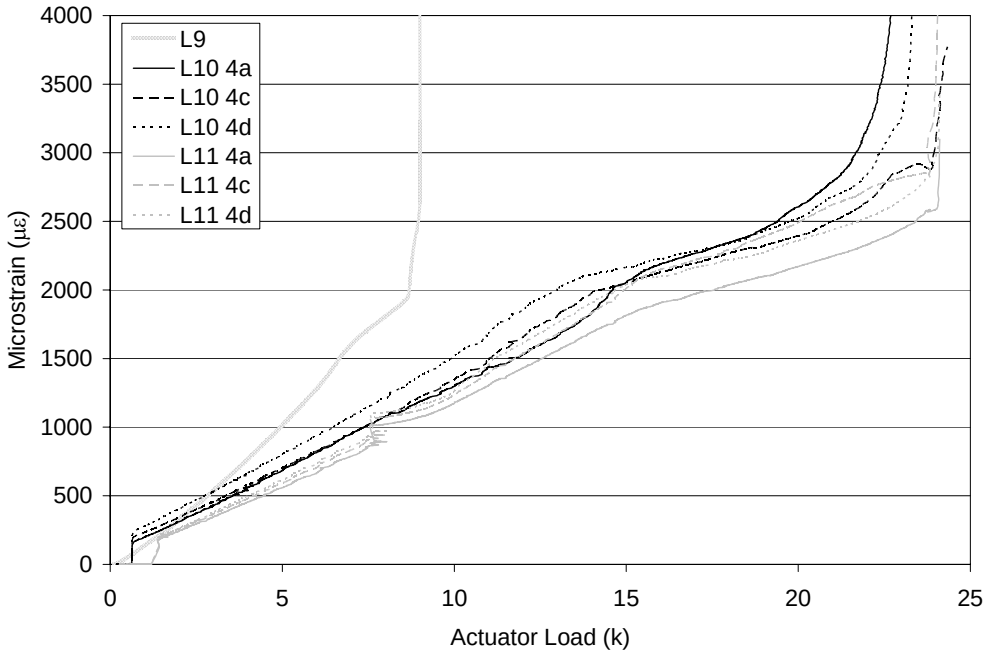

Fig. 83. Measured reinforcing strain at gage position 4 in L9 – L11

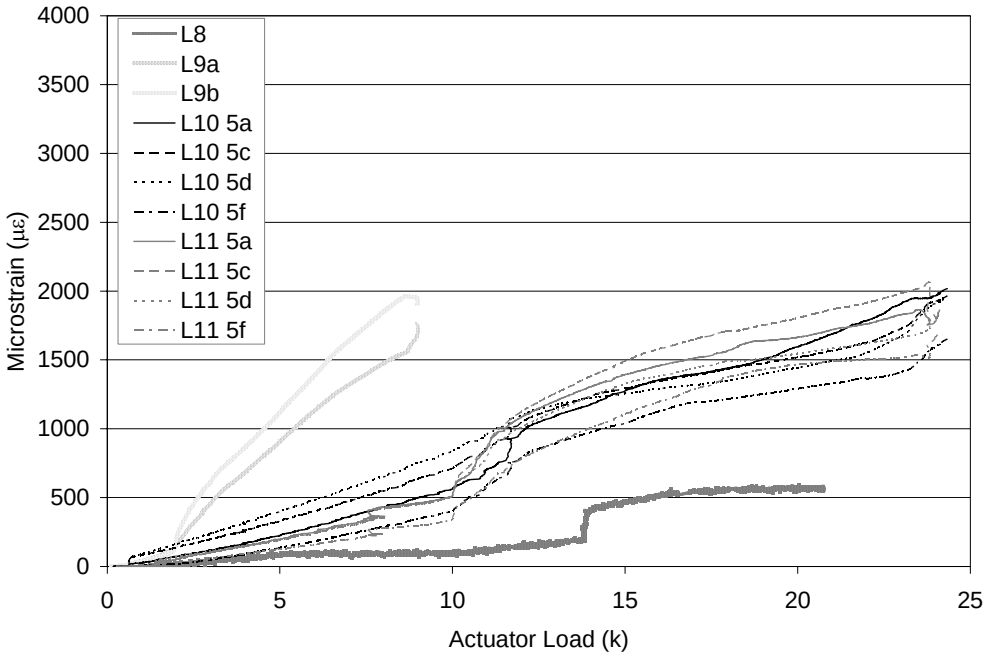

Fig. 84. Measured reinforcing strain at gage position 5 in L8 – L11

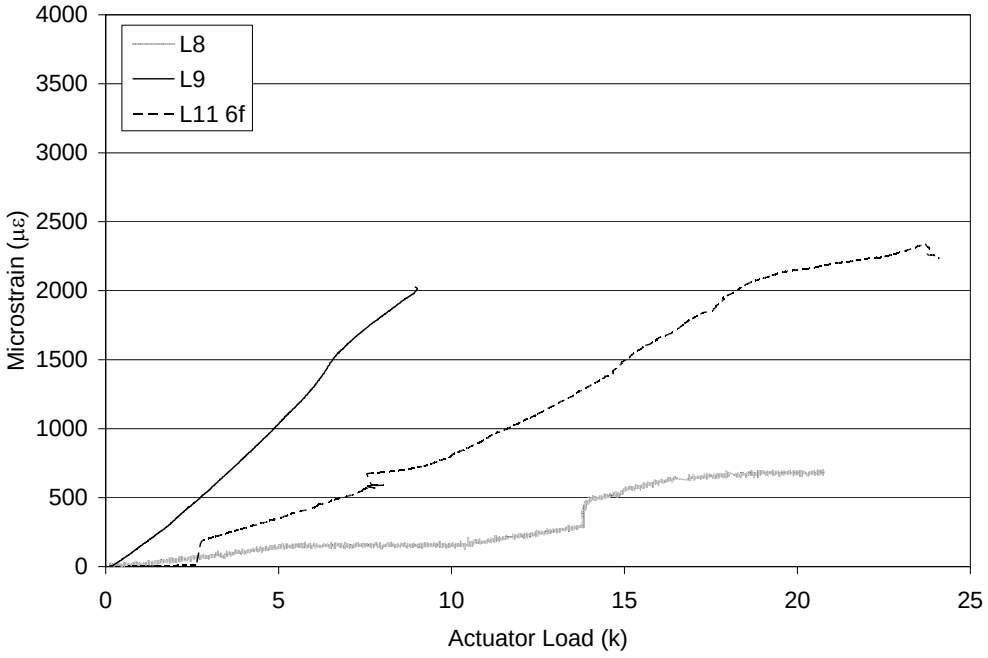

Fig. 85. Measured reinforcing strain at gage position 6 in L8, L9, L11

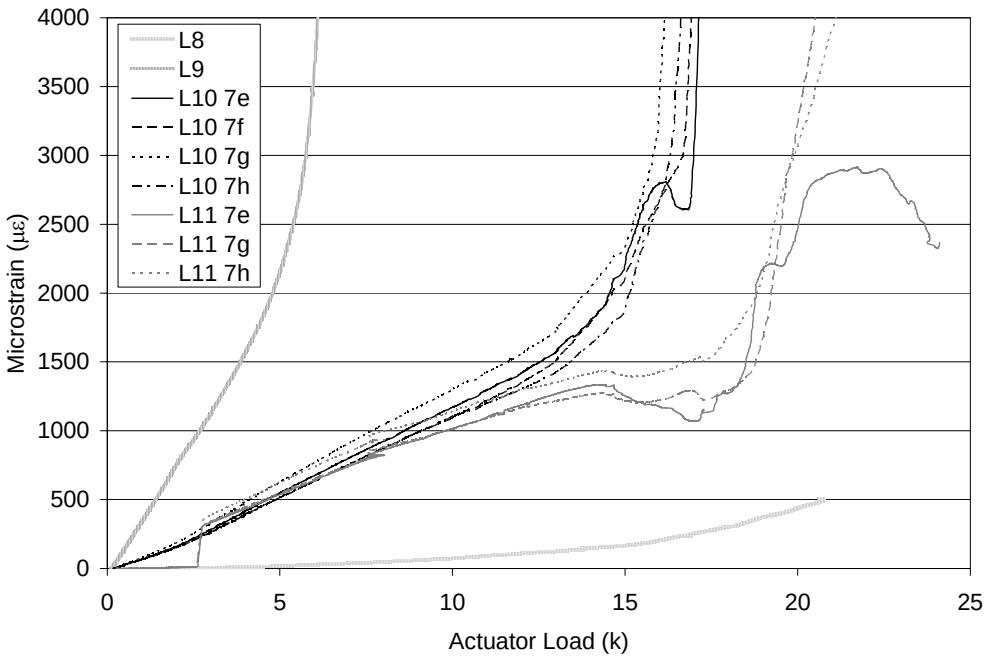

Fig. 86. Measured reinforcing strain at gage position 7 in L8 – L11

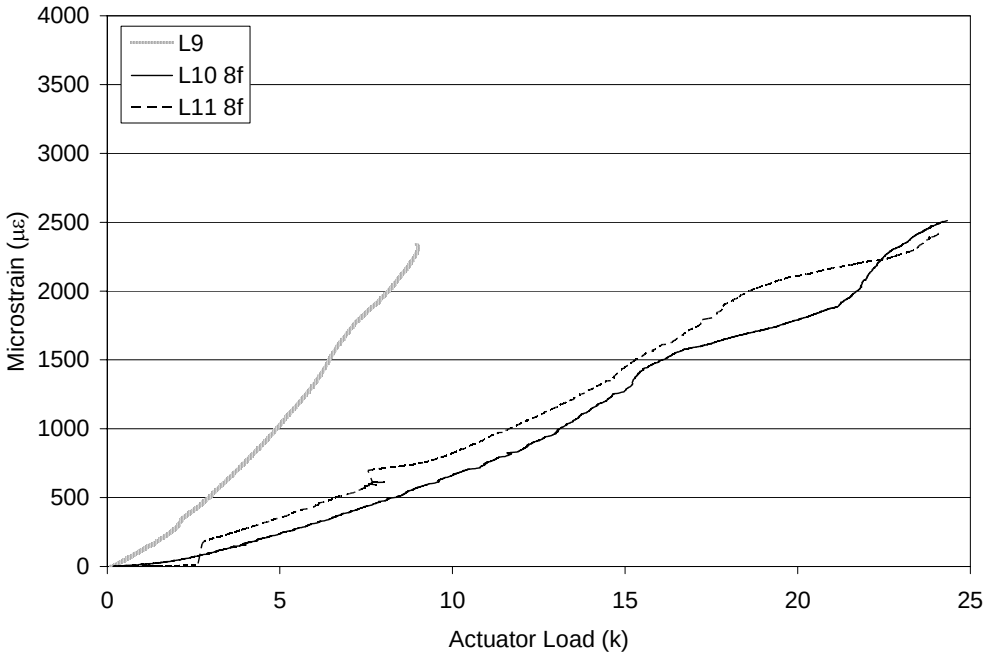

Fig. 87. Measured reinforcing strain at gage position 8 in L9 – L11

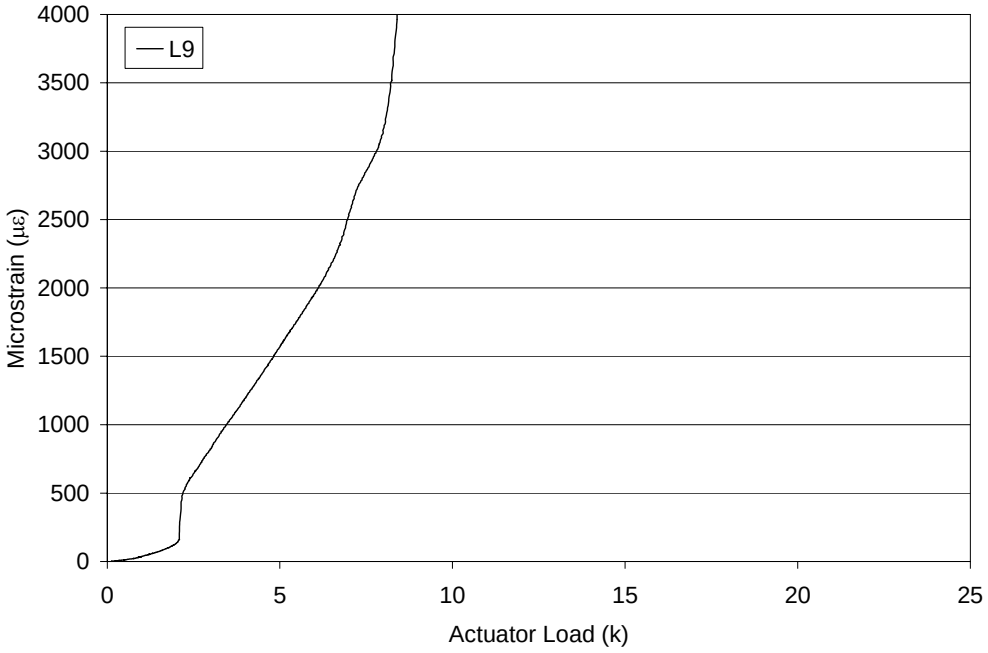

Fig. 88. Measured reinforcing strain at gage position 9 in L9

VITA

Natalie Camille Brush received her Bachelor of Science in civil engineering from Texas A&M University in the summer of 2002. She began working towards her Master of Science in civil engineering in the fall of 2002. Ms. Brush worked as an assistant researcher for Dr. Ray James and Dr. Harry Jones.

1604 Pineridge St.

Longview, Texas 75604

USA

(903) 297 – 9587